Dependence of natural fragmentation characteristics of a casing material on explosive parameters

SAN Alqarni

orcid.org / 0000-0002-5814-4598

Thesis accepted in fulfilment of the requirements for the degree Doctor of Philosophy in Mechanical Engineering at the North-West University

Promoter: Prof JH Wichers

Graduation: July 2020

Student number: 27359808

PREFACE

It was a great pleasure to study at North West University and to train in parallel at Rheinmetall Denel Munition (Pty) Ltd (RDM) over the past four years; this was the critical time in my work life. This continuous enrichment from people around me at that time has undoubtedly motivated me and has inspired my research. Therefore, I would like to acknowledge and thank the many people that have helped me along the way toward the successful completion of this thesis. To them I am eternally grateful.

First: I would like to thank Prof. JH Wichers for giving me the opportunity to study for my doctorate degree under his supervision.

Especial grateful to the one who was supporting and motivating me during the process of this work; my promoter, Dr Frikkie Mostert; thank you for your positive feedbacks, for your patience and guidance, without you, none of this would have been possible.

RDM has fully sponsored this work, for them, I would like to express my thanks and gratitude for their support and cooperative help.

My Wife and my Kids, words cannot express my appreciation to you. Your love and persistent confidence in me, have taken the load off my shoulders.

Finally, my friends and my dear family, I would not have been able to write this manuscript without you. Thanks for your precious support and enthusiasm.

ABSTRACT

Since the prediction of warhead performance is crucial in the early stages of design and the scaling of this procedure is complex and expensive, it is beneficial to have measurable parameters in one optimal model to improve the efficiency of prediction.

In general, the type of explosive, mechanical properties and warhead geometries have been proven in previous approaches to provide critical parameters, in terms of size, spatial and velocity distribution, in warhead fragmentation. Statistical approaches have been developed to describe this fragmentation with a combination of these parameters (statistical factors with mechanical properties or explosive properties), and thus, the possibility of developing an integrated model that encompass the effect of detonation behaviour on natural fragmentation characteristics for the same casing material in one scale factor still exists.

A literature review describes how the current models based on statistical factors have been investigated with only a single donor explosive is assumed (most commonly TNT or Composition B) in most of these studies. However, it is clear from the trends in munitions development that explosives with characteristics quite different from TNT and Composition B are being increasingly used. Therefore, limited research has been performed on the changes in fragmentation that occur in a specific material due to either changing the explosive type or changing the detonation characteristics of the same explosive.

This study investigates the dominant explosive parameters that dictate the fragmentation process. In addition, this study pursues the possibility of developing an integrated model that includes both explosive and material parameters in one simple analytical model.

Key terms

Natural fragmentation characteristics, High explosive material, Insensitive Munition, Explosive Parameters, Detonation products, Cylinder test, Arena test

ABBREVIATIONS, SYMBOLS AND TERMINOLOGIES

ABBREVIATION	
HE	High explosive
IM	Insensitive munition
JWL	Jones-Wilkins-Lee (JWL) equation of state
TNT	Type of explosive **Trinitrotoluene**
RDX	Type of explosive known as hexogen, cyclonite and cyclotrimethylenetrinitramine
NTO	Type of explosive **Nitrogen tetroxide**
ONTELIT	Mixture of explosive 50%TNT and 50%NTO
MCX-6002	Mixture of explosive 51%NTO, 34%RDX and 15%TNT
Comp-B	Composition B mixture of 60% RDX and 40% TNT
RXHT-80	Mixture of 80%RDX and 20% liquid polymer binder
PBX	plastic-bonded explosive or a polymer-bonded explosive
HTPB	Hydroxy-terminated polybutadiene
N/A	Not applicable
PAFRAG	Picatinny Arsenal Fragmentation (simulation program)
FE	Finite Element
HSV	High speed video
BEW	Bridge electric wire
ITOP	International Test Operations Procedure
STANAG	Standardization agreement
AL	Aluminium
SYMBOLS	
σ	Mechanical stress
ε	Strain
$\dot{\varepsilon}$	Strain rate
Y	Yielding stress
UTS	Ultimate tensile strength
P_{CJ}	Chapman–Jouget pressure
C-J point	Chapman–Jouget point
$\acute{\gamma}$	The isentropic constant
D	Detonation velocity
D	Damage criteria
d	Diameters
d_i	Inner diameter

d_o	Outer diameters
R	Radius
R_i	Inner radius
R_o	Outer radius
R_m	Central radius
v_f	The final velocity where the fragments takes place
$\sqrt{2e}$	Gurney constant
v_G	Gurney velocity
e	Gurney energy
ΔE_i	internal energy of explosion or internal energy of detonation
ΔH_d	Heat of explosion or heat of detonation and enthalpy of detonation
ΔH_c	Heat of combustion and enthalpy of combustion
ΔE_c	Internal energy of combustion
ΔS	Entropy of explosion
E_f^o	Internal energy of formation
H_f^o	Enthalpy of formation and heat of formation
t	time
t	thickness
V	volume
m	Fragments mass
$N(m)$	Total number of fragments
$N(> m)$	Cumulative number distribution of fragments their mass $> m$
μ	Average fragments mass factor
$\bar{m}$	Average fragments mass =2μ
$M(m)$	Total mass of fragments
$M(> m)$	Cumulative mass distribution of fragments their mass $> m$
C	The mass of the explosive material
M	The mass of the cylindrical case material
B and λ	Held empirical paramters
γ	Gold distribution factor
$\grave{\gamma}$ and $\grave{C}$	Mott empirical parameters
β and μ	Mott parameters of the distribution fuction
A_M, B_M and C_M	Gurney–Sarmousakis, Mott and Magis empirical parameters.
n_k, m_k and a_k	Empirical parameters of Randers-Pehrsod, Hennequin and König
$F(t)$	The radial displacement as a function of time
a_i and b_i	Equation of motion empirical parameters

TERMINOLOGIES

Chapman–Jouget point	Is the condition where the velocity of the shock front reaches the detonation velocity of the explosive and the detonation is considered to reach a state of equilibrium.
Detonation	A form of reaction given by an explosive substance in which the exothermic chemical reaction produces a shock wave. High temperature and pressure gradients are created in the wave front so that the chemical reaction is initiated instantaneously.
Detonation pressure	The dynamic pressure in the shock front of a detonation wave.
Brisance	The shattering effect of an explosive upon its casing, or the ability of an explosive to perform such mechanical work.
Gurney velocity	Is the final velocity imparted to an explosively loaded case.
Gurney energy	Is the chemical energy in the initial state that is converted to kinetic energy in the final state. The kinetic energy is partitioned between the casing metal and the detonation products gases.

TABLE OF CONTENTS

LIST OF TABLES

LIST OF FIGURES

CHAPTER 1: INTRODUCTION

Weapons systems are integrated systems controlled by governments to protect their communities and to defend their property. There are various sub-systems enshrined within the weapons systems that featured different warheads and apply varying mechanisms to neutralise various threat. The high-explosive (HE) fragmentation warhead is one such sub-system that forms the core of this research.

In a simplified definition, the HE warhead artillery round is a cylindrical metal casing filled with energetic material (explosive) adjusted with an initiation system to release the chemical energy (compound) of that explosive. Figure 1-1 is across-section illustrating the different part of the warhead including the initiation system, casing material and HE filling.

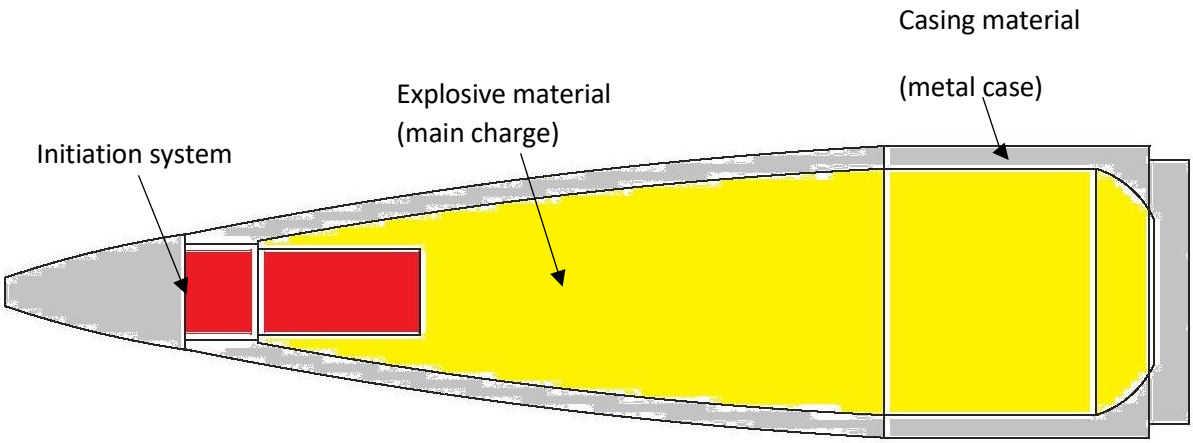

Figure 1-1: The main structure of the high-explosive (HE) fragmentation warhead.

The initiation system consist of explosive composition in a detonator and booster to the main charge to complete the explosive train. The energy released from detonation is, therefore, converted into various types of energy for different utilizations to neutralise specific threats

Two main types of effects from HE warheads are of concern in this investigation, namely the blast effect and the fragment effect. The **blast effect** is an effect in which the compression of the surrounding medium (typically air) by the liberated hot and high-velocity explosive gases results in the development of a shock wave that expands three-dimensionally away from the explosive event. This shock wave is further enhanced when aerobic reactions continue to occur when the explosive particles mix with the air, such as in the instance of aluminised or otherwise highly

oxygen-deficient mixtures. These mixtures generate additional blast energy through exothermic reactions with the surrounding air (i.e. after-burn) [1].

The **fragment effect** is an effect in which the energy released from the casing body shattering into fragments is converted into kinetic energy. The expansion of the casing normally overcomes the yield strength of the material and fractures under a dominant fracture mechanism into fragments. The final form of these fragments and their behaviour are critical factors in measuring HE warhead efficiency and lethality. The distinction between these two effects is that a blast wave has a very limited and short effect due the energy dissipating very rapidly in the air, while, the fragment effect is subjected to air drag as the main resistance force. Therefore, fragments can deposit higher energetic effects at larger distances. This study focuses on the high-explosive fragmentation warhead as outlined below.

1.1 High-explosive fragmenting warhead

High-explosive warheads are common in defence systems all over the world, since they are part of one of the most cost-effective weapon systems. Like with any other system in other fields, there are critical parameters that must be determined in the design and development phases, especially in the early stage of design, to measure whether the performance of the system will meet the requirements for neutralising a specific threat. In the case of the HE fragmentation warhead system, the warhead's lethality can be measured through the terminal effects of the fragments. Three types of fragmentation warhead exist, namely pre-fragmented warheads (warheads that contain fragments of a specific shape and size), controlled fragmentation warheads (normally dictated by grooves or other gauging mechanisms in the casing) and natural fragmentation warheads (the casing fragmentation is only dictated by the material parameters of the casing) [2]. The terminal effects of natural fragments depend highly on their final form and behaviour, which are controlled by three main factors: type of casing material and its behaviour, type of explosive material and its behaviour and the warhead's geometry. Figure 1-2 is an illustration of an integrated warhead system and how the three main factors must be considered by warhead designer to predict the warhead effectiveness under the final fragments characteristics.

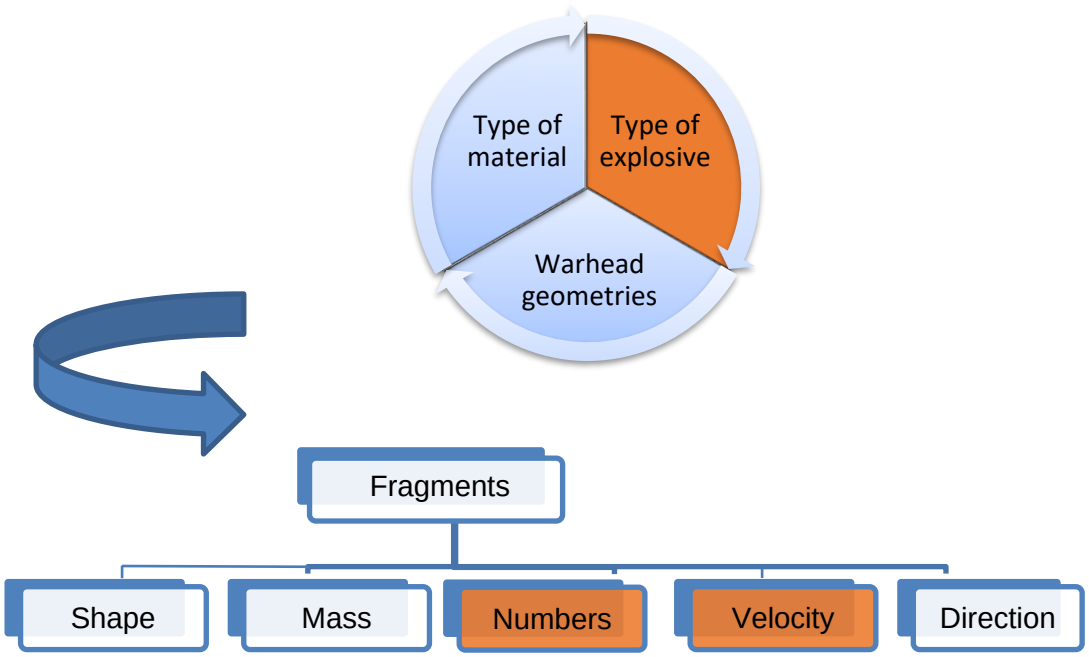

Figure 1-2 : Diagram of an integrated warhead system.

Therefore, the designer of this type of warhead as a complete system must be aware of the fragment characteristics that result from a particular material and design in order to predict its lethality. Furthermore, the designer must also understand how different choices of materials and geometries can be used to control and balance certain features of the fragments. The aim of this study is to provide data on aspects of natural fragmentation warheads that can be used to simplify and enhance predictions of the characteristics of the resulting fragments. In particular, it aims to zoom into the contributions of specific changes in the explosives to the changes observed in the fragment characteristics.

1.2 Research problem and background

From the material science perspective, fragments are a result of multiple fractures to the warhead casing material that has shattered under the stress of detonation load. The material resists the stress effect for a certain time before it fracture at a condition known as the *material failure mode*.

Material behaviour

Materials under stress loading pass through different stages before reaching a final stage when failure occurs. The transformation stages under stress load depend on the material properties and the type of stress. The mechanical behaviour of the material in this process has been described through mechanical variables such as stress (σ), strain (ε) and strain rate ($\dot{\varepsilon}$) [3]. Figure 1-3 describe the material behaviour under stress load where the three main points used to

characterize the material based on their behaviour. The point between the elastic and plastic formation (***P)*** is the yielding point of the material (Y). (***M)*** is the distinguished point for the ultimate tensile strength (*UTS*) where the material withstands a load and tends to elongate and (***F)*** is the failure point where the material fracture.

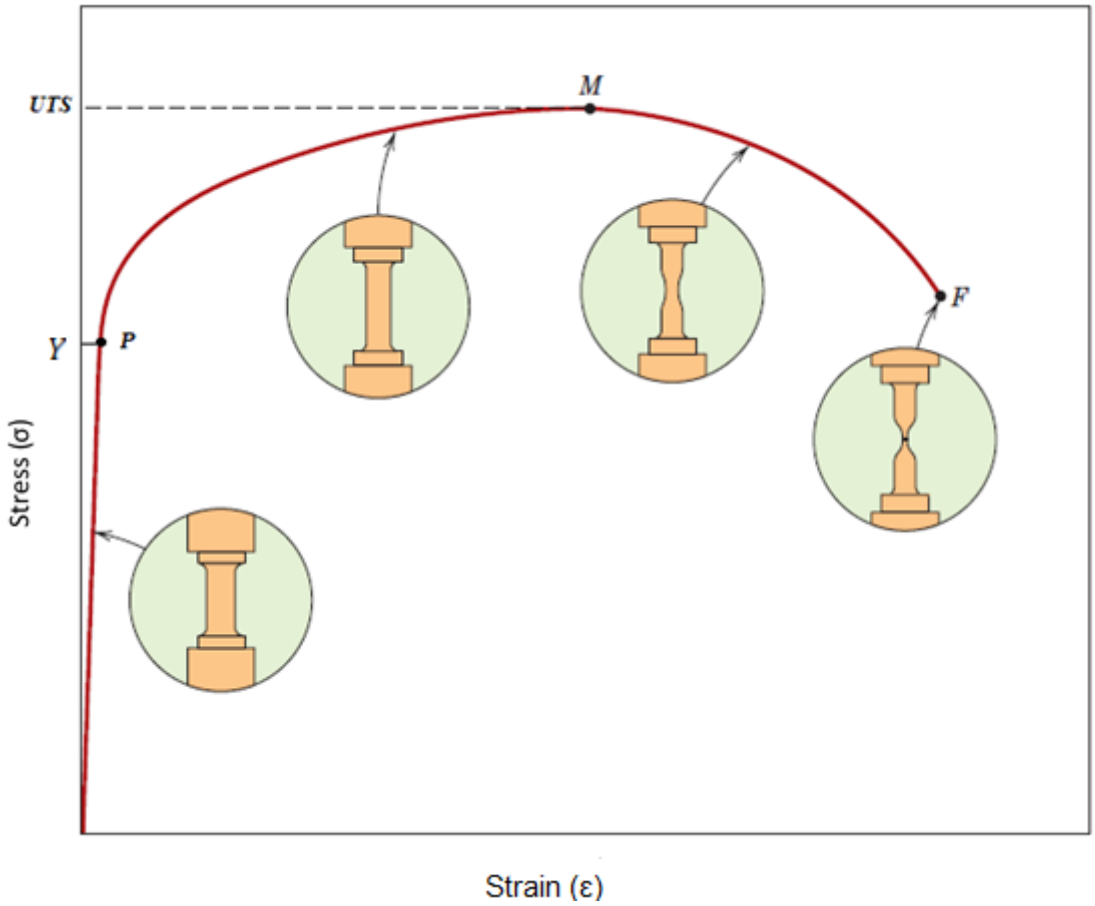

Figure 1-3: Typical engineering stress– strain behaviour to fracture [3].

Constitutive model

Based on the mechanical definition of the material behaviour under stress loading, several constitutive models have been developed to describe the strength and hardening response of a metal material under different loads. One of the most common models is the empirical model developed by Johnson–Cook [4], namely:

$$\sigma = \left[Y + b\varepsilon_p^n\right]\left[1 + c\, ln\frac{\dot{\varepsilon}}{\dot{\varepsilon}_o}\right][1 - T^{*\epsilon}], \qquad 1\text{-}1$$

The first square bracket on the right hand side of equation (1-1) describes the influence of the plastic strain, where Y is the yield stress, b represents the hardening modules, n is the hardening

exponent and ε_p is the plastic strain. The second square bracket describe the influence of the strain rate on the material behaviour under stress load, where c is strain rate coefficient, $\dot{\varepsilon}$ is the strain rate and $\dot{\varepsilon}_o$ is the reference strain rate. The last square bracket describe the influence of the temperature change, where $T^{*\epsilon}$ is the homologous temperature and ϵ is temperature coefficient.

The solid material under this characterisation, has been classified into two main types of material: brittle and ductile materials. Figure 1-4 illustrate the behaviour of both material where the area under each curve represent the energy absorbed by the material before fracture which known as the toughness of the material. The energy observed by ductile material is higher than the energy observed by the brittle material during expansion, which affects the final shape of the fracture.

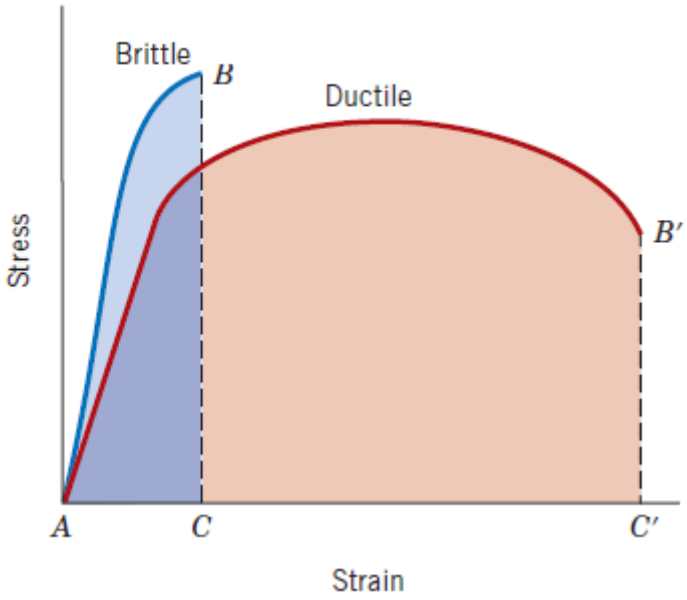

Figure 1-4: Type of solid material based on their responsibility of mechanical stress loading [3].

Ductile materials will be elongated before failure, and yielding occurs not due to separation but to the sliding of atoms (the movement of dislocations), as depicted in Figure 1-5. Thus, the stress or energy required for yielding is much less than that required for separating the atomic planes. Hence, for a ductile material, the maximum shear stress causes yielding of the material. The ductile material exhibits larger elongation compared to brittle materials before fracture, which for similar stress levels can be interpreted as toughness.

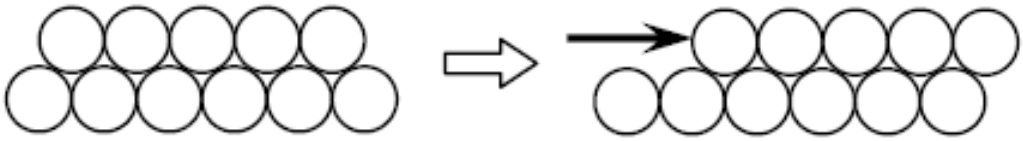

Figure 1-5: Material atoms under mechanical stress [3].

In brittle materials, stress–strain behaviour is almost linear up to the point of failure Figure 1-4, and they can fail abruptly. The failure or rupture occurs due to the separation of atomic planes. However, the high value of stress required is provided locally by concentrations of stress caused by small pre-existing cracks or flaws in the material. The stress concentration factors can be in the order of 100 to 1,000. That is, the applied stress is very highly amplified due to the presence of cracks and is sufficient to separate the atoms. When this process becomes unstable, the material separates over a large area, causing the failure of the material [3].

Explosive parameters

Explosive properties are an important consideration for the fragmentation process since they are the source terms for the stress in the casing that eventually generates the fragments. Explosive properties are a combination of the shock imparted on the surrounding medium and the kinetic energy of the gases produced, which perform work on the surrounding medium. A shock wave, in principle, is a wave with a discontinuity at its front and which moves at supersonic speed. Depending on the medium it propagates through, a shock wave can be classified as one of two types: an unreactive shock wave (inert wave) and a reactive shock wave (detonation wave).

The detonation is defined as a special form of shock wave moving with a rapid exothermic chemical reaction and occurring in a region just behind the shock front. Theoretically, the shock wave is a very high-pressure wave moving at a supersonic velocity through the explosive material; the energy of this wave is capable of breaking the explosive molecular compound in a process of exothermic reaction to convert the explosive material from a solid to gas state. This process is accompanied by a very high energy release.

Detonation behaviour

Based on existing models, the detonation wave is the result of a self-sustaining shock wave (self-sustaining due to the liberation of the chemical energy in the explosion) that passes through explosive material with a rapid exothermic reaction occurring just behind the shock front [5].

According to detonation theory, when an initiation of an explosive material from one side a detonation wave will move in the same line of the initiation point and a detonation products will expand vertically to the detonation axis. The shock front, the chemical reaction zone and leading edge of the rarefaction are all in equilibrium, so they all assumed to move at the same speed, known as the *velocity of detonation (D) or the detonation rate*. Figure 1-6 is an illustration of the detonation behaviour in a confined explosive material inside a cylindrical metal tube where the curved red line is representing the detonation front, the reaction zone is located between the curve red line and the purple curved line and the green line is representing the sonic line. The critical parameters to characterize detonation behaviour is the detonation front point (D), Chapman–Jouget point (P_{CJ}) and the point at fracture (v_a).

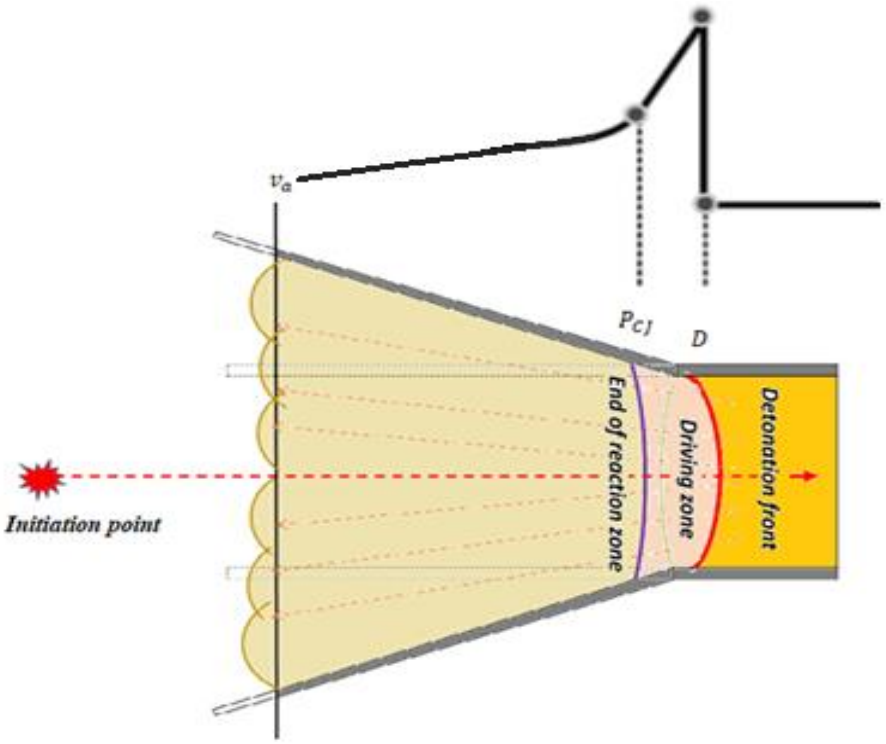

Figure 1-6: Schematic representation of the detonation process.

The Chapman–Jouget point hypothesised the state at the end of the reaction zone and the beginning of the released wave. The slope of the Rayleigh line at C-J point yields the detonation velocity *D* [5]. $v_a$is the point of interest where Gurney velocity, internal energy of explosive and the other explosive parameters can be predicted. The gas expansion, or rarefaction wave, behind the C–J point are not a fixed characteristic of the explosive.

Equation of State model

Several equations of state were developed to characterise detonation behaviour. One of the most commonly models used is the empirical equation of state model developed by Jones-Wilkins-Lee (JWL) [6, 7, 8]:

$$P = A\left(1 - \frac{\omega}{R_1 V}\right)e^{-R_1 V} + B\left(1 - \frac{\omega}{R_2 V}\right)e^{-R_2 V} + \frac{\omega E(V)}{V}, \qquad 1\text{-}2$$

where P, V and E are the pressure, specific volume and internal energy, respectively. A, B, R_1 and R_2 are the JWL empirical parameters related to each region and specific to each explosive, and ω is the isentropic expansion factor

Based on the detonation front point (D), Chapman–Jouget point (P_{CJ}) and the point at fracture (v_a); an analytical method have been developed to determine the empirical parameters for each type of explosive such as cylinder test [9]. JWL models therefore divides the detonation behaviour into three stages, where the parameters A and R_1 contribute to modelling the first stage of detonation behaviour at high pressure and low expansion ratio at the shock front. The parameters B and R_2 contribute to define the detonation behaviour at the intermediate pressure zone of the detonation products where C and ω describe the pressure and specific volume relationship of the detonation products at low pressures and high expansion ratios.

Several energies contribute to the determination of the failure point, such as Gurney energy, particle energy, deformation energy and the internal energy at failure. Several fracture models have been developed to determine the effective mechanical parameters at a very high strain rate such as detonation.

Fragmentation behaviour

In our case, the fragmentation is the result of a **dynamic** fracture that is the consequence of an explosive detonation, impulsive internal pressure, rapid gas product expansion and the behaviour of the casing material [10]. Figure 1-7 provide a numerical illustration of the detonation behaviour inside warhead body. The detonation front presented in the red colour move with the detonation velocity where the yellow colour present the end of the reaction zone and the green is the presented colour of the detonation products.

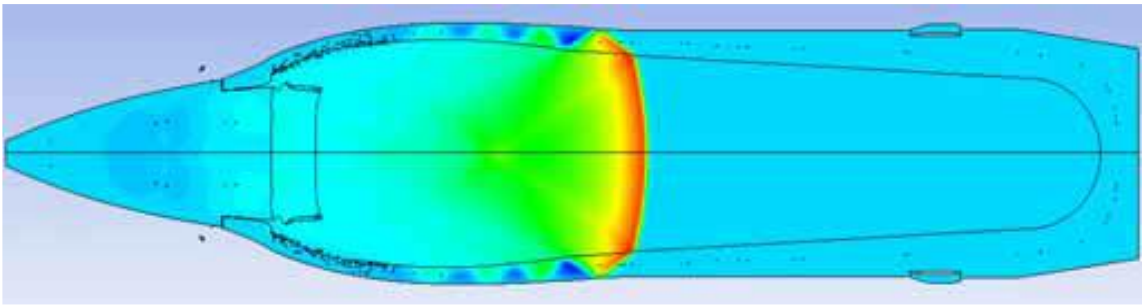

Figure 1-7: Detonation behaviour in high-explosive warheads (FE simulation) [10].

Subsequently, the fragmentation process is the result of an interaction between the detonation wave effect and the material response. The specific result of the detonation effect is an increase in the strain rate during the expansion of the material by the products of detonation. This kinetic effect is accounted for in the constitutive models. However, the temperature transients and shock effects of the detonation wave on the casing and their effect on the casing's in-situ microstructure are normally not incorporated in the models. It is therefore important to investigate the effect of the explosive contribution itself on the fragmentation process.

The cylinder test is the standard test to determine the empirical parameters of the detonation behaviour as well as the empirical parameters of failure model, as presented in the next section.

1.3 Cylinder test

The cylinder test is the technique used to extract the equation of state parameters and other explosive characteristics such as the Gurney constant. This test piece is a hollow cylindrical metal tube filled with an HE material. The explosive confined inside the tube adjusted with an initiation system from one side and left opened from the other side. When the detonation front move vertically in the longitudinal axis, the detonation products expands the tube horizontally in the radial axis to the point at which the tube reaches its final velocity. Using various techniques, this event can be recorded at a certain cross-section along the longitudinal axis of the cylinder during the test, such as with a streak camera or velocity spectrogram technique [9]. Figure 1-8 illustrate the streak camera method to record the expansion behaviour of the detonation products. An analytical model have been developed and improved through time by several scientist to obtain the optimum values of the empirical models such as Gurney and JWL models.

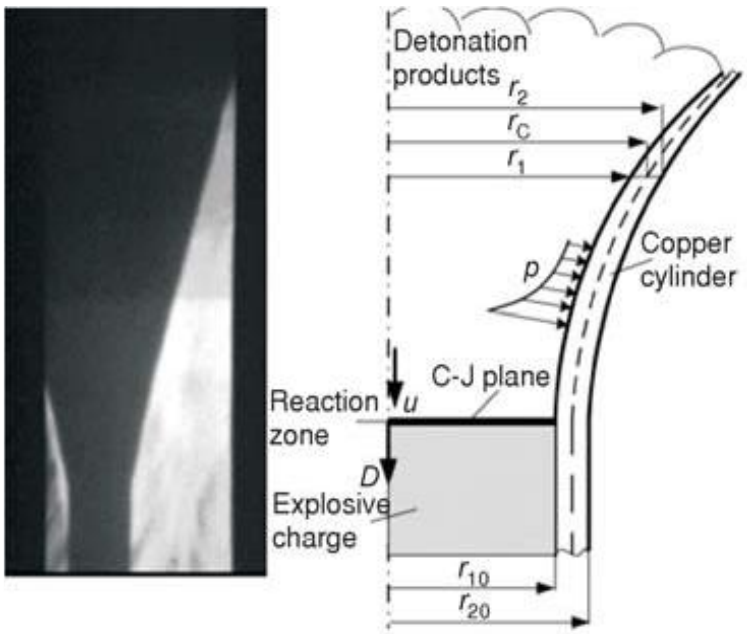

Figure 1-8: Streak photograph of detonation behaviour by [11].

The data obtained from the cylinder test rely on the time history of the metal wall expanding under the products of detonation. The JWL equation of state relates the pressure of the expanded gas to the fragmentation process and the time of expansion process. The velocity spectrogram technique is one of the existing methods used to record expansion event. Figure 1-9 shows an oscillation of the wall during expansion until it reach its final velocity before fracturing [11]. The figure provides an illustration of the expansion behaviour of the detonation product in velocity vs time diagram. The curve in red colour represent the velocity history of the wall during interaction between detonation and the wall material. The acceleration time of the detonation products is the time of motion from initial to final stage of expansion where the wall start to fracture and velocity start to stable. This time also known as the after burning time of the detonation products.

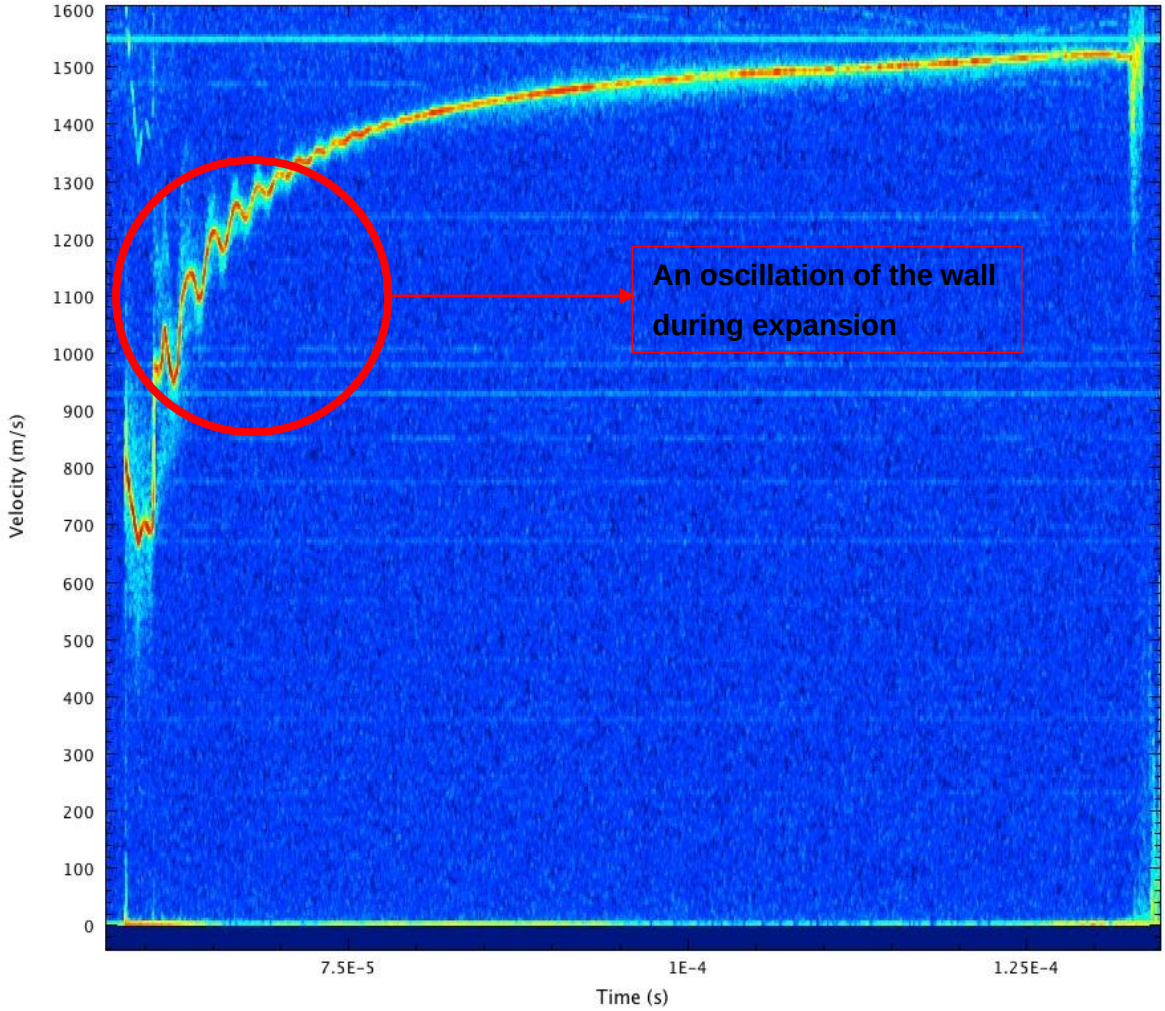

Figure 1-9: Expansion behaviour of detonation products recorded by spectrogram technique [11].

The wall material of the cylinder under detonation effect withstand the detonation wave during acceleration and an oscillation on the wall is the results of the material resistance, which can affect the kinetic energy imparted to the wall before fracture. Because of the rapidity of the detonation process, the acceleration time is not considered as a major parameter in fragmentation model. In addition, a detonation products of different explosive material can results to different acceleration time especially with those contain metallic material such aluminium. However, a situation where two fragments have the same final velocity with different acceleration times can be found. The effect of the acceleration time of the detonation products on the final fragments characteristics is unpredictable through the existing model and that may be significant.

1.4 Fragmentation and failure models

Due to the complexity of the fragmentation process, simple models have been developed, based on assumptions on the expansion of ring elements, to describe fragment characteristics and material failure modes.

The results of these models are empirical factors with mechanical parameters that describe fragment characteristics and behaviour at a failure condition. The most important models were developed by Taylor [12,13], Mott [14], and Grady et al. [15]. The main concern of these models is to predict the characteristics of the fragments at failure as formulated in the following equations.

The model developed by Mott [14] is widely used to predict the average fragment breadth relative to the effective strain rate at failure, namely:

$$\bar{x} = (\frac{2\sigma_f}{\rho\grave{\gamma}})^{\frac{1}{2}}\frac{1}{\dot{\varepsilon}}, \qquad 1\text{-}3$$

where σ_f is the failure stress or the stress at which fragmentation takes place, ρ is the material density, γ' is a semi-empirical constant determining the dynamic fracture properties of the material and $\dot{\varepsilon}$ is the effective strain rate.

The other important model used to predict the average fragment size at failure is the model developed by Grady et al. [15], namely:

$$\bar{x} = (\frac{\sqrt{24}K_f}{\rho c\dot{\varepsilon}})^{\frac{2}{3}}, \qquad 1\text{-}4$$

where K_f is the material toughness or the energy observed by the fragments before being formed, ρ is the material density, c is the speed of sound and $\dot{\varepsilon}$ is the effective strain rate.

The model developed by Taylor is also one of the most important models used to predict the effective radius at failure, namely:

$$\frac{a}{a_0} = (\frac{P_o}{Y})^{\frac{1}{2\acute{\gamma}}}, \qquad 1\text{-}5$$

where a is the radius at a failure mode, a_0 is the initial radius of the expanded ring, P_o is the effective detonation pressure acting on the inside surface of the casing material, $\acute{\gamma}$ is the isentropic constant and Y is the yielding point of the material at the circumferential failure radius. This model is also used to evaluate the effective thickness of fragments at failure.

In the simple fragmentation models, the fragmentation process is coupled to the casing material properties through mechanical variables such as stress, strain and strain rate, where the Gurney velocity is the only explosive parameter involved in the determination of fragmentation characteristics to estimate the effective strain at failure. The initial pressure of the detonation product has been coupled indirectly through the Taylor model to the fragmentation process. Another empirical model have also indirectly coupled the Chapman–Jouget pressure to the fragments characteristics. These models and other provide quite well estimation method to predict the fragmentation characteristics from prompt energy release.

Moreover, the fragmentation process is indirectly coupled to the expansion of the casing (to the failure stress and strain) by the JWL equation of state (explosive properties) through the gas expansion volume of the detonation products. Tests must be conduct in every case to extract the empirical parameters for each model to characterize the explosive parameters for any change in the explosive formulation. The fragmentation and failure models discussed in more detail in next chapter.

1.5 Purpose and problem statement

A constitutive model has been developed to characterise material response to stress load. Consequently, a fracture model has also been developed to characterise the fracture behaviour of a material subjected to dynamic loading conditions such as high-strain impact or explosive detonation. The fragmentation process therefore has been modelled in a simple fragmentation model through mechanical properties (strain, strain rate and stress at failure). Expansion properties have also been used to model explosive behaviour (Jones-Wilkins-Lee equation of state) [6, 7 and 8]. These mechanical and equation of state properties have been combined with material properties in statistical and empirical models to describe the fragmentation process, such as the fracture strain model by [12, 14 and 15]. Moreover, these models have been investigated for different material properties such as ultimate tensile strength, hardness and fracture toughness [10, 16, 17 and 18] rather than different explosive properties such as heat transfer (explosives with higher afterburning rates) and detonation characteristics, which also have an effect on mechanical properties on a microstructural level.

As previously mentioned, warhead performance prediction depends on a comprehensive database of the natural fragmentation features of warheads, including data on fragment mass, number and shape, initial fragment velocities, warhead case and explosive material performance and spatial fragment distributions.

Thus, the overall problem statement has been formulated on the following premises:

- There is no integrated model that includes all material or explosive parameters required to conduct a warhead fragmentation simulation.
- The existing models do not properly address the effects of afterburning rates (detonation products).
- In most of the existing studies investigating material properties, parameters were derived for limited explosive types (most commonly TNT or Composition B [Comp-B]).
- All detonation characteristics of explosives have not been explicitly included in these models.

Therefore, the problem to be researched is: to study the dependence of natural fragmentation characteristics of a casing material on explosive parameters.

1.6 Research aim and objectives

The aim of this research aim to develop an integrated model to characterize fragment based on explosive parameters.

The specific theoretical objectives of this study are to:

- To determine the effects of different explosive charges on the fragmentation characteristics in terms of size, mass and number distribution, velocity and spray angle.
- To determine the material's response to the explosive effects through mechanical properties (strain, strain rate) of the fragments.
- To develop an integrated model by relating the material parameters with explosive parameters in one model that can predict the statistical distribution of the fragmentation pattern in the early stages of design.

1.7 Research scope and methodology

The scope for this study is divided into three parts, namely literature analysis, experimental work and analysis of results. For the purposes of this study, the following equipment was used:

- Cylinder tests scaled with a high-speed framing camera and a streak camera in order to measure the strain and strain rate of the cylinder pipe.
- A well characterised material used for fragmentation of the cylinder pipe.

- A capture technique and other measurements applied to catch the fragments to investigate their characteristics.
- Five different explosives with widely varying detonative parameters for investigation.

1.8 Contributions and limitations

This research will contribute to the field of science, engineering and technology in the manner outlined below.

- To characterise the effects of different explosives on fragmenting behaviour.
- To ensure the proposed model is useful in terms of munitions assessment and design.
- To provide a reference for the selection and design of fragmenting warhead shell material.
- To enhance prediction in the early stages of design by providing reference data for different type of explosive in terms of fragmentation in order to minimise risks in later phases of the design verification.

The test proposed will be limited to the explosives material and the filling process available at the RDM company as a supporter for this research. The candidate explosive materials for this study are presented in

Table 1-1. The five candidate are mainly fabricated form three main types of explosive, namely (TNT, RDX and NTO).

Table 1-1: Candidate explosive materials for study.

	Type of explosive	Empirical formula
1 -	TNT	$C_7H_5N_3O_6$
2 -	Comp-B (RDX-TNT) (60-40)	$C_{4.6}H_{5.6}N_{4.8}O_6$
3 -	ONTELIT (NTO-TNT) (50-50)	$C_{4.5}H_{3.5}N_{3.5}O_{4.5}$
4 -	MCX-6002 (NTO-RDX-TNT) (51-34-15)	$C_{3.09}H_{3.81}N_{4.53}O_{4.47}$
5 -	RXHT-80 (RDX 80%)	$C_{2.4}H_{4.8}N_{4.8}O_{4.8}$

1.9 Knowledge gap to be closed

This study will investigate the dependence of natural fragmentation characteristics on explosive parameters inclusive of (afterburning rate) through material parameters (the strain and the strain rate sensitivity). This investigation depends on the characterization of the expansion behaviour of the detonation products. The cylinder test is the standard to be used as a guideline for this investigation. This investigation aims to answer the question if there are any other explosive parameters other than the initial pressure or the final velocity that have an effect the final characteristics of natural fragmentation.

CHAPTER 2: LITERATURE REVIEW

There are many studies on natural fragmentation of metallic casings. These studies vary based on the approaches they use, and there are statistics-based studies and energy-based studies. Recently, a numerical simulation approach based on strength and failure models has been in use.

2.1 Natural fragmentation characteristics

Regarding the shell design of HE warheads, there are several varieties of fragments, mainly natural, preformed, controlled and embossed. These groups are schematically illustrated in Figure 2-1, which also further illustrates controlled fragmentation [19].

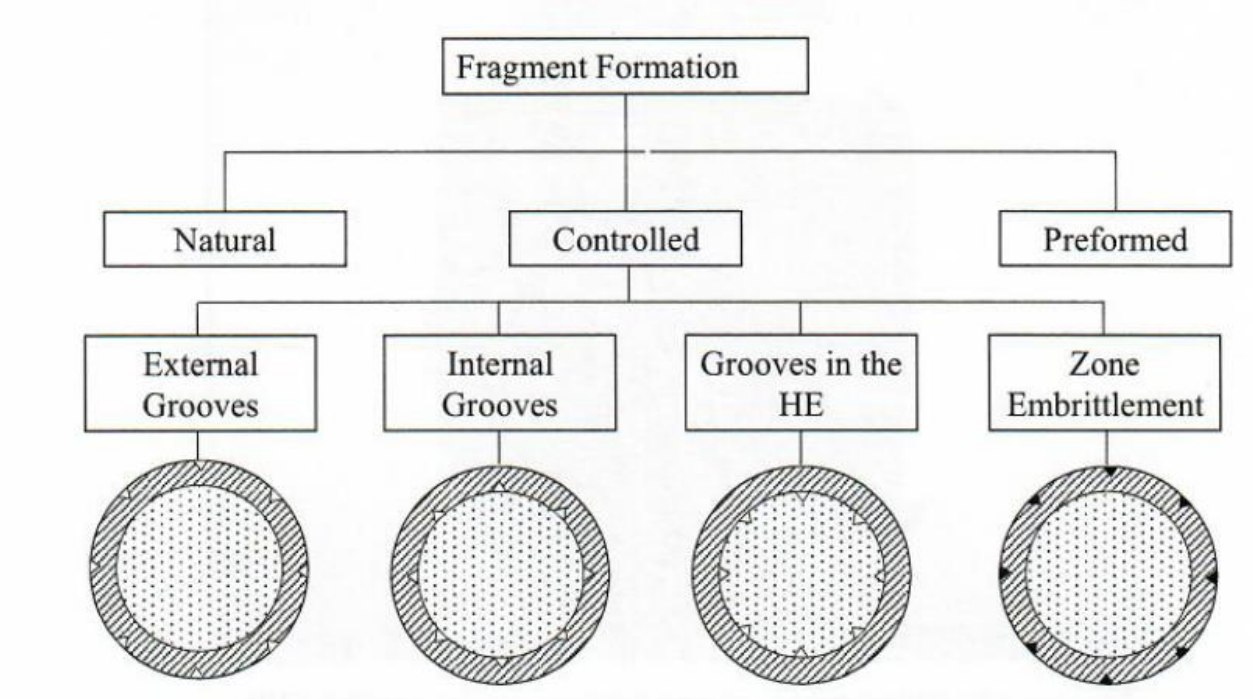

Figure 2-1: Methods for generating controlled fragments [19].

The differences between these fragmentation types from the perspective of design are their manufacturing cost, efficiency and manufacturing process. These criteria were evaluated in a comparative study presented by Zecevic et al. [2], to support a warhead designer in selecting and optimising a fragmentation warhead. The results of Zecevic study are summarised in the following points:

- The natural fragmentation warhead is characterised by wasted mass and energy, lowest cost of manufacturing and least mass efficiency at certain target among all fragmentation types.
- The controlled fragmentation warhead is characterised by less wasted mass and energy, improved lethality over the natural fragmentation warhead and low cost of manufacturing, but this technique is limited to rocket warheads and hand grenades because the grooving process reduces casing strength and can result in explosive pinching in gun systems, causing barrel system damage.
- The preformed fragmentation warhead is characterised by efficient mass and energy, optimised lethality, higher cost of manufacturing than the controlled fragmentation warhead and highest mass coefficient among all fragmentation types [2].

Accordingly, the natural fragmentation warhead is preferable in terms of the manufacturing process and cost effectiveness.

Performance is an important part of the warhead design process. An evaluation of the efficiency of a design depends on its fragmentation characteristics and the energy delivered by the fragments to a certain target, which should be predicted in the early stage of design based on a simple analysis tool.

The natural fragmentation process of an HE warhead is the result of multiple fractures in the casing material under the detonation loading, which depends on many factors. Fragment characteristics are therefore difficult to predict without extensive testing. However, the fragment characteristics of controlled and preformed fragmentation warheads are considered easier to predict, since fragment parameters, such as size and mass, are a priori known.

2.1.1 Fracture behaviour

According to the strength and failure models, a material under stress load will stretch to reach a point where it begins to fail. The failure process differs based on the material structure itself, the type of stress load, and other external criteria, as discussed along with the failure models.

Material behaviour is the critical factor in fracture formation, where a ductile material exhibits a ductile fracture, which differs from a brittle fracture, as illustrated in Figure 2-2. A ductile fracture, according to [3], is a failure process in which a material sustains plastic deformation before it separates into pieces due to an imposed stress at a temperature is lower than its melting temperature.

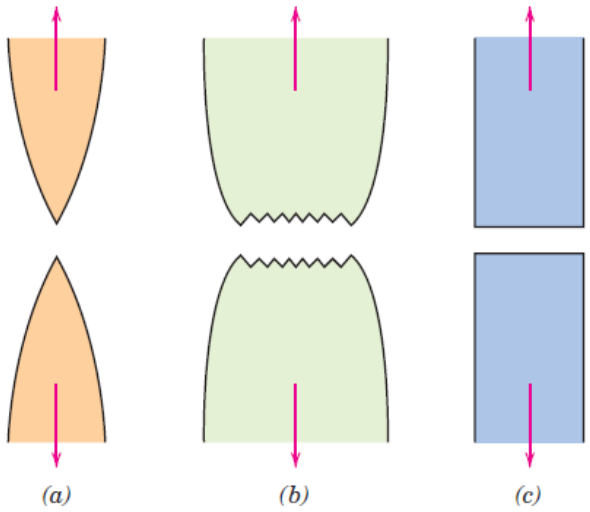

Figure 2-2: (a) Highly ductile fracture in which the specimen necks down to a point. (b) Moderately ductile fracture after some necking. (c) Brittle fracture without any plastic deformation. [3].

As shown in Figure 2-2, a ductile fracture's surface has the special feature of necking regions and is rougher and more irregular than that of a brittle fracture.

For cases in which fragmentation is the result of a multiple fractures formed under a radial detonation load, several models have been developed to characterise the fragmentation based on a circumferential failure mode. These models consider two predominant modes of fracture in the breakup of an expanding metal shell: the first is **tensile fracture**, where failure proceeded by crack propagation, and the second is **shear fracture**, initiated by adiabatic shear banding [20]. Figure 2-3 illustrate the type of radial fracture that occur in expanded ring under radial stress.

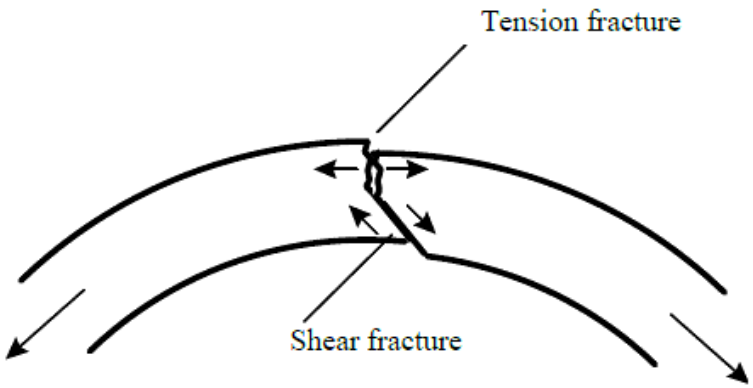

Figure 2-3: Tension and shear fractures as the two basic failure modes [21].

Fragmentation process

The fragmentation process is defined as the result of the dynamic interaction between the effect of detonation and the material response. According to Taylor, Hoggatt and Recht, among others [12, 21], the fracture usually begins from the outside diameter of the casing, forming tensile cracks joining together with shear cracks initiated from the inside surface.

The fragmentation process was described by [22] as a dynamic process that can be split into several stages. Figure 2-4 illustrate the natural fragmentation behaviour under the dynamic behaviour of the detonation products.

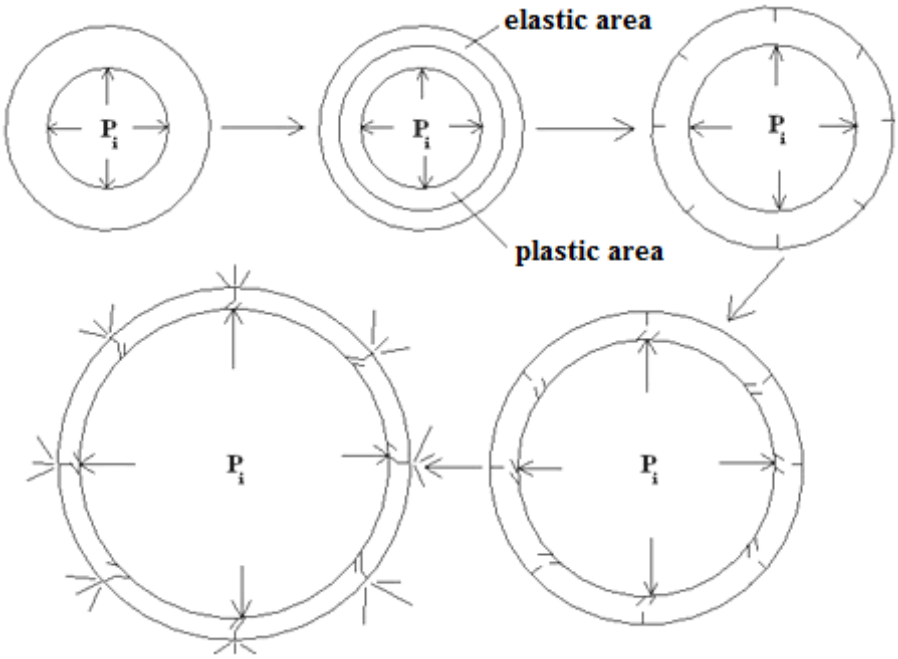

Figure 2-4: Stages in natural fragmentation behaviour [22].

First, the shell wall is driven and compressed by the shock waves and gases, and suffers elastic deformations. Once the flow stress threshold is exceeded, at the interior face, plastic deformation begins, and the area affected is expanded toward the exterior face of the wall. Having a radial displacement, the shell continuously increases in diameter. This results in a level of circumferential strain and corresponding stress under which the shell material fails and breaks. These cracks evolve from the outside of the shell toward the interior. Subsequently, **micro-flaws** generate cracks at the level of the interior face that propagate toward the exterior surface at a 45° angle. When these two types of cracks join or pass through the entire thickness of the wall, fragments are generated. The compressed gasses flow through the openings and **continue to accelerate** the fragments until the maximum value of expansion velocity is reached. This argument shows that plays a role is not only the Chapman–Jouget pressure but also the full

acceleration history of the casing and the detonation products properties. The process of the natural fragmentation of steel envelopes is considered finished at the moment when the exterior shell radius reaches a value of 80% higher than the original. Implicitly, this assumption boils down to accepting that the metal will always fragment at a fixed value of strain [21].

Fragment types and modelling

The process according to Ugrčić [10], is described as the following. The fragmentation begins from the outside diameter through the formation of sharp radial cracks of longitudinal orientation, is known as **brittle** normal disruption or **tensile cracks**. These cracks then join with **shear cracks** from the inside of the material (or not, if the material is extremely **brittle**). The cracks then coalesce into long, longitudinal cracks. If the casing material is resilient enough (**mild**), as the casing expands radially, the wall will **thin out** somewhat, as in the Taylor, Hoggatt and Recht models. Regardless, the metallic casing will fragment completely, and the described scheme of casing fragmentation is depicted in Figure 2-5.

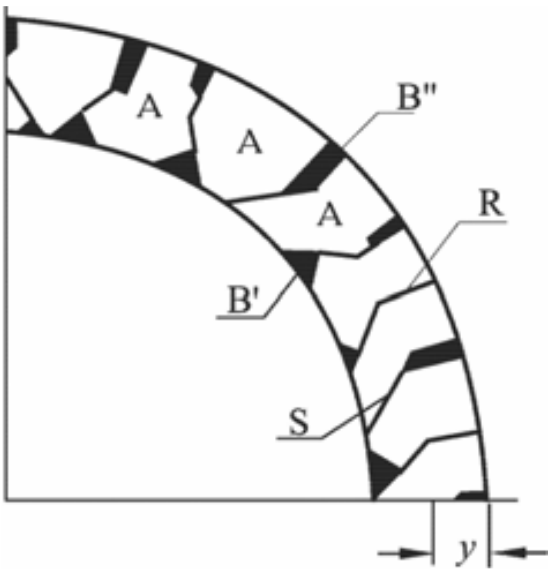

Figure 2-5: The scheme of casing rupture and fragments generation; (A) principal and (B) seed fragments [10].

Two types of fragments arise as a results of this characterization: **large massive** or **principal fragments** (Type A) and **small light** or **seed fragments** (Type B) [Figure 2-5]. The massive fragments comprise casing surfaces from both the inner and outer surfaces, and they are generated by principal stresses. The crack surfaces of massive fragments are characterised by two zones: the surfaces of **brittle** normal disruption (zone R in Figure 2-5) adjacent to the outer

surface of the fragment, and the surface of **shear** cracking along the sliding region (zone S in Figure 2-5) adjacent to the inner fragment surface.

The small fragments comprise one external surface (outer or inner) only. Figure 2-6 illustrate the variety of the small fragments includes two subtypes: B', the fragments of the explosive contact zone formed by shear cracks, and B", the fragments of the outer casing zone formed by a sharp rupture along the radial direction (typical for high-carbon steel).

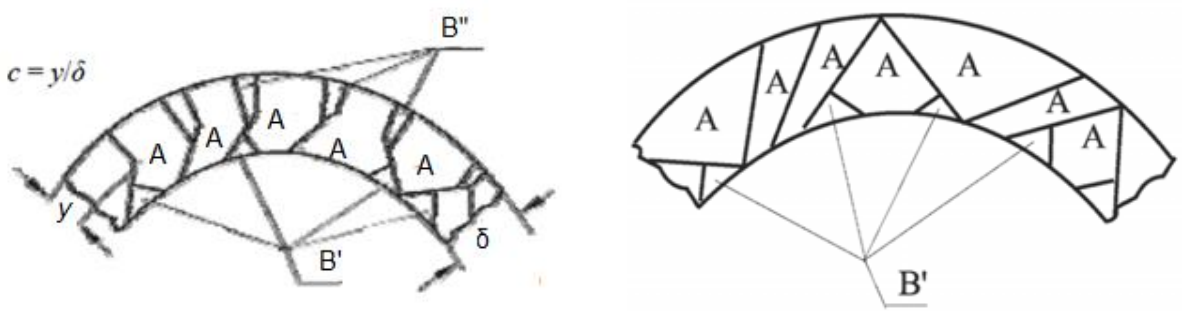

Figure 2-6: Casing crack scheme: brittle steel (left) and plastic steel (right) [10].

Based on this classification, the type of crack and the fragment characteristics can be described by the joint point of fracture [10]. By denoting the zone of the brittle normal disruption *y* and wall thickness δ, then the type of cracking can be described by the ratio $c = y/\delta$. Where the ratio varies between 0 and 1, the smaller the ratio, the more likely a shear fracture is occur such as in the plastic steel. The fragments of brittle material take the value of c between 0.5 and 0.8.

2.1.2 Strain-to-failure model

Several model have been developed to investigate the fragmentation characteristics at failure point based on the dynamic behaviour of the explosion of a cylindrical casing material.

An analytical model developed by Taylor [12] to predict the effective strain radius of an expanding ring of a casing martial during detonation process. During expansion of the casing material, Taylor assumed a development of two regions; a compressive hoop stress region developed in the interior surface of the ring and a tensile hoop stress region in the outer surface of the ring. Figure 2-7 illustrate the expansion behaviour of ring elements under the effect of detonation products.

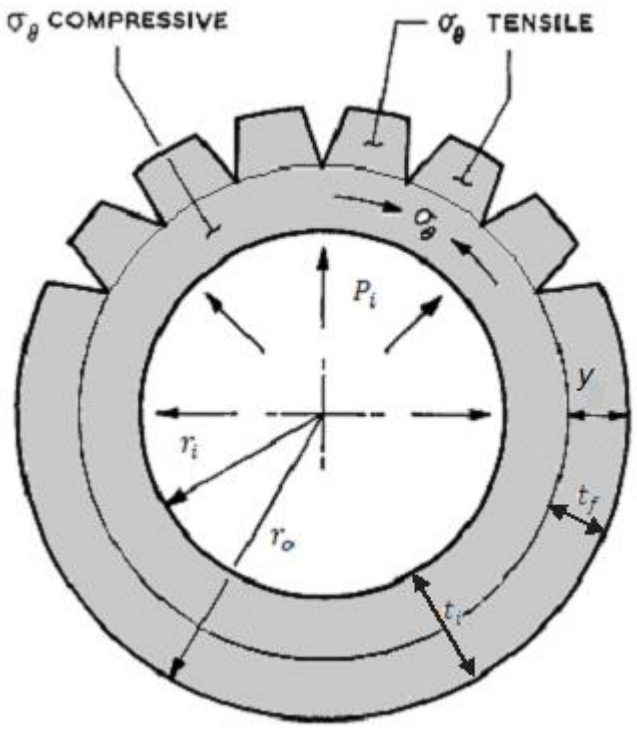

Figure 2-7: expansion of ring elements Tylor model.

A radial cracks assumed to occur only in tensile region penetrating to depth $(y = \frac{t_o Y}{P_i})$ until the compressive region completely disappears where the fragments formed. The boundary between compressive and tensile hoop stress can be analyse to determine the fragments characteristics at failure. Accordingly, the depth of the crack (y) conditionally related to the wall thickness (t_o), the tensile strength (Y) and the internal pressure (P_i). Thus, if the condition for complete fragmentation is given by $y = t_f$, when $P_i = Y$, then if P_i is known as a function of radius r, the effective radius at failure may be deduced which can be used to represent the effective strain of fragments after formation ε_f.

The result of Tylor analysis is an analytical function to predict the effective strain of expanded ring based on the effective radius at fracture:

$$\frac{r}{r_i} = (\frac{P_i}{Y})^{\frac{1}{2\acute{\gamma}}} \qquad 2\text{-}1$$

Where P_i is the initial pressure of the detonation product inherited from Chapman–Jouget pressure and Y is the yielding stress of the casing material, $\acute{\gamma}$ the isentropic constant of expansion gas. An investigation study of the effective radius of different type of explosive have been discussed through different study.

According to Taylor model, by considering only the radial crack in the tensile stressed region and neglecting the yielding stress value which is very small compare to the detonation pressure value and assuming $\acute{\gamma} \approx 3$; the effective radius considered to be a constant value for different type of explosive equal to ($\frac{r}{r_o} \approx 1.8$), 80% of the original radius increase, corresponding approximately to ($\frac{V}{V_o} \approx 3.24$).

Another model developed by Hoggatt and Recht [21] to investigate the effective radius value of cylindrical case at fracture, where a shear fracture have been taking into consideration. According to Hoggatt and Recht model, the effective radius have been considered to be equal to ($\frac{r}{r_o} = 1.74$) for different explosive material corresponding approximately to ($\frac{V}{V_o} \approx 3.0286$).

An experimental study have been conducted by Pearson [23], to investigate of the effective radius at fracture. A conclusion of Pearson model that the fragmentation of shells with idealized cylindrical geometries occurs at approximately three volume expansions, whereas the instant of fragmentation is defined as the time at which the detonation products first escape from the fractures in the shell.

These models have deduced a constant value of the effective strain at fracture, which is almost three times the initial volume of the expanded case. These models have been considered in Gold model [43] to predict the average fragments mass at constant strain.

A cumulative-damage fracture model by Johnson and Cook

Taking into consideration the change in material properties from static-to-dynamic events such as detonation loading, the cumulative-damage fracture model developed by Johnson–Cook [24] was established to distinguish *dynamic* material properties from *static* material properties. The underlying assumption in this model is that the differences between the dynamic and static properties must be due to the strain rate effects only. However, the model is an adaptation of the strain-to-failure model developed by Hancock and Mackenzie [25] to investigate the effect of stress triaxiality at the failure point. The strain rate and temperature terms were used by Johnson and Cook to study their effect on the fragmentation characteristics at a failure:

$$\varepsilon^f = [\mathrm{D}_1 + \mathrm{D}_2\, exp(\mathrm{D}_3\sigma^*)][1 + \mathrm{D}_4 ln\dot{\varepsilon}^*][1 + \mathrm{D}_5 T^*], \qquad 2\text{-}2$$

The parameters in the first bracket represent the effect of stress triaxiality, where $\sigma*$ is a dimensionless pressure–stress ratio defined as $\sigma^* = \frac{\sigma_m}{\bar{\sigma}}$, $\sigma_{\mathrm{m}}$is the average of the three normal

stresses and $\bar{\sigma}$ is the von Mises equivalent stress. The damage parameters follow the equation presented by Hancock and Mackenzie, where D_1 is the void nucleation strain, D_2 is the material constant and D_3 is generalised to be equal to 1.5. The second bracket represents the effect of the strain rate $\dot{\varepsilon}$ through D_4, and the third bracket represents the effect of the temperature T^* through D_5.

The material is presumed to fail when the damage scale parameter in equation (2-3) reaches unity (D = 1.0):

$$\mathrm{D} = \sum \frac{\Delta\varepsilon}{\varepsilon^f} = \sum \frac{\dot{\varepsilon^p}\Delta t}{\varepsilon^f}, \qquad 2\text{-}3$$

This fracture model depends on fracture strain at constants σ^*, $\dot{\varepsilon}^*$ and T^*, and is accurate under constant conditions to the extent that the equivalent stress, $\bar{\sigma}$, equivalent strain, ε, and equivalent strain rate, $\dot{\varepsilon}^*$, represent the more complicated stress and strain relationships:

$$\bar{\sigma} = \sqrt{\frac{1}{2}[(\sigma_1 - \sigma_2)^2 + (\sigma_2 - \sigma_3)^2 + (\sigma_3 - \sigma_1)^2}, \qquad 2\text{-}4$$

$$\bar{\varepsilon} = \sqrt{\frac{2}{9}[(\varepsilon_1 - \varepsilon_2)^2 + (\varepsilon_2 - \varepsilon_3)^2 + (\varepsilon_3 - \varepsilon_1)^2}, \qquad 2\text{-}5$$

$$\dot{\varepsilon} = \frac{\Delta\varepsilon}{\Delta t}. \qquad 2\text{-}6$$

The fracture model is intended to show the relative effects of various parameters. It also attempts to account for path dependency by accumulating damage as the deformation proceeds, which can be used to calibrate the material parameters of the strength model [26].

2.1.3 The effect of strain and the strain rate of explosively driven material at a failure mode

A modification model developed by Goto et, al. [26] to investigate the fracture and fragmentation of explosively driven rings and cylinders. The Johnson–Cook failure model was statistically compensated with a Weibull distribution derived from the measured strain to failure of the steel fragments recovered from the experiment. The data were used to determine relevant coefficients for the Johnson–Cook (Hancock–McKenzie) fracture model. This model is considered to be a constrained version of the more general Johnson–Cook fracture model.

In this study, cylinders and rings fabricated from AerMet-100 alloy and AISI-1018 steel were explosively driven to fragmentation by LX-17 explosive in order to determine the fracture strains for these materials under plane strain and uniaxial stress conditions. The phenomena associated with the dynamic expansion and subsequent breakup of the cylinders were monitored using high-speed diagnostics.

Detailed numerical simulations were used to relate the final thickness of the fragments to the total equivalent plastic strain up to the point where it fractured. The sensitivity of the effective strain and strain rate of fragments during fracture were investigated.

The study compared the fracture strain data with the high-speed imaging data, finding that the thickness measurements yielded a lower fracture strain than might be inferred from either optical or X-ray images. The study also found that using smoke of detonation products as the indicator of fracture significantly overestimated the fracture strain.

The study conducted by Zecevic et, al. [27] examined the effects of **the ratio of tensile strength to yield strength** of the warhead steel cases on fragmentation characteristics. It conducted a series of tests on fragmentation warheads by varying the ratios of tensile strength to yield strength of the warhead steel cases (R_m/R_v). They found that a steel case with a larger ratio of R_m/R_v generated a greater number of fragments but with less mean mass. This phenomenon were explained by the authors as the result of a warhead's expansion ability during detonation. The same study also found that during the expansion of a warhead case, the relative volume increases and the relative case thickness decreases. The relation between the effective volume at fracture of the expanded metal and the effective thickness at fracture is defined as:

$$\frac{t_o}{t} = \left(\frac{V_o}{V}\right)^{-0.5}. \qquad 2\text{-}7$$

Where $\frac{t_o}{t}$ is the ratio between the initial thickness (t_o) and the final thickness (t) at fracture. $\frac{V_o}{V}$ is the ratio between the initial volume V_o of the expanded metal and the final volume V at fracture. According to this formula, an increase of the expansion volume to 4 times the initial volume will results to a decrease in the relative thickness to the half of the original thickness.

In addition, when the ratio R_m/R_v increases, the ratio $\frac{V_o}{V}$ increases while the ratio $\frac{t_o}{t}$ decreases. This relationship results in a greater number of fragments with a lower average fragment mass.

According to this viewpoint, for two types of explosives cased with the same metal expanding to the same level, this model predicts that they will have nearly identical fragment thickness.

Effects of the material properties of a high-explosive warhead casing on natural fragmentation

Material behaviour has been characterised based on mechanical properties extracted from the stress–strain curve. These material properties depend on the models and the tests used to characterise the material's behaviour. The analytical fragmentation models, such as those by Mott and Grady, address the material properties only at the failure point, whereas other properties such as the points of initial yield and ultimate strength can also have an effect on the final fragmentation distribution. Taking this principle into consideration, a different study investigating the effects of material properties on fragmentation characteristics is highlighted in this section.

The numerical study presented by Tanapornraweekit and Kulsirikasem [16] focuses its investigation on the effects of the material properties of a warhead casing – **failure strain**, **initial yield** and **ultimate strength** – on the characteristics of warhead fragmentation in terms of initial velocities, spray angles of fragments and fragment mass distribution. The results of Tanapornraweekit study reveal that the initial yield and ultimate strength of a casing have minimal effects on the initial velocities and spray angles of fragments. Moreover, a brittle warhead casing with low failure strain tends to produce a higher number of fragments with a lower average fragment mass.

Another numerical study presented by Shahraini [28], investigated the effect of casing toughness on fragmentation characteristics. Two types of material with the same hardness but different toughness were investigated. The results of Shahraini study revealed that a casing with higher toughness generates a higher number of small fragments but a lower number of large fragments.

Several numerical studies have been performed to investigate the effects of the mechanical properties on fragmentation characteristics. Numerical simulation has been used, employing the empirical strength models together with the empirical equations of state to characterise the material response and expansion behaviour of detonation product. The simulation results reveal that the yield strength, ultimate strength and failure strain of the casing do not have significant effects on the initial velocities or spray angles of its fragments.

However, these numerical models are known to be tedious and time consuming in terms of setting up a problem. Moreover, these models have been investigated through mechanical properties such as ultimate tensile strength, hardness and fracture toughness rather than explosive properties such as heat transfer (explosives with higher afterburning rates) and detonation characteristics, which also can affect the mechanical properties of the casing material on a microstructural level.

Because of the complexity of the numerical models, several simple statistical and empirical models have been developed to characterise fragmentation in the early stages of design. The most emphasised models used by warhead designers have been discussed in the section below.

2.2 Natural fragmentation of high-explosive warheads

Several criteria play critical roles in the design of warhead, such as simplicity, manufacturability and performance. These criteria must be taken into consideration when designing HE fragmentation warheads, where lethality is the determining factor in warhead efficiency.

The effectiveness of HE fragmentation warheads therefore depends on their fragmentation characteristics and fragmentation behaviour, in terms of mass, size, number, velocity and projection angle. Fragmentation characteristics are a result of the interaction between the detonation shock and the detonation product expansion of the casing material. The complexity of this process has led to the postulation of this event as a natural event with inherent variability. Thus, several statistical models have been developed to predict these fragmentation characteristics. Since natural fragmentation is random in terms of the physics of the process, the following section is presented to clarify the fragmentation characterization process and to discuss the most common models used to characterise natural fragment patterns.

2.2.1 Number and mass distribution models

The detonation of an explosive device creates fragments with different masses m from the fragmentation source, a casing with a starting mass M_0. This process is commonly described statically through a probability distribution function treating the fragment mass as the random variable.

Two types of distribution functions, the cumulative distribution function and the probability density function, can be utilised. For natural fragments, the cumulative distribution function is less sensitive to the scatter of the fragment mass data [29]. The following section highlights the principle roles of mathematics and statistics in characterising fragment distribution. The cumulative number of fragments $N(>m)$, defined as the total number of fragments with individual mass greater than m, and the cumulative fragment mass $M(>m)$, defined as the total mass of all fragments each with individual mass greater than m. The relative (normalised) cumulative distribution is given by:

$$N(m) = \frac{N(>m)}{N_o} \overset{or}{\Rightarrow} N(>m) = N_o N(m), \qquad 2\text{-}8$$

$$M(m) = \frac{M(>m)}{M_o} \overset{or}{\Rightarrow} M(>m) = M_o M(m), \quad \text{2-9}$$

Where $N(m)$ and $M(m)$ is the total number and the total mass of the produced fragments with individual mass equal to m, respectively. M_o is the total mass of all produced fragments (i.e. shell body) and N_o is the total number of all produced fragments. The relation between the two distributions is given by:

$$\frac{dM}{dm} = \frac{m}{\overline{m}} \frac{dN}{dm}, \quad \text{2-10}$$

The mean of this distribution is the average fragment mass $\overline{\mathrm{m}}$ that determined by:

$$\overline{m} = \frac{M_o}{N_o} = \int_0^\infty N(m) dm \quad \text{2-11}$$

Generally, these are the basic methodical ways of normalising fragmentation distribution through the mass and number of fragments [29]. Several other approaches have been developed through mathematical derivation and data analysis to present the distribution laws of fragment mass and number. Some of these approaches are based on problems – probabilistic [30,31 and 32] energetic [33] and fracture mechanics [34]. These functions for characterising fragment distribution are presented in the next section.

The Mott distribution function [34] in the general form is the most common function used to describe the number of fragments based on geometric considerations:

$$N(m) = e^{-(\frac{m}{\mu})^{\frac{1}{j}}}, \quad \text{2-12}$$

Where: *j* is a parameter known as the dimensionality and depends on geometric considerations such as wall thickness ($\mathrm{t_o}$) or the explosive mass (C) to metal mass (M) ratio (C/M). μ defined as the ½ of the average fragments mass $\overline{m} = 2\mu$. For normal wall thickness (i.e., $C/M < 2$), Mott proposed the first derivation of this formula known as the two-dimensional case (i.e. *j* equal to 2):

$$N(m) = e^{-(\frac{m}{\mu})^{\frac{1}{2}}}, \quad \text{2-13}$$

In the situation where the cylindrical wall is very thick (i.e., C/M << 2), the exponent (½) was argued by Grady and Kipp [30], and *j* was proposed to be equal to 3 instead of 2 in the exponent, as in equation (2-14), known as the three-dimensional case:

$$N(m) = e^{-\left(\frac{m}{\mu}\right)^{\frac{1}{3}}}, \quad 2\text{-}14$$

In the case where the cylindrical wall is very thin (i.e., C/M > 2), [30] also derived the simple linear exponential distribution where *j* is proposed to be equal to 1:

$$N(m) = e^{-\left(\frac{m}{\mu}\right)}, \quad 2\text{-}15$$

These functions are used to characterise fragmentation distribution through the number of fragments with mass greater than m, [$N(> m)$]. The other method of characterising fragmentation distribution uses the total mass of fragments each with individual mass greater than m. This method is the two-parameter (λ and μ) Weibull distribution function [29]:

$$M(m) = e^{-\left(\frac{m}{\mu}\right)^{\lambda}} \quad 2\text{-}16$$

Where λ is the exponent parameter.

Held [35] proposed another method of characterising fragmentation distribution based on the optimisation of empirical constants through regression analysis, where the largest fragments are discarded. The equation introduced by Held defines the relation between the cumulative mass and the cumulative fragment number:

$$M(n) = M_o\left[1 - e^{-Bn(m)^{\lambda}}\right], \quad 2\text{-}17$$

Where B and λ are empirical fitting parameters; $B = constant\sqrt{(d_i/\mathrm{t_o})}$, where d_i is the initial diameter of the casing materail and $\mathrm{t_o}$ is the casing material thickness; *B* is of order of 10^{-2}; and λ is of the order of 2/3 (≈0.77) [36,37]. $n(m)$ is the cumulative number of fragments sorted in descending order, and $M(n)$ is the total mass of these fragments.

The differentiation of Held equation $M(n)$ with respect to n gives the definition of the approximate mass of the n^{th} fragments:

$$m(n) = \frac{dM}{dn} = M_o B\lambda n(m)^{\lambda-1}e^{-Bn(m)^{\lambda}}, \quad 2\text{-}18$$

The mass of each fragment can be calculated by:

$$m_n = M(n) - M(n-1), \quad 2\text{-}19$$

Held's method depends on the determination of the fitting empirical parameters (*B* and λ). The M_o is the best fit of the total mass in Held equation with the necessity to discard some of a number of heaviest fragments to match the best results for curve fitting. The model developed by Strømsøe et al. [38] claims to avoid overestimation of the number of very large fragments. It has been demonstrated [29] that the Strømsøe-Ingebrigtsen distribution does not represent substantial improvement to Mott's law.

The sensitivity of the distribution function models was investigated by [29] through regression analysis for $N(m)$ functions and the relative error of the median $\tilde{\mathrm{m}}_{\mathrm{M}}$ for the three analysed distributions (generalised Mott, Grady and Weibull) based on 30 experimental fragmentation test results. The study found that the generalised Grady distribution provides the best description of the mass distribution of fragments generated by the detonation of HE warheads. The properties of the generalised Grady distribution imply two types of fragment: fine and coarse. Two interpretations were proposed by the authors. First, the fine and coarse fragments can be related to the central cylindrical and residual portion of the warhead, respectively. The other explanation is that different fragment formation mechanisms in the inner and outer sections of the warhead casing influence the bimodal distribution.

In overall, the fragmentation distribution model is a statistical model derived to describe natural fragment distribution based on mass and number distributions. Experiments must be conducted for each warhead with a unique combination of explosive and material to characterise the fragments based on their mass and number group.

The sensitivity of these models depends on certain criteria such as the C/M ratio, the fracture mechanism, the number of fragments collected and the method used to collect the fragments. However, although these models are useful for preliminary analysis, it is difficult to derive certain conclusions from them regarding the influence of statistical parameters on the fragmentation process [29,37].

2.2.2 Average fragment mass models

The prediction process is simplified when the distribution parameters can be determined without conducting excessive experiments with complex procedures when the design changes. For this purpose, other semi-empirical approaches have been derived based on the geometric considerations to predict the mean distribution (average mass), since it is the dominant parameter controlling the distribution. A cylindrical metal case filled with a certain type of explosive is shown in Figure 2-8, where $\mathrm{t_o}$ is the thickness of the case wall, d_i is the internal diameter (explosive diameter) and C/M is the ratio of explosive mass to metal mass.

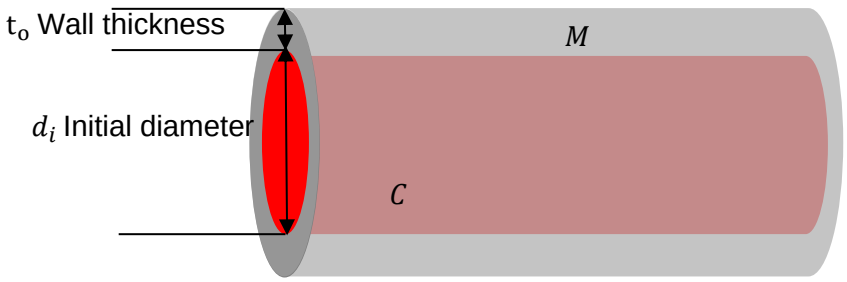

Figure 2-8: Cylindrical metal tube filled with explosive material.

Semi-empirical approaches

Serval model have been approached to address the effect of the explosive material and the casing material on the fragments distribution through the mean parameters. Taking into consideration that the average fragment mass $\bar{m}$ equal to 2μ, the following section present the significant models to characterize the fragment distribution.

One of the most common methods of defining the average fragment mass is the Mott's model [14,36], namely:

$$\mu = B_M^2 t_o^{\frac{5}{3}} d_i^{\frac{2}{3}} (1 + \frac{t_o}{d_i})^2, \qquad 2\text{-}20$$

Where B_M is an empirical constant that depends on the type of explosive and material used.

The other approach, developed by Magis [39], is considered to be more appropriate for the large calibre case:

$$\bar{m} = 2\mu = C_M \frac{(t_0 d_i^{\frac{1}{3}})}{(1 + 2\frac{C}{M})}, \qquad 2\text{-}21$$

Where C_M, is also an empirical constant that depends on explosive and material type used.

The Gurney–Sarmousakis model [40],is a noteworthy model for assessing the average fragment mass:

$$\mu = A_M^2 \left(\frac{t_o}{d_i}\right)^2 (t_o + d_i)^3 \left(1 + \frac{C}{2M}\right), \qquad 2\text{-}22$$

Where A_M is an empirical constant for this model that depends on the type of explosive and material used. The empirical constant A_M was found to be approximately equal to 338.1/Chapman–Jouget pressure (P_{CJ}) for mild steel [36].

These models are useful for warhead designers to predict changes in fragmentation distribution using the parameters C/M, $\mathrm{t_o}$ and d_i. The Gurney–Sarmousakis model is also the only model that considers an explicit explosive parameter in the analytical prediction of fragmentation characteristics.

Generally, the final fragmentation characteristics are determined by a complex mechanism of explosive and material interaction. These models, however, approximate this interaction by considering the warhead's geometry, the material properties, a single explosive property and an empirical constant to be extracted or estimated from other test data. The value of the P_{CJ} for the explosive is the only explosive parameter that approaches a correlation with the empirical constants A_M, B_M and C_M, as in the Gurney–Sarmousakis constant. However, this is not the only explosive parameter involved in fragment characteristics, since this pressure (P_{CJ}) is only the initial detonation pressure. The evolution of the pressure history of detonation products may also play a role in the fragmentation process and should be investigated. It is, therefore, at the core of this study to investigate the dependence of natural fragment characteristics on *all* the explosive parameters and to investigate the methods used to extract these parameters.

2.2.3 Mott models

Material properties play a critical role in fracture behaviour. Based on the fracture mechanism, different models have been developed to predict the average fragment size produced by ductile materials. Attempting to evaluate the dependence of fragmentation characteristics on the material and the explosive parameters, the simple analytical models derived by Mott, [14] and Grady and Kipp [15] are the most common and widely used models for predicting the average fragment sizes produced from dynamic detonation loading. The following section discusses the fragmentation process and the material and the explosive criteria used to predict the average fragment size.

Evaluation of fragment size by Mott (statistics-based model)

In attempting to evaluate the fragment size from a failure generated by a cylindrical bomb, Mott in his work [14] presented a simple numerical model based on statistical theory that accounts for the mechanical properties of the material, such as fracture stress and strain at the moment of fracture having a statistical nature. The statistical nature depends on irregularities in the material structure (voids, inclusions, micro-cracks) that vary from one sample to another. Considering the case of a cylindrical bomb, the model was derived under certain assumptions.

Statistic strain-to-failure formula

Assuming a cylindrical case expand under the effect of detonation products, the stress of detonation will increase the strain of the material until it reach the failure point. From point of view, the higher the strain the higher the number of fracture is expected. Relatively, a hypothesis formula is proposed by Mott in an exponential form to evaluate the probability of failure based on the change in strain from ε to $\varepsilon + d\varepsilon$:

$$\grave{C}e^{\grave{\gamma}\varepsilon}d\varepsilon. \qquad 2\text{-}23$$

Where $\grave{C}$ and $\grave{\gamma}$ are probability parameters represent the characteristics of material:

$$\grave{\gamma} \approx 160\frac{\sigma_P}{\sigma_F(1+\varepsilon_F)}\ , \qquad 2\text{-}24$$

$$\grave{C} = \grave{\gamma}e^{-(\bar{\varepsilon}\grave{\gamma}+0.5772)}\ , \qquad 2\text{-}25$$

σ_F, σ_P and ε_F are the material characteristics in the stress–strain curve [41].

According to Mott formula the change of number of fracture dn will increase with the increase of strain $d\varepsilon$. The exponential function was chosen because it provides a rapid increase in fracture probability with increasing strain. It is possible to choose different increasing functions for modelling the increase in fracture probability with increasing strain. Grady [42] used the power function to modify the basic Mott model.

Mott wave

In attempting to evaluate the fragment characteristics of cylindrical material expand radially, the casing material is considered as a sum of independent rings that have similar thickness and similar width. During expansion a release area in the circumferential direction of the rings material assumed by Mott known as Mott wave Figure 2-9. The model implies that the formation of each new crack triggers a new Mott wave, which increases the number of unstressed regions of the ring. The process of crack formation, or fragment generation, proceeds until the entire ring material is free of stress.

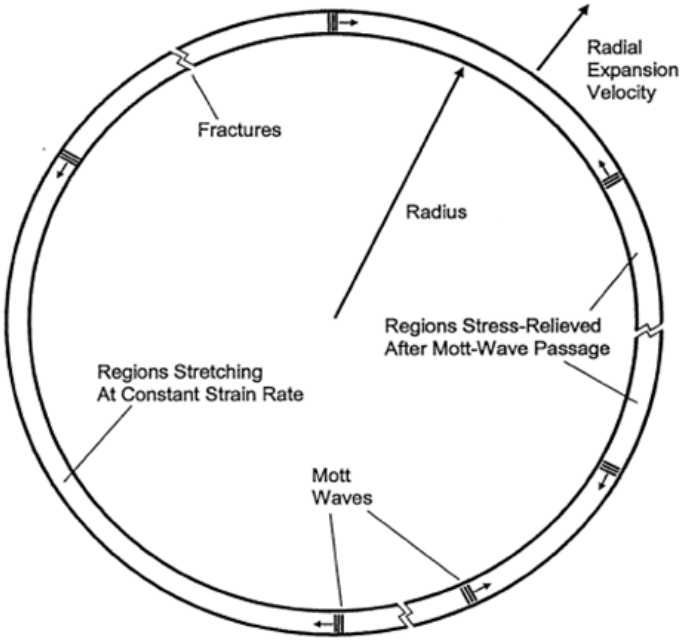

Figure 2-9: Expanding Mott ring [42].

The evaluation of the wave motion under load stress is used to evaluate the average fragments length l Figure 2-10. Two regions are assumed during expansion; the released area representing the width of Mott wave AB, and tension area where extra fracture are probable.

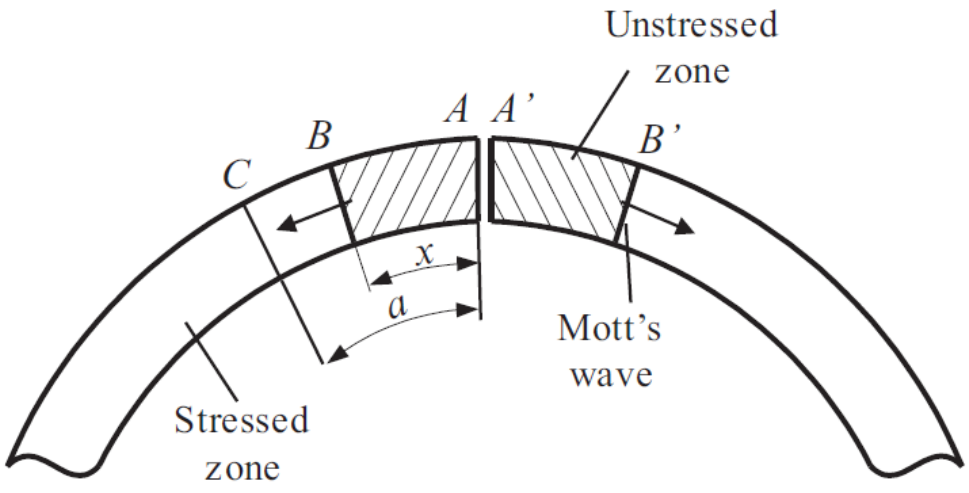

Figure 2-10: Release wave propagation in a crack's neighbourhood [41]

For the calculation of the release wave velocity v the hypothesis of a constant value for ring radius r and radial outward velocity v is used. The hypothesis covers the situations when the wall

thickness is small compared with r and the time interval for whole process of break-up is short enough to neglect the change in v and r. The strain rate therefore may be written as:

$$\frac{d\varepsilon}{dt} = \dot{\varepsilon} = \frac{v}{r} \ , \qquad 2\text{-}26$$

Mott assumed the release wave to propagate from a crack to its neighbouring region, where no crack will occur in a stress-relieved area. The distance travelled by Mott wave is assumed to be the fragment length, which can be calculated through the relative velocity v_{rel} of AB stress-free area to C section the wave:

$$v_{rel} = \frac{a - x}{r} v \ , \qquad 2\text{-}27$$

For this purpose, an equation of motion was formulated to describe the release wave's movement:

$$\sigma_F = -\rho x \frac{d}{dt}\left((a - x)\frac{v}{r}\right), \qquad 2\text{-}28$$

Where ρ is the casing material density and σ_F is fracture flow stress for the rates of strain concerned. The integration of the above relation, using the hypothesis of a constant value for $\frac{v}{r}$, the relation between the limit of the unstressed region and the time elapsed since fracturing is defined by Mott in the form:

Mott $$x = \sqrt{\frac{2\sigma_F r}{\rho v}}\sqrt{t}, \qquad 2\text{-}29$$

or $$x = \sqrt{\frac{2\sigma_F}{\rho \dot{\varepsilon}}}\sqrt{t}, \qquad 2\text{-}30$$

This equation used to evaluate the length of the fragments x obtained at fragmentation of ring together with the hypothesis probability formula of Mott to obtain the average fragments length x_o at constant strain rate $\dot{\varepsilon}$.

Average fragment length

According to Mott probability formula $\grave{C}e^{\grave{\gamma}\varepsilon}d\varepsilon$, the increase rate of the fracture number n at the ring of circumference $l = 2\pi r$, is given by:

$$\frac{dn}{d\varepsilon} = lf\grave{C}e^{\grave{\gamma}\varepsilon} \qquad 2\text{-}31$$

Where f value is the proportion constant of the ring that is still stressed. By introducing a new variable $\alpha = \grave{\gamma}\varepsilon$, the above equation becomes:

$$\frac{dn}{d\alpha} = \frac{lf\grave{C}}{\grave{\gamma}}e^{\alpha}, \qquad 2\text{-}32$$

If the fracture occurs at the strain ε_1 (i.e. corresponding value α_1), the region safe from further fracture and the time interval Δt to the moment with the strain ($\varepsilon > \varepsilon_1$) is:

$$\Delta t = \frac{d\varepsilon}{\dot{\varepsilon}} = \frac{r(\varepsilon - \varepsilon_1)}{v} = \frac{r(\alpha - \alpha_1)}{\grave{\gamma}v}, \qquad 2\text{-}33$$

The length of the safe region where further fracture is prevented can be calculated by:

$$\Delta x = x_o\sqrt{(\alpha - \alpha_1)} = \sqrt{\frac{2\sigma_F}{\rho\grave{\gamma}}}\left(\frac{1}{\dot{\varepsilon}}\right)\sqrt{(\alpha - \alpha_1)}, \qquad 2\text{-}34$$

The value of (x_o) defined by the following equation:

$$x_o = \sqrt{\frac{2\sigma_f}{\rho\grave{\gamma}}}\frac{1}{\dot{\varepsilon}} \qquad 2\text{-}35$$

The average fragment lengthl_o is proportional to the value of x_o. The fragmentation characteristics according to Mott approach depend material density ρ, fracture stress σ_F, ring radius at fracture r, the velocity of ring at fracture v and the scatter of the fracture limit trough material parameters $\grave{\gamma}$.

The value of x_o is used to predict the average fragment mass and to characterize the naturel fragmentation distribution. The strain rate in this model is proposed to be calculated from a constant value of $\dot{\varepsilon} = \frac{v}{r}$ due to the short duration of the detonation process. It is assumed that the radial ring expansion velocity v, as well as the ring radius r, do not significantly change during fragmentation. Therefore, the velocity of this wave can be estimate through the Gurney velocity, which is the only explosive parameter that can included in this model. The acceleration time during fragmentation process for some explosive material can be significant which may have a significant change on the final shape of fragments.

2.2.4 Gold's average fragment mass model

Following Mott's model for predicting the average fragment size (breadth), Gold, et al. [43] developed a modified analytical model for predicting the average fragment mass, taking into consideration that the average fragment mass is the critical factor for the fragmentation distribution models and is central to the determination of warhead performance and lethality. Based on the fact that the Mott model takes only the Gurney velocity as an explosive parameter to predict the fragmentation characteristics for different explosives, Gold also studied the effect of explosive detonation pressures on fragmentation characteristics.

The average fragment mass factor (μ)

By taking advantage of the Mott's model [14], Gold et al, developed a prediction model of the average fragment mass by giving the rugged-shaped fragments an idealised simple geometric shape such as a parallelepiped; having an averages of longitudinal length l_o, breadth $\bar{x}$ and thickness t_o, the average fragment mass takes the following form:

$$\bar{m} = 2\mu = \alpha\rho {x_o}^3, \qquad 2\text{-}36$$

By defining the shape facto α as:

$$\alpha = \frac{l_o}{x_o}\frac{t_o}{x_o}. \qquad 2\text{-}37$$

By substituting Mott equation (x_o) and the shape factor α into equation (2-38), Gold calculated the average fragment mass factor (μ), as:

$$\mu = \frac{1}{2}\left(\frac{2\sigma_F}{\rho^{-\frac{1}{3}}\alpha^{-\frac{2}{3}}\grave{\gamma}}\right)^{\frac{3}{2}}\left(\frac{r}{v}\right)^3. \qquad 2\text{-}38$$

Even though the fragment distribution relationship warrants a knowledge of the average mass but not the shape, Gold also reduced the analysis to the mass by combining the shape factor (α) with the Mott factor ($\grave{\gamma}$) in the new statistical factor:

$$\gamma = \alpha^{-\frac{2}{3}}\grave{\gamma}. \qquad 2\text{-}39$$

Therefore, Gold defined in his derivation the average fragment mass using the following approach:

$$\mu = \frac{1}{2}\left(\frac{2\sigma_F}{\rho^{\frac{1}{3}}\gamma}\right)^{\frac{3}{2}}\left(\frac{r}{v}\right)^3. \qquad 2\text{-}40$$

The model developed by Gold can be used to predict the mass distribution of a cylindrical warhead by determining the distribution factor μ depending on the density and the dynamic stress of the material and the final velocity of the expanded metal under the effect of the detonation products. The Gurney velocity is inherently an explosive parameter that can related to the average fragment mass, as in the Gold's model. The final velocity of the expanded metal is very sensitive to the determination of the fragments characteristics, which have been related to the average fragments mass factor to the power 3 as been addressed by Gold.

The semi-empirical factor γ at this stage must be determined empirically for different material–explosive combinations, which include the shape factor and all the other predominant parameters, whether for the case material or the explosive. Different techniques can be used to determine the γ, such as a ring bomb test, the cylinder test or any fragmentation test.

Effect of explosive detonation pressures on fragmentation characteristics of explosive fragmentation munitions

The Gold model depends on several material and explosive empirical parameters extracted from experiments and hinges on specific assumptions. The model can distinguish between the different materials through the density and the strength of the material, which are the dominant parameters for materials. As far as explosives are concerned, the model can only distinguish between different explosives through the Gurney velocity, which effectively translates into the determination of fragment formation through a strain rate calculation. The model also requires the statistical factor, which must be determined experimentally. This statistical factor represents all the other predominant parameters that can affect the fragmentation.

Gold proposed the strain rate to be the variable that can be measured through the value of v/r as proposed by Mott. Gold, however, followed the investigation of the effective strain at fracture by the Pearson model [23], where he assumed the fragmentation of shells with idealised cylindrical geometries occur at a constant strain (approximately three volume expansions). The instant of fragmentation is defined as the time at which the products of detonation first escape from the fractures in the shell. Under this assumption, the radius r at failure must be constant,

and the velocity v is the variable that can be measured. Furthermore, Gold determined the dependence of the fragmentation characteristics on explosive parameters through the statistical factor γ. Therefore, the statistical factor γ, the final velocity of expansion v, the average mass factor μ and the stress σ_F at a failure point must be determined experimentally, which is not easy to achieve.

Gold in another publication [44] studied the dependence of the fragmentation characteristics on explosive parameters. Gold studied the dependence of the fragmentation characteristics on explosive parameters through the statistical factor γ as the fragmentation factor and Chapman–Jouget pressure as the explosive parameters P_{CJ}.

Different techniques have been used by Gold to determine the previous fragmentation parameters such as sawdust pit test and the fragmentation arena test to collect the fragments for μ measurements and the PAFRAG[1] modelling methodology to record the γ, v and σ_F parameters. A fitting possess have been used in the simulation program to fit the optimum value of μ to match the test result of the collected fragments. A numerical program known as the CALE code that incorporate the equations of state of the explosive materials as well as material strength models is also employed in Gold study to extract time of the shell breakup at three volume expansions.

The γ value for different types of explosives, with a wide range of detonation pressures, were extracted through a curve fitting method to match the test results. The results of Gold study display a linear relationship between the semi-empirical factor γ and the detonation pressure P_{CJ} of the explosive.

[1] The PAFRAG (Picatinny Arsenal Fragmentation) is modelling methodology that links three-dimensional axial symmetric high-strain-rate CALE hydrocode analyses with a semi-empirical fragmentation model PAFRAG-Mott [44].

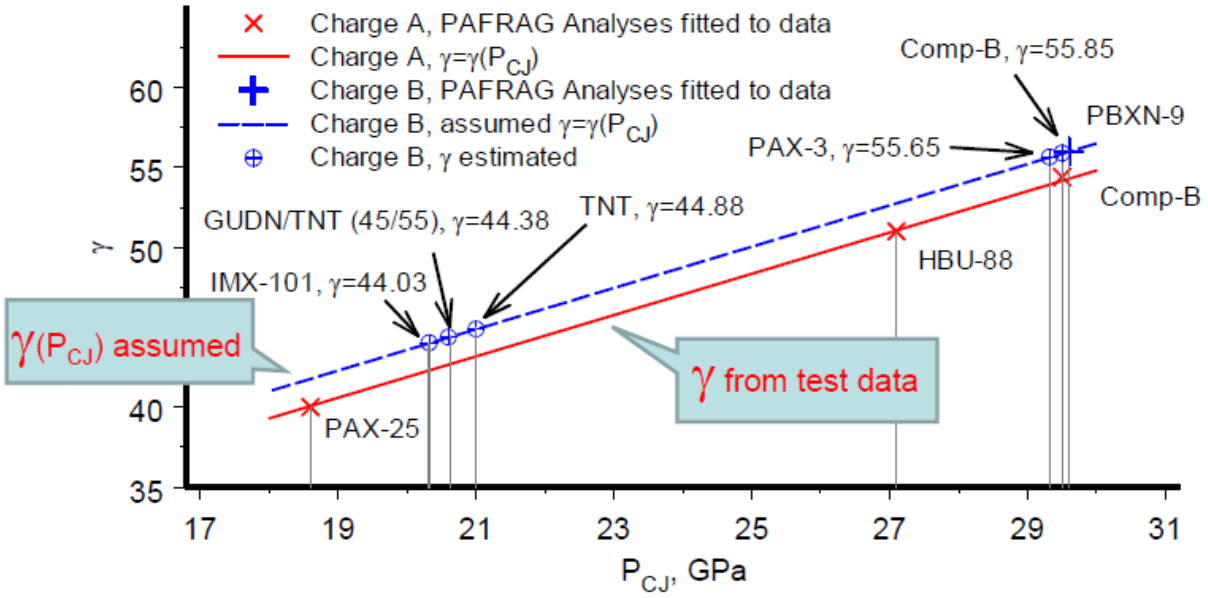

Figure 2-11: Parameter γ versus explosive detonation Chapman–Jouguet (C–J) pressure [44].

Figure 2-11 illustrate the linear relationship between the statistical distribution factor γ and the initial pressure factor P_{CJ} as provided by Gold. Defining this relationship between the semi-empirical factor γ and the detonation pressure of the explosive P_{CJ}, the result of a certain known warhead can be used to predict the mass distribution of an unknown warhead with a different explosive. The process of predicting the semi-empirical factor for different explosives is addressed in Gold's work. However, this process suggests that the use of different explosives will not affect the material constants or the shape factor of the casing.

Gold in his model defined the dependence of the natural fragmentation characteristic through (γ) factor on the explosive parameters through the initial pressure factor (P_{CJ}). The acceleration time of the detonation products from the initial point of expansion to the final stage of expansion where the fragmentation takes place did not considered by Gold as critical parameters for the determination of the fragmentation characteristics.

Length over diameter model (L/D)

A more advanced numerical computer model developed by Gold [45] is the final version of the PAFRAG simulation code for fragmentation. Gold in the previous code identified PAFRAG as the

one-region model, referring to the body of the casing where he assumed the mass distribution for the whole casing is controlled by one statistical factor γ. A relationship was indicated between the semi-empirical constant γ and the detonation pressure P_{CJ} as an explosive parameter, where the semi-empirical constant can be predicted for different explosives analytically.

In a recent study of Gold [45], the use of one statistical factor for a long warhead was identified as a problem that could lead to poor fragmentation predictions. This can be explained as the result of using the ring expansion assumption in the models of Mott and Pearson. However, the one-region model can yield good predictions for warheads with a small length to diameter ratio (*L*/*D*; with ratios of length over diameter between 2 and 2.5, referred by Gold). Gold therefore proposed the analytical length over diameter model to resolve this problem [45].

The problem inherent in the one-region model can be understood by looking at the differences between the two versions and the assumptions made. In the one-region model, fragmentation is assumed to expand into the same level of expansion when the expansion volume ratio V/V_o is equal to 3, which means the metal will fracture at a fixed value of strain.

To overcome this problem, in the newly developed multi-region model, the shell is subdivided into several regions; for each of the shell regions, the breakup is assumed to occur instantaneously, whereas the entire shell is modelled to fragment at multiple times. This method of characterisation generates a different semi-empirical constants for each region depending on the affected strain of that region and the resulting affected strain rate. Non-dimensional time parameter was proposed to minimise the error of the mass distribution by using a different values of μ for the different regions rather than one μ per region.

In conclusion, the analytical model developed by Gold is a continuation of the Mott model, and it was implemented into simple code to predict the mass distribution for different explosives. The dependence of the fragmentation characteristics, as predicted by the model, is very sensitive to the actual strain and the strain rate. Following Mott and Gold's models, the number of fragments for the same material is proportional to the velocities to the power of 3 where the strain and the strain rate are adjusted as v/r:

$$\frac{N_2}{N_1} = \left(\frac{\gamma_2}{\gamma_1}\right)^{\frac{3}{2}} = \left(\frac{v_2}{v_1}\right)^3. \qquad \text{2-41}$$

The fragments characteristics is very sensitive to the final velocity at fracture. The sensitivity is in the microsecond range, where a 1 μs change in the strain rate leads to tripling the number of fragments, according to this model. Conversely, the velocities of the fragments at the time of

breakup are usually empirically obtained. The actual moment of breakup is difficult to measure, and the determination methods sometimes affect the final results, as discussed in Pearson's investigation [23].

This analytical study of Gold will be used as a guideline in this study to investigate the dependence of the natural fragmentation characteristics on the explosive parameters at the time of breakup through the final velocity of an expanded metal under the effect of the detonation products of different type of explosives.

2.3 Fragmentation behaviour under detonation load

The other critical factor in the determination of the fragmentation warheads efficiency is the velocity of the fragments. The calculation of the initial fragment velocities of explosively accelerating items can be approached through sophisticated numerical codes that incorporate the equations of state of the materials as well as material strength models. Less complex empirical and/or analytical procedures are often preferred in estimating the initial velocity and the projection angles of explosively accelerating items.

The seminal and most commonly used models for predicting fragment velocity are the analytical models developed by Gurney [46]. Gurney developed these models for different warhead geometries to predict the velocities of fragments from bombs, shells and grenades in order to assess the efficiency of these warheads and compare them with other warheads. These relatively simple equations are based on energy balance methods of estimating the final velocity of metal driven by detonation, as discussed in this section.

2.3.1 Gurney model in cylindrical case

In attempting to predict the kinetic energy of fragments, as well as their initial velocity after acceleration by the products of detonation, Gurney [46] developed a model for a cylindrical case based on the considerations on detonation behaviour with certain simplifying assumptions. The model considers a simple cylindrical charge with mass per unit length C and radius R, surrounded by a thin casing metal with mass per unit length M, as illustrated in Figure 2-12

.

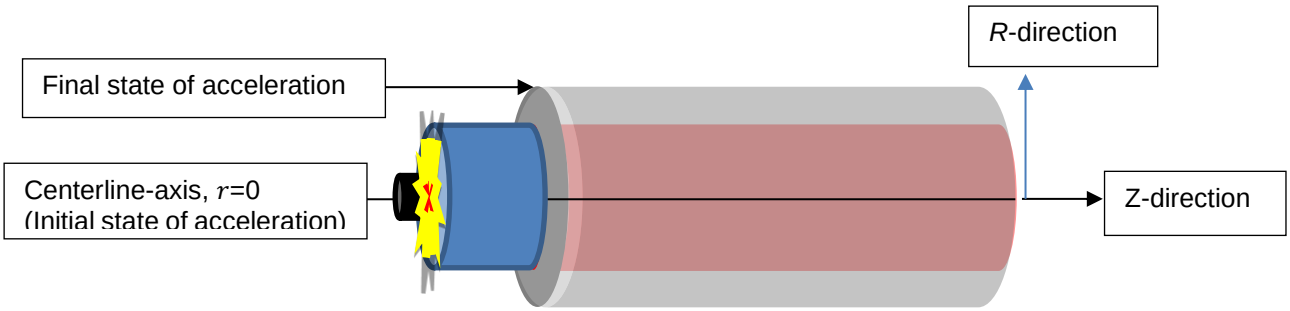

Figure 2-12: The diagram of a cylindrical explosive charge surrounded by a shell; Gurney model.

Initiation from one end generates a detonation wave that moves in the z-direction at a uniform velocity along the longitudinal axis of the cylinder (i.e., initial radius $r = 0$).

Gurney assumed the cylindrical case to be of infinite length (open ended) and the detonation wave to have no significant effect in the z-direction. From detonation theory, the passing of the detonation wave through a point in the z-direction is followed by the release of gas from chemical reactions in the detonation front. These gases expand rapidly outward in the radial direction (*R*-direction), causing the case to also expand radially outward. The model assumes that the chemical reaction in the detonation front proceeds instantaneously and there is an instantaneous energy release. For simplicity, Gurney defines an energy parameter, known as the Gurney energy (e), which represents the chemical energy of the explosive material at the initial state (i.e., r = 0). The chemical energy of the explosive material will convert through detonation process into a kinetic energy. Accordingly, the kinetic energy of flying fragments plus the energy of expanding explosion products equals the internal energy of explosion.

Therefore, the chemical energy of the explosive charge in the initial state (Gurney energy e) is converted into kinetic energy at the final stage for both the fragments and products of detonation (KE_f and KE_c):

$$e = KE_f + KE_c = \frac{1}{2}Mv^2 + \frac{1}{4}Cv^2, \qquad 2\text{-}42$$

Where KE_f is the total kinetic energy of the accelerating metal under expansion of detonation products, equal to $\frac{1}{2}Mv^2$, M is the mass per unit length of the casing material and v is the velocity of the metal wall. In the case of fragmentation, it is assumed that the fragments move with the same velocity of the detonation products when $R = r$.

KE_c is the total kinetic energy of the gases products, equal to $\frac{1}{4}Cv^2$, C is the mass per unit length of the explosive charge and v is the velocity of the metal wall derived as described below.

The derivation of the total kinetic energy of the gases comes from the change in the kinetic energy of the detonation products. The mass elements of the detonation products dm accelerate from the centreline of the explosive charge $r = 0$ during detonation until it reach the final stage at the outer radius of the casing material $r = R$.

The kinetic energy of this element therefore is:

$$dKE_C = \frac{1}{2}dmv(r)^2, \quad \text{2-43}$$

Where the velocity of the gases as a function of the radial displacement $\mathrm{v(r)}$ assumed to varies linearly in the radial direction form the centreline to the metal casing:

$$v(r) = \frac{r}{R}v, \quad \text{2-44}$$

The density during expansion assumed to be constant and the change of the mass elements only considered in the change of the volume per unit length V under the following equation:

$$dm = \rho dV = \rho r dr d\theta, \quad \text{2-45}$$

Where the density of the explosive charge before detonation is:

$$\rho = \frac{C}{\pi R^2}, \quad \text{2-46}$$

By substituting the previous equations dm and $v(r)$ into dKE_C the following equation is obtained:

$$KE_c = \int dKE_c = \frac{1}{2}\int v(r)^2\, dm = \frac{1}{2}\frac{C}{\pi R^4}v^2 \int_0^R r^3 dr \int_0^{2\pi} d\theta, \quad \text{2-47}$$

The integration of previous equation will results to the following approach:

$$KE_c = \frac{1}{4}Cv^2, \quad \text{2-48}$$

Therefore, the final velocity of the accelerating fragments under the effect of detonation-produced gases as formulated by Gurney for the cylindrical case; namely:

$$v_G = \sqrt{2e}\left(\frac{M}{C}+\frac{1}{2}\right)^{-\frac{1}{2}}, \qquad 2\text{-}49$$

Where $\sqrt{2e}$ is an empirical constant, known as the Gurney constant, combining the effect of the explosive with the effect of the material in one constant.

Restrictions on the Gurney model

The simple analytical model developed by Gurney for cylindrical warhead is a one-dimensional model used to predict the fragment velocity from the M/C ratio and the empirical Gurney constant. The Gurney equation is derived from general considerations of energy balance up to the moment before gas leakage occurs. This derivation assumes a linear velocity profile and a constant density for the reactant gases. The model does not consider the interaction process between the detonation products and the material. As a result, the same (M/C) ratios with different materials but with the same explosive will yield different velocity histories.

The velocity of the fragmentation based on this model is a result of the pressure of the detonation products. The time of this process is very sensitive to the detonation products where early break-up of the warhead or any escape of the gas will generate a different velocity history, as in end effect and gas leakage models.

Although useful for first order predictions, the simplicity of this model exhibits major shortcomings or constraints, which limits it applicability. Most of these shortcomings or constrains were investigated, and a list of the findings are summarized by Kennedy [47] as in Table 2-1.

Table 2-1: Restrictions and constraints of the Gurney model.

Restriction	Remarks and Recommendations
Range of M/C ratio	Henry (1967) claims accuracy for 0.1 < M/C < 5, and Kennedy (1970) states a range of 0.2 < M/C < 10 for velocity calculations. Impulse calculations are usually acceptable for M/C > 0.2.
Acceleration phase	The Gurney method, in its basic form is not capable of analyzing motion during acceleration. However, Henry (1967) and Jones et al. (1980) used the assumption of a linear velocity profile in the uniformly dense gases in conjunction with an equation of state of the gases to yield acceleration solutions for flying metal plates. The detonation product gases must be allowed to expand sufficiently to complete the acceleration. The flying metal will reach its calculated velocity only if no external forces (or interactions) are applied during the initial acceleration phase.
Direction of detonation propagation	The detonation of the HE drives the metal at a given velocity (approximately) for a given M/C regardless of the angle between the detonation front and the metal. The direction in which the metal is driven will vary slightly with the angle. (Refer to the Taylor angle discussion later in this literature review).
Gas velocity profile assumption	The assumed linear velocity profile and constant density gas expansion are major assumptions. Ignoring the effects of both rarefaction waves and of pressure peaks near the metal surface would seem to be canceling errors. However, these assumptions are inherent to the simplicity of the Gurney method.
One-dimensional motion	The Gurney approach is not valid for the estimate of variations in the local velocity of a plate driven by a charge with a tapered thickness (or a tapered metal thickness). In this case, an average value of M/C could be used to estimate the final velocity of the entire plate.
Metal strength effects	Forces exerted by the metal to oppose deformation are not considered, other than inertia. Hoop stresses in cylinders and spheres can reduce the metal velocity in explosions and the strength effect is greater in implosions.
Metal spallations	Metal spallation may occur when M/C < 2 for high-density explosives and metals. Spallation can, in some cases, be avoided by introducing an air gap of a few millimetres between the explosive and the metal. This what results in a small decrease in metal velocity.
Early case fracture	The leakage of the detonation product gases through fractures in the metal case can decrease the final metal velocity perhaps significantly depending on the nature and extent of the leakage.

2.3.1.1 **The dependence of Gurney constant on explosive parameters**

The Gurney constant is an important characteristic property of an explosive, which indicate the chemical energy of explosive material imparted to casing metal. A value for this constant can be determined experimentally from direct measurements of fragment velocities or by the cylinder test which known as one of the most common methods for extracting this constant [48]. Alternatively, the $\sqrt{2e}$ value can be estimated from empirical and theoretical methods as discussed below.

Thermodynamic behaviour of detonation products

One of the method used to predict Gurney constant it through the empirical thermodynamic parameters of detonation such as the internal energies of formation and the heat of formation of explosive under certain assumptions. This estimation method assumed an isothermal process where the decrement in the internal energy ΔE_i of the system correspond to the increment on the heat ΔH_d of the system (explosion in this case). The heat of explosive represent the isothermal internal energy of the explosion corresponding to Gurney energy (e). This method assumed a nominal products compositions, where the theoretical value of internal energy of explosion equal to the difference between the empirical internal energy of formation for the products and the reactants:

$$\Delta H_d = -\Delta E_i = -\left(\sum_i^p n_i E_f^o - \sum_j^r n_i E_f^o\right) = e \qquad \text{2-50}$$

Where; p refer to the products and n_i is the number of moles of products. r refer to the reactants (i.e. explosive material) and n_i is the number of moles of the reactant. E_f^o is the internal energy of formation at constant volume.

One of the main problem of this method is only valid for prompt energy release from chemical energy of the explosive where no loss in energy during detonation process. Another issue of this method is the leak of data of variety of explosive material that used nowadays.

In addition, the method used to extract thermodynamic parameters of detonation from direct measurement is somewhat difficult, where the calorimeter must be able to withstand the explosion. Alternatively, indirect measurements that avoid some of the various difficulties associated with direct determination of thermodynamic parameters from detonation are those obtained from combustion. The reaction in this method is a relatively simple combustion process at constant volume in the presence of excess oxygen.

During the generation of this study, a paper have been published in 2019 by Frem [49], considering a model to predict Gurney energy from heat of combustion (ΔH_c^o) for different explosive material. The Gurney constant obtained from this model depends on the density of explosive and the heat of combustion and empirical parameters related to the type of explosive:

$$\sqrt{2e} = 2.2608 + 0.5941(\rho) + 0.0448(\Delta H_c^o) - 0.1394(\xi) + 0.3(\phi) \qquad 2\text{-}51$$

Where ρ is the density of the explosive, ΔH_c^o is the heat of combustion that can be obtained theoretically from the different in the heat of formation between products (p) and reactants (r). ξ and $\phi$is an empirical parameter depends on the type of explosive.

Gurney constant as a function of detonation velocity

The velocity of detonation is an indicated factor of the chemical energy of explosive material released during detonation. Hence, several models have been approach to predict the Gurney constant of explosive material based on their velocity of detonation value D such as the model developed by Koch et al. [50], Cooper [5] and Roth [51].:

Koch	$\sqrt{2e} = 0.325D$	2-52
Cooper	$\sqrt{2e} = 0.327D$	2-53
Roth	$\sqrt{2e} = 0.303D$	2-54

These models illuminate the dependency of the fragmentation characteristics on the detonation behaviour, which is an indicated factor of the initial stage of the expansion behaviour. Based on the assumptions of these models, the time from detonation front until the moment of breakup is not properly addressed. This time of expansion based on these models is constant for all explosive material. The time however for prompt detonation is fairly small enough to be considered as constant and that might not affect the final shape of fragments. Although not all the energy of the explosive released from detonation is imparted to the casing material, it is still depends on the time of the detonation products at fracture.

In overall, different values for Gurney constant will be a result of different models based on different assumption. The effective strain of fragments is very sensitive to the time at fracture and that will reflect on the final shape of fragments. This study will investigate the dependence of the natural fragments characteristics on the final velocity at the time of breakup.

2.3.2 Fragmentation projection angle

The direction of fragments is a considered factor in the determination of the lethality and effectiveness of a warhead. The spatial distribution of natural fragments from a warhead casing, is a complex function that depends on the internal and external geometry of the warhead's surface, the warhead's mechanical properties and the energetic characteristics of the explosive. The two-dimensional analytical model developed by Taylor [52] is a corrected the Gurney model, which takes into consideration both the axial velocity of the detonation wave and the radial velocity of the fragments. The results of this analysis are discussed in the section below.

Taylor model for cylindrical cases

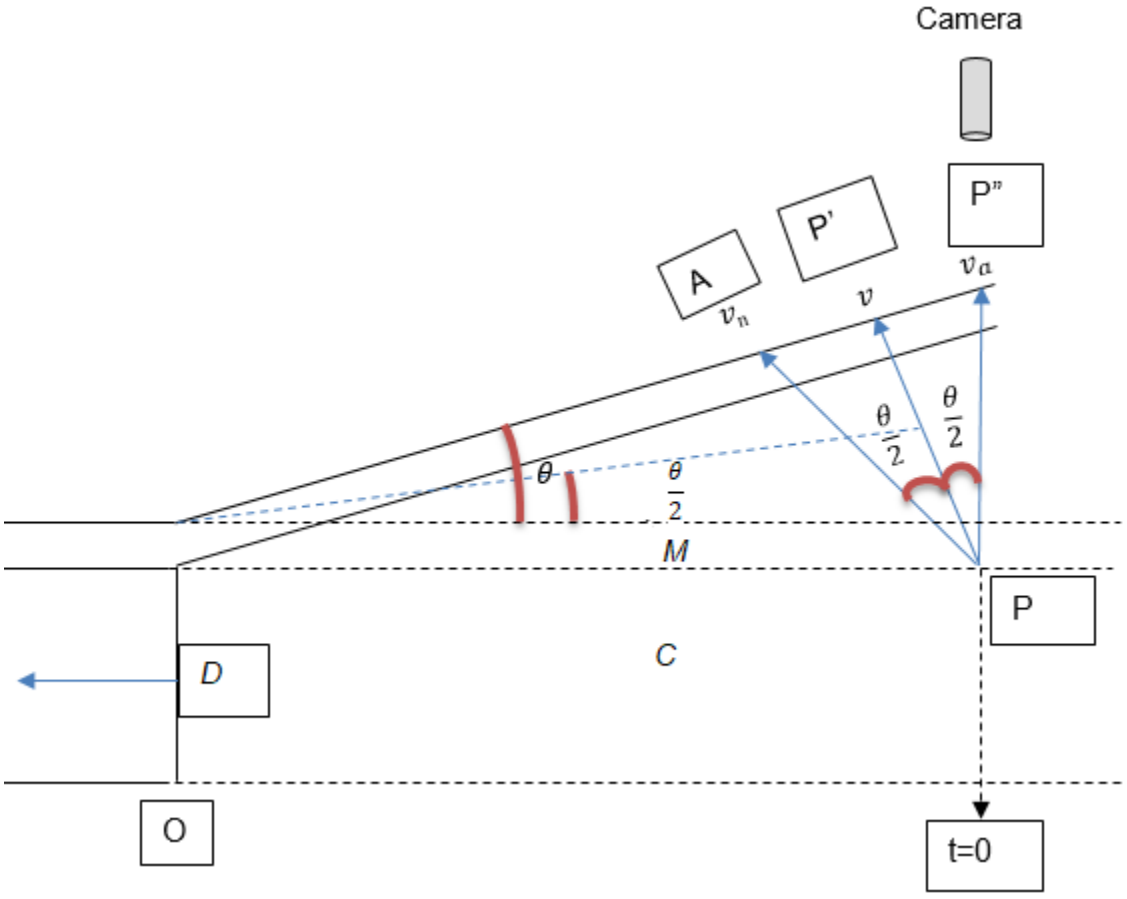

Figure 2-13: Direction of metal projection by a grazing detonation wave (Taylor model).

Figure 2-13 shows a schematic for the Taylor expansion angle approximation based on an analysis of the expansion of a cylindrical metal tube under the effects of a detonation wave as it passes from point P to point O. The one-dimensional Gurney model assumes that the metal moves in a direction normal to its surface (in the radial direction), and based on this assumption, the metal will expand from point P to point P"; in the real case, as rectified in the Taylor analysis,

there is an acceleration component in the direction of the detonation. The correction to this problem proposed by Taylor was to account for the grazing angle instead of the normal incidence. For this purpose, Taylor assumed that when the detonation wave moves from P to O, the metal will expand from P to P' instead of P".

The time elapsed between the two points (P to P') is the main concern of this analysis in determining the actual fragment velocity and direction, and this elapsed time is also the critical factor for the other empirical explosive parameters. A high speed camera is often used to record the expansion behaviour of the casing metal at point P" perpendicular to the detonation wave axis where the apparent velocity v_a is defined. When a detonation wave pass through point P to the point O, the time t is measured between P and P' where the actual velocity v is defined. The results of this model, based on a triangular geometric analysis, yielded the following velocity functions:

$$\overline{\mathrm{PO}} = Dt, \qquad \text{2-55}$$

$$\overline{\mathrm{PP'}} = vt \qquad \text{2-56}$$

$$\overline{\mathrm{PP''}} = v_a t \qquad \text{2-57}$$

$$\overline{PA} = v_n t \qquad \text{2-58}$$

Where D is the detonation velocity from P to O.

Therefore, from the triangle ΔPP'O, the actual velocity v from the grazing incidence of the detonation wave to the casing metal:

$$\sin\frac{\theta}{2} = \frac{\overline{\mathrm{PP'}}/_2}{\overline{\mathrm{PO}}} = \frac{vt}{2Dt} = \frac{v}{2D} \qquad \text{2-59}$$

For the triangle ΔPP"O, the apparent velocity v_a of the recorded camera:

$$\tan\theta = \frac{\overline{\mathrm{PP''}}}{\overline{\mathrm{PO}}} = \frac{v_a t}{Dt} = \frac{v_a}{D} \qquad \text{2-60}$$

For the triangle ΔPAO, the normal velocity v_n from the normal incidence of the detonation wave to the casing metal:

$$\sin\theta = \frac{\overline{PA}}{\overline{\mathrm{PO}}} = \frac{v_n t}{Dt} = \frac{v_n}{D} \qquad \text{2-61}$$

The result of this model is a method of measuring the components of fragment velocity and the effective projection angle of the fragments. This analysis is also used for the analysis of the streak camera technique to extract explosive parameters such as the Gurney constant and the equation of state parameters. The key point of this approximation is to determine the actual value of the acceleration behaviour of the effective pressure between points P and P'.

2.3.3 Correction models

Since the pressure from the detonation products provides the force that accelerates the warhead body to its final velocity, the acceleration of the fragments depends on the gas released by the detonation wave and the expansion behaviour of the detonation products. Therefore, different physical effects may contribute to the fragmentation process, such as the heat of the detonation products, the physical interaction of these products with the material of the casing and the shock reflections in the casing during the expansion process. Relying on this postulation, other criteria could be accounted for when dealing with fragmentation, such as the end effects at the geometric limits of the case and the release of pressure when the gas escapes from cracks in the early breakup of the warhead. In Figure 2-14, a numerical computation illustrates gas released at the initiation end of a cylindrical warhead.

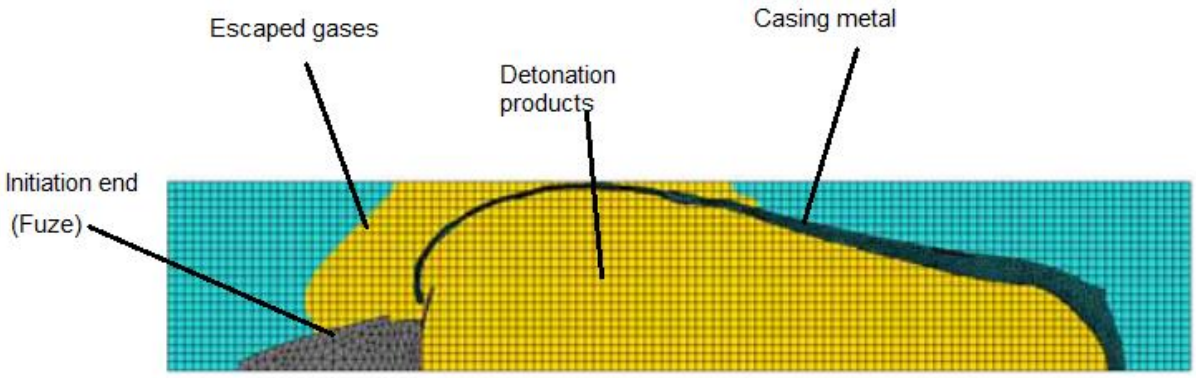

Figure 2-14: Two-dimensional expansion model of the warhead casing t = 75 μs [10].

End effect model

The velocity found in the Gurney and Taylor models is the maximum velocity achieved by fragments during their acceleration phase and applies to the expanding warhead's case fragments only at distances from the warhead centre greater than approximately twice the warhead's initial radius.

In order to account for the end effect to the fragments velocity, models developed by several researchers Randers-Pehrsod, Hennequin and König [53, 54 and 55] estimated the reduction in

the velocity of the fragments at both ends of a cylindrical warhead. The derivation of these models relies on the fact that the reduction in the velocity at the ends is due to waves of released detonation gas. A correction factor F_x was proposed by Randers-Pehrsod [53] to be added to the explosive mass term C in the Gurney equation to reduce the effective mass acting on the warhead wall:

$$v_G = \sqrt{2e}\left(\frac{M}{F_x C} + \frac{1}{2}\right)^{\frac{1}{2}} \qquad 2\text{-}62$$

The calculation of this factor was estimated by assuming a conical shape for the release wave at both ends (as suggested by Hennequin [54]). Figure 2-15 illustrate the virtual release cones as proposed by Hennequin.

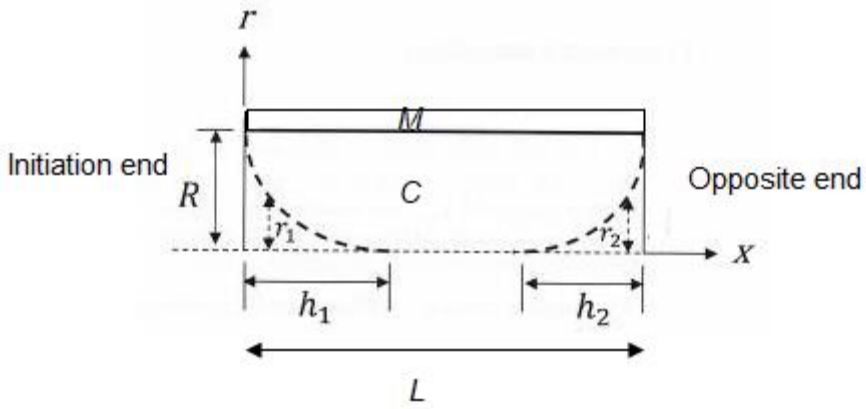

Figure 2-15: The Hennequin model of cylindrical warhead [54].

The dimensions of this cone are the critical values for the calculation of the reduction factor F_x. Where r is the radius of the cone at the point of interest, and h is the height of the cone at end of interest. These heights are the minimum distance from the respective end of the warhead where release waves would have no effect. The calculation of this factor as proposed by Hennequin:

$$F_x = \left[1 - \left(\frac{r_1}{R}\right)^2\right]\left[1 - \left(\frac{r_2}{R}\right)^2\right] \qquad 2\text{-}63$$

R is the radius of the warhead:

(Initiation end) $$\frac{r_1}{R} = 1 - n_k\left(\frac{x}{d}\right)^{n_k} \qquad 2\text{-}64$$

(Opposite end) $$\frac{r_2}{R} = 1 - 2n_k\left(\frac{L-x}{d}\right)^{n_k} \qquad 2\text{-}65$$

Where L and d is the length and diameter of the warhead. n_k takes the value of 1 and 2 referring to initial and the opposite end of the warhead, respectively.

The numerical values of n_k depend on the charge-to-metal mass ratio (C/M) of the warhead. The heights of the release cones h relative to the warhead diameter d*:*

(Initiation end) $$\frac{h_1}{d} = k_1 \left(\frac{M}{C} + \frac{1}{2}\right)^{\frac{1}{2}} \quad \text{2-66}$$

(Opposite end) $$\frac{h_2}{d} = k_2 \left(\frac{M}{C} + \frac{1}{2}\right)^{\frac{1}{2}} \quad \text{2-67}$$

where k_1 and k_2 are empirical constants.

This model was also adapted by König [55] to correct for the projection angle's deviation from the Taylor model prediction near the ends of a warhead, the correction factor of the projection angle (α_c) proposed by König:

(Initiation end) $$\alpha_c = -a_k \left\{\left(\frac{dF_x}{dx}\right)\right\}^{m_k} \left(\frac{h_1}{d}\right) \quad \text{2-68}$$

(Opposite end) $$\alpha_c = a_k \left\{\left(\frac{dF_x}{dx}\right)\right\}^{m_k} \left(\frac{h_2}{d}\right) \quad \text{2-69}$$

The constants a_k and m_k are empirically determined.

Other researchers have contributed to the corrections to velocity, and projection angle for end effects and for non-cylindrical warheads as presented in [56]. This semi-empirical model is a time-dependent model, and it can be used in combination with other fragmentation models to develop an integration model for fragmentation characteristics, as in the focus of this study. In other words, these models can be used to predict the effective velocity of a warhead at a certain distance to characterise the fragments at that point.

2.4 Experimental methodology of investigating explosive behaviour

Several numerical and analytical models have been used to characterise the detonation and fragmentation behaviour. These models rely on empirical parameters that must be determined to characterise fragmentation and detonation behaviour; these parameters include Mott and Gurney constants and the parameters for the empirical equations of state [48]. The cylinder test is the standard test which, in combination with other techniques, is used as a guideline for this investigation [57].

Cylinder test technique

The cylinder test technique is a method proposed by Los Alamos National Laboratory and Lawrence Livermore National Laboratory to investigate HE material performance [58]. The cylinder geometries used for the standard test at Lawrence Livermore National Laboratory, are illustrated in Figure 2-16.

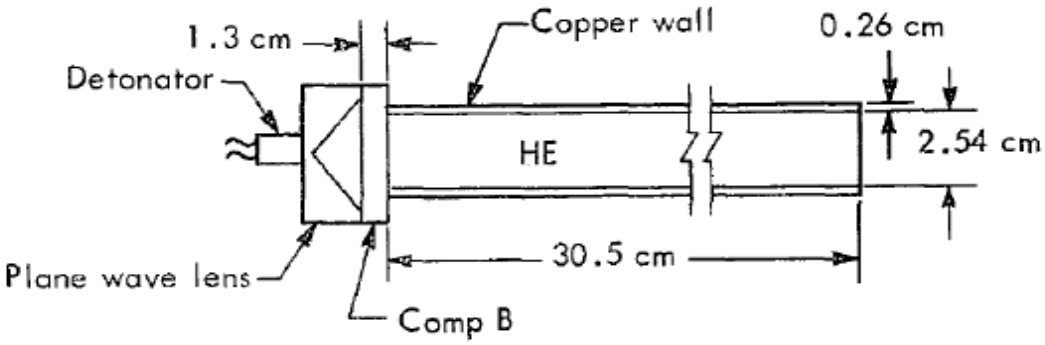

Figure 2-16: The cylinder expansion test setup proposed by Lee et al. [58].

Based on the detonation theory, by initiating the HE material from one side, a detonation wave propagates toward the open side, and the detonation products expand the tube radially. A recording method normally used at certain point to record the expansion behaviour of the cylinder wall accelerated under the effect of the detonation products. Figure 2-17 is an illustration of the standard cylinder test setup provided by [59]. The schematic illustrate the standard method used to characterize the behaviour of the detonation including the cylinder material, the cylinder dimensions, the illumination source and the suggestion point of record.

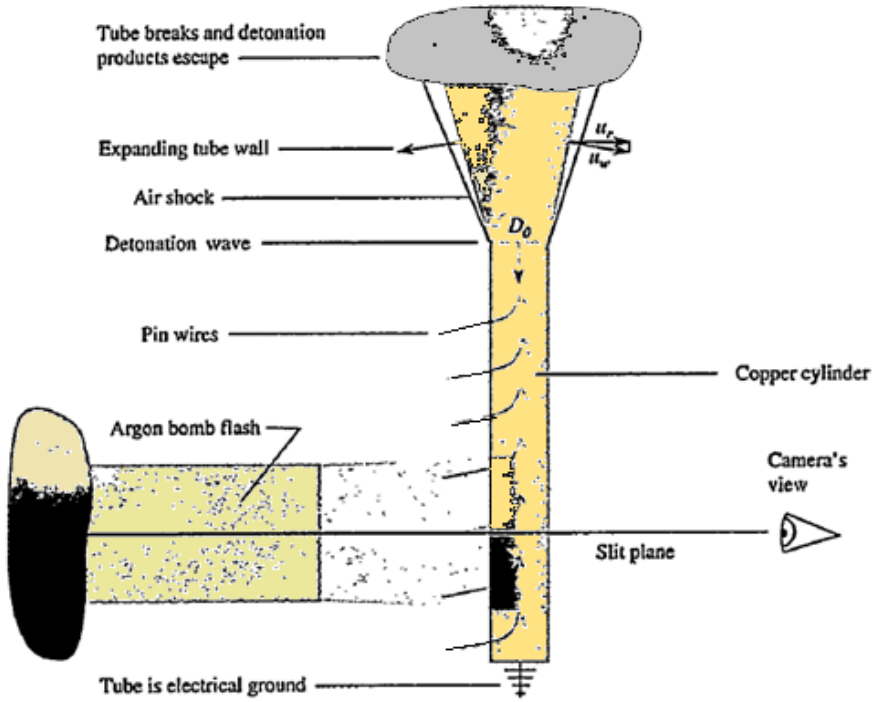

Figure 2-17: Schematic of the test setup used by Los Alamos National Laboratory [59].

The test was originally used to investigate the transfer of energy from an explosive charge to a casing material and Gurney constant. Several technical reports have been published to establish the basic principles of the cylinder expansion test [59].

Recently, the test has been used in an analytical procedure to extract the JWL equation of state parameters in an iterative process, as proposed by Elek et al. [9]. The model developed by Elek is an analytical method to extract the optimum empirical parameters of JWL equation of state through the analysis of the cylinder wall motion. Elek normally rely on the analysis of the streak camera record of the detonation products at certain point to consider the equation of motion parameters of the cylinder wall. The equation of motion parameters used later to derive the velocity and the acceleration of the detonation products. By defining the acceleration of the detonation products the pressure of the detonation products and the other explosive parameters have been deduced. An iteration process to extract JWL empirical parameters have been provided by the Elek model.

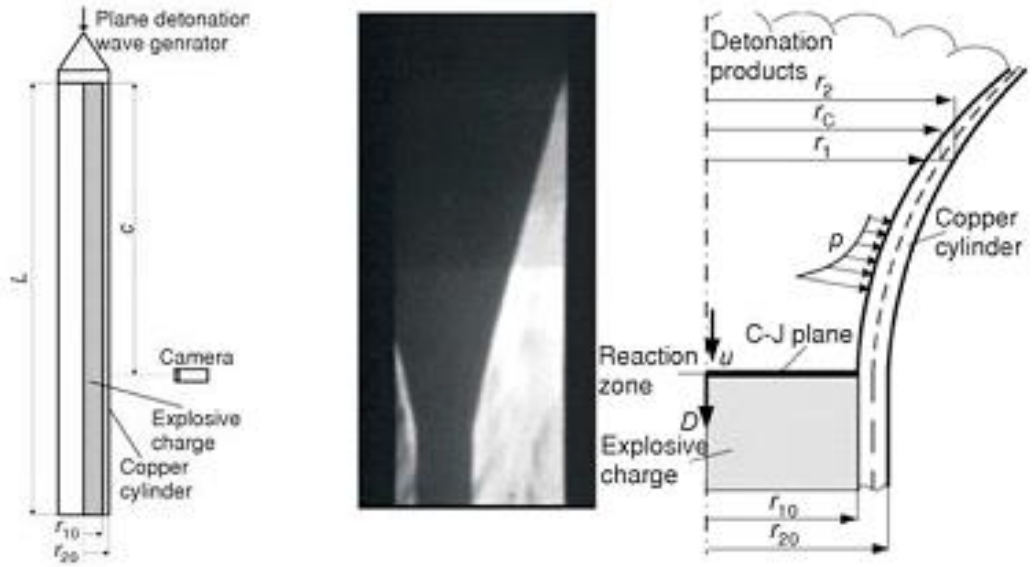

Figure 2-18: A typical streak camera recording with a schematic of the motion of a copper tube under the action of detonation products, by [9].

Elek [9] in his study developed a combination models from different perspective to specify the ideal method to extract the optimum explosive parameters from cylinder test through streak camera record. The cylinder test has also been used by Goto et al. [26], to investigate the fracturing and natural fragmentation behaviour of steel and copper hollow cylinders filled with explosive. Figure 2-19 is schematic figure of the cylinders used by Goto to investigate the fragmentation characteristics produced by the cylinder material.

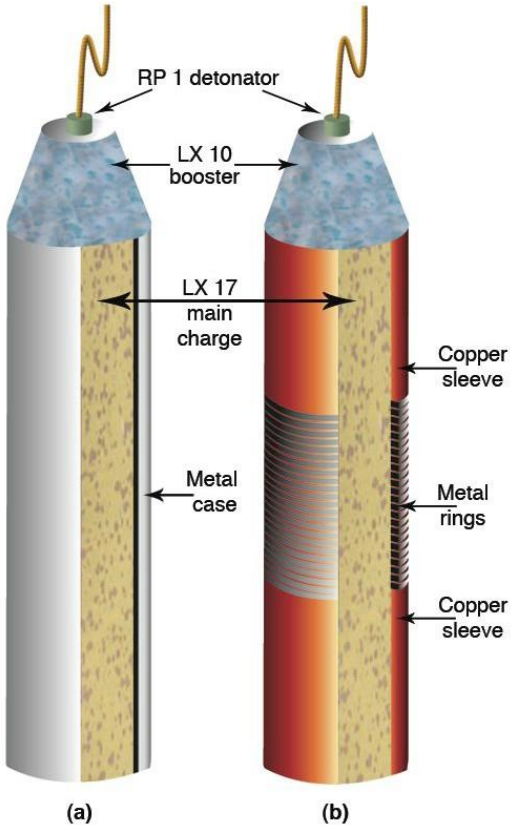

Figure 2-19: Schematic of (a) standard cylinder to investigate plane strain and (b) ring loaded cylinder [26].

The test investigates a hollow cylindrical metal tube filled with HE material. The case is typically made of copper to study detonation behaviour, but in the case of fragmentation, the case is made of the material under investigation. The explosive contained inside the tube initiates from one side and opens from the other side. A modification model developed by Goto to characterize the effective strain of the collected fragments from the effective thickness. The cumulative damage of Johnson-Cook have been used in a combination with a statistical distribution function in a numerical program to investigate the fragments distribution of the detonated tube. This model typically developed to calibrate a statistics-compensated Johnson-Cook fracture model for numerical simulation program.

Determination of the empirical explosive parameters depends on the methods used to record the expansion behaviour. An optical technique normally used to record the expansion behaviour such as in the case of Elek; [9]. An analysis method used to extract the empirical equation of motion parameters from streak picture photography.

The expansion event also can be recorded electronically by using an electronic pin probes or contact pins in different distance, as in [59 and 60], Figure 2-20. The electronic probes used to

record the expansion event in different time at different distance, which can be determined beforehand.

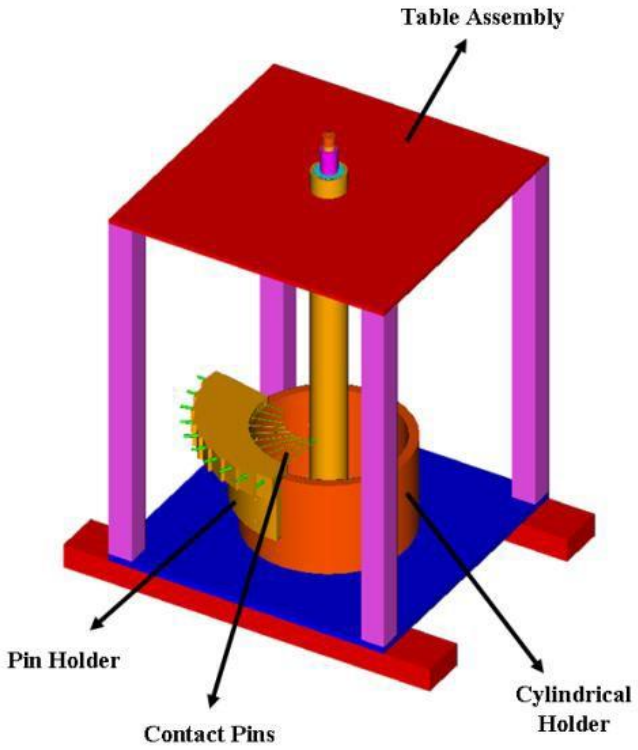

Figure 2-20 : A schematic of the cylinder test setup using electronic pin probes by [60].

Direct measurement of the velocity of the wall verses time can be obtained through various velocity interferometer techniques, such as photon doppler velocimetry, used by Jackson [11]

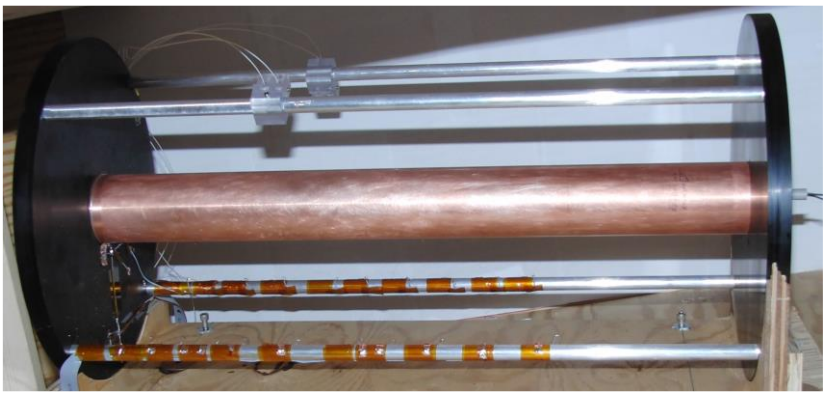

Figure 2-21: a cylinder test prepared for photon doppler velocimetry recording used by [11].

The recording devices are located during the test at a certain cross-section along the longitudinal axis of the cylinder in a position that ensures a full detonation and prevents side effects (normally, 2/3 L is recommended).

Characterisation of the expansion behaviour of the detonation products is the main concern of the cylinder analysis. The behaviour of wall motion under the effects of the detonation products is used to characterise the detonation behaviour in terms of velocity, acceleration and pressure. The main output of this characterisation is the displacement versus time of this wall motion.

Several analytical models have been developed to characterise the expansion behaviour of detonation products to extract the optimum explosive parameters thereof [57]. There are two well known analytical models that characterise expansion behaviour. The first is the fitting function developed by Hornberg and Lan et al.,[61,62]:

$$F(t) = \sum_{j}^{1,2} a_j \left[t_i - \frac{1}{b_j}\left(1 - e^{-b_j t_i}\right) \right], \qquad 2\text{-}70$$

This model assumes that the pressure of the detonation product drops exponentially, where a and b are the empirical parameters to be optimised from the experiment results for one or two addends.

The second function is the function in the following equation, by Hill [63]:

$$F(t) = \frac{v_\infty t g(t)}{\frac{2v_\infty}{a_o}\dot{g}(0) + g(t)}, \qquad 2\text{-}71$$

where a_o is the initial cylinder acceleration,v_∞ is the asymptotic radial cylinder velocity and the function $g(t)$ is defined as:

$$g(t) = (1 + t)^\beta - 1. \qquad 2\text{-}72$$

where β is an empirical parameter determined to minimise the deviation of the function defined from experiment results.

The cylinder test is used to fit the empirical parameters of these models. Fitting procedures were discussed and developed in several studies to extract the optimum parameters of these models [64,17].

In conclusion, the main purpose of this test is to characterise the radial expansion behaviour of a detonation products to extract the explosive parameters in an optimisation process. However, the test can also be used to determine fragmentation characteristics and the explosive parameters at the same time. Therefore, the cylinder test in combination with other techniques is used as a

guideline along with the arena test to characterise the fragmentation and expansion behaviour of different explosives, as discussed in the next chapter.

2.5 Conclusion

To simulate the effectiveness of the configuration of a given natural fragmentation warhead, it is necessary to estimate the fragmentation characteristics: mass, number, velocity and direction. The estimation of these characteristics depends on the model used for their prediction. Different analytical, empirical and semi-empirical models have been derived from studying fragmentation characteristics and behaviour in terms of mass, velocity and spatial distribution. The simplicity of these models is the result of mathematical derivation under certain conditions and assumptions, which have limitations. However, these models are an attractive approach to deriving the fragmentation characteristics for initial design purposes.

Numerical models deliver more accurate results but are time consuming and expensive to run. Typically, these models are used in the final design stages of a weapon system. The accuracy of these models strongly depends on the results of the experiments employed to extract the constants of these models.

Several studies has been reviewed through three parts in this chapter. The first part of this chapter was a review of the fracture behaviour under mechanical stress load, this include the strain-to-failure model and the mechanical parameters that contribute to the determination of fragmentation characteristics of cylindrical case.

The second part was a review of the statistical model that developed to characterize the natural fragmentation distribution. Simple empirical and analytical models were discussed and summarised in the second part, where the mass, velocity and direction of the fragments were combined with empirical parameters to characterise the fragmentation.

The third part was a review of the contribution of the explosive parameters in the determination of fragmentation characteristics. The methods used to characterise detonation behaviour in a cylindrical tube and how these parameters contribute to the determination of the fragmentation characteristics is also reviewed.

The models discussed are the results of mathematical and analytical derivations built under certain assumptions to characterise fragmentation based on material and explosive parameters. In contrast, fragmentation is the result of the dynamic interaction between detonation of explosive and casing material that causes failure at certain points of expansion. Accordingly, the

fragmentation models were adjusted to use the stress, strain and strain rate as the dominant factors in the determination of the failure points of a material, where the Chapman–Jouguet pressure and the expansion velocity are contributing factors to these models. Hence, there are two significant points to be discussed in this study: The first is to investigate the models used to characterise fragmentation, and the second is to investigate the methods used to extract the empirical parameters of these models.

The main challenge of this study is to characterise fragmentation and detonation behaviour using one test to cover all possible effects from the method used that can cause a variation in the final results.

One main problem is the effective strain at fracture is approved to different model to be constant for the same casing material and different explosive. Due to the prompt event of the detonation process, the final velocity assumed to occur at the same strain for the same casing material and different explosive material where the acceleration time of the detonation products is not concern.

However, the objective of this research is to study the sensitivity of explosive parameters and the effect of these parameters on the fragment characteristics in their final form. The aim of this study is to enhance the predictive accuracy in a simple way by attempting to include other explosive parameters through an existing analytical model.

CHAPTER 3: RESEARCH METHODOLOGY

This chapter presents the methodology used to investigate the dependence of natural fragmentation characteristics of a casing material on explosive parameters. The proposed methodology of this study is an experimental study to characterise both the fragmentation behaviour and the detonation behaviour of cylinder samples filled with different types of explosive. Therefore, the test designed herein is a combination test based on local availability and accessibility following the guidelines given in the publications and the literature presented in the previous chapter.

Fragmentation behaviour has been characterised by employing an international standards test for fragmentation characterisation (known as the arena test). The cylinder test is the standards test employed to characterise the expansion behaviour of a metallic cylinder that expands under the effect of explosive detonation products. The remainder of this chapter describes the method used for the preparation of the sample items, the arena test setup and the cylinder test setup. This chapter also illustrates the procedures for gathering the required measurements and values relating to the distribution of fragments and the expansion behaviour using optical and capture box techniques.

3.1 Sample items (material selection and preparation)

The material used in this test must meet the requirements of the study. It must be able to achieve a certain level of expansion to be visualised by the camera as well as to break apart to such an extent that an optimum number of fragments are produced for characterisation. The specification of the material used in this study and the preparation process for the samples are detailed in the following section.

3.1.1 Cylinder material

A decision was made to use steel for the casing material, which has properties that ensure sufficient fragmentation and expansion behaviour at the same time. Based on the literature review [10, 16], the mechanical properties of the material, such as the brittleness, ductility and toughness, are the principle criteria in the selection of the material. These parameters can be predicted through the history of the stress–strain curve for the material.

For sufficient expansion, however, the metal involved must have a very high ultimate strain (e.g., ductile material has sufficient elongation), where explosive gases can drive the metal for a long

period of gas expansion. On the other hand, brittle material generates a sufficient number of fragments, but the optimum expansion process will not be achieved properly.

In this case, therefore, the selected material for this purpose must satisfy both aspects: optimum expansion with optimum fragmentation. Consequently, alloy steel (EN19) was selected, which has a sufficient level of ductility and sufficient tensile properties. The specification of the sample items, guided by the literature, and the dimensions specified for the standard cylinder test are presented in Table 3-1.

Table 3-1: Cylinder item specification.

Steel Type	Yielding point Y	Ultimate tensile stress UTS	Strain failure (ε_F)	Length (L)	Outer diameter (OD)	Thickness (t)
	(MPa)	(MPa)		(mm)	(mm)	(mm)
EN19	755	1000	0.12	200	50	5

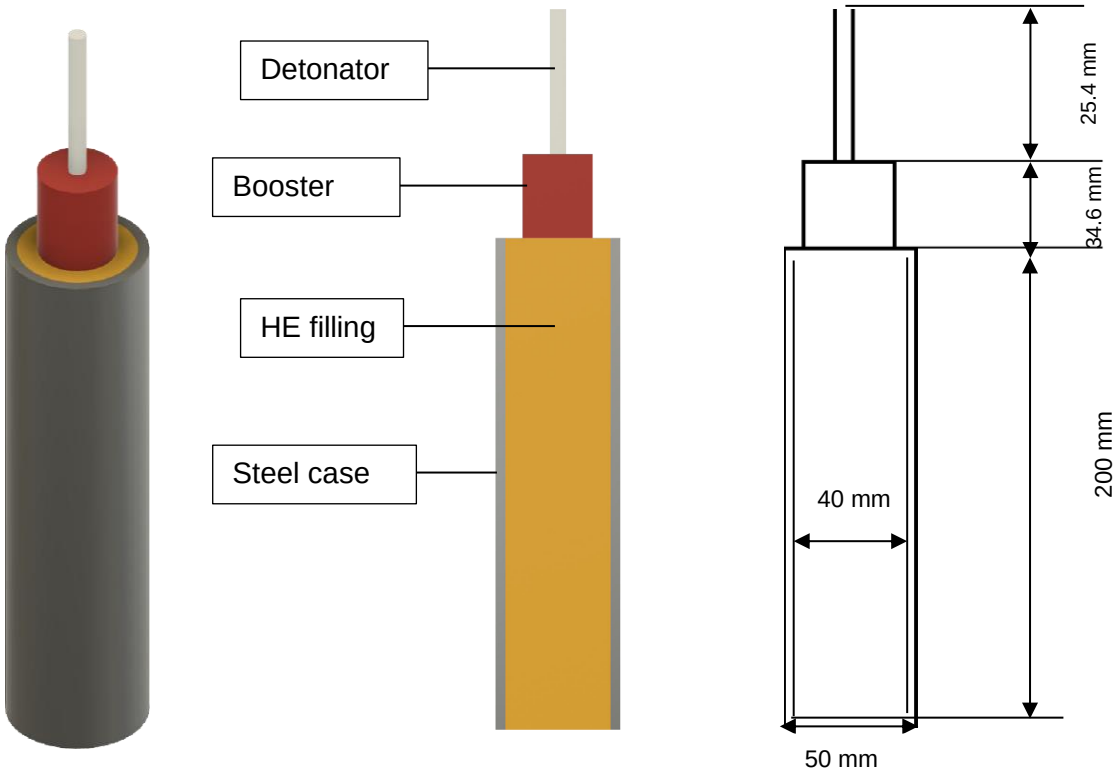

Figure 3-1: Sample item specification.

Machining process

As the performance of HE warhead is dependent on its manufacturing properties, attention must be paid to the preparation of the samples to ensure consistency and to avoid any discrepancy in the results. Furthermore, the material properties can be fabricated with a certain limit to achieve optimum fracturability, which results in enough fragments for the main goal of this test.

For these reasons, the preparation of the samples began when a long rod (round bar) made of EN19 steel was received from the supplier. Figure 3-1 illustrate the samples dimension were cut and machined into pieces as specified for this test and to match the dimensions used in the literature.

A heat treatment process was also applied to the samples to increase the hardness of the material, which led to the enhancement of the brittleness of the material as well. This process can enhance the fragmentation behaviour of the material as discussed in [17].

Finally, the samples went through a quality and control process to record the weight and dimensions of both sides of the samples for analysis, as shown in Appendix 1. This was followed by the next step, which was the filling process.

3.1.2 High-explosive material

Several critical parameters played leading roles in the selection of the HE materials required to accomplish the objectives of this study. The difficulties in choosing the best explosives for this study are summarised in the following three points:

- The first factor was the availability of the explosive material and the filling process, which were the main concerns in the selection of the material.
- The second factor was the performance of the HE material. In accordance with the aim of this study to offer a clear relation showing the dependence of fragmentation characteristics on explosive parameters, this can be achieved by using different types of explosive with large variations in explosive properties; the larger the variation, the stronger the relation we could achieve.
- The third critical factor was the insensitive munition (IM) characteristics, or sensitivity properties of the HE material. Due to the recent tendency in the munitions development field to change from HE to IMs for safety purposes, we focused on IMs without studying their fragmentation characteristics.

Considering these points, five types of explosive were designated for this study: TNT, Comb-B, ONTALITE, MCX-6002 and RXHT-80, as shown in Table 3-2. These five candidates, which are formulated from three main bases (TNT, RDX and NTO), were used purely or in a mixture as filling, as described later in detail. The variety of these explosive materials was intended to yield different explosive parameters such as strain, strain rate and others.

Table 3-2: Explosive properties (data in this table obtained from [5, 65, 66, 67 and 68]).

Explosive Type	$^*\rho_o$	D	P_{CJ}	$\sqrt{2e}$	ΔH_d
Units	(g/cc)	(mm/μs)	(GPa)	(mm/μs)	(kJ/kg)
1. TNT	1.65	6.86	19.57	2.31	4092
2. Comp-B	1.73	7.95	26.30	2.68	4684
3. ONTALITE	1.71	7.37	22.60	2.48	3626
4. MCX-6002	1.79	7.97	27.22	2.86	3790
5. RXHT-80	1.51	7.68	22.20	2.58	4060

* The theoretical maximum density (TMD), or the calculated density from the crystal densities of the ingredients of an explosive formulation, considering their relative proportions.

TNT ($C_7H_5N_3O_6$) or 2,4,6-trinitrotoluene is well known as an HE material and has been widely used in military applications since WWI. It has advantages such as low manufacturing cost, cheap raw materials, safety of handling, low sensitivity to impact and friction, and relatively HE power. These advantages make TNT preferable to other materials. It also has a high chemical and thermal stability, strong compatibility with other explosives, a low melting point for casting and moderate toxicity. Table 3-3 presented the TNT properties obtained from [65].

In our study, two of these advantages determined TNT as our best choice: its availability and low melting point for casting. TNT is used as a base material for other explosive materials such as Comp-B and MCX-6002. TNT was also assigned as a guideline for this study since many studies have used it, and these studies can be used for validation and comparison purposes.

Table 3-3: TNT properties from [65].

Characteristics	Values	Units
Molecular weight	227.13	g/mol
Melting temperature	80.70	^{o}C
Density at 20^{o}C	1.65	g/cc
Enthalpy of formation	–62.07	kJ/mol
Energy formation	–45.44	kJ/mol

RDX is the other candidate available for this study, and it is also known as hexogen, cyclonite and cyclotrimethylenetrinitramine ($C_3H_6N_6O_6$). RDX has a high chemical stability and stronger explosive power when compared to TNT in terms of the energy released during detonation. Pure

RDX is very sensitive to initiation by impact and friction. It can be desensitised by coating the crystals with wax, as in RXHT-80, the final candidate for this study [66].

RDX has a high melting point, as listed in Table 3-4, which makes it difficult to cast, but this can be solved by mixing it with TNT, which results in the mixture known as Comp-B, the second candidate for this study.

Table 3-4: RDX properties from [65].

Characteristics	Values	Units
Molecular weight	222.117	g/mol
Melting temperature	202–204	^{o}C
Density at 20^{o}C	1.816	g/cc
Enthalpy of formation	+70.29	kJ/mol
Energy formation	+92.59	kJ/mol

Comp-B is a mixture of 60% RDX and 40% TNT. It is a relatively high-power explosive with a density that can vary from 1.69 g/cc to 1.75 g/cc and a velocity of detonation between 7.89 mm/µs and 8.2 mm/µs. Comp-B has a low sensitivity to impact and friction and has a HE power in terms of the energy released during detonation.

The main purpose of this study was to have a wide variety of explosives, and **Comp-B** was assigned as one of the most powerful explosives available. It was also chosen with TNTs for a comparison purpose as many studies have been conducted on these two types of explosive.

Overall, five types of explosive with a wide range of properties were sufficient to achieve our goals in this research. Since TNT and Comp-B were used as guidelines in our research, the other three candidates were chosen due to their IM characteristics as replacement material in the future for TNT and Comp-B.

Insensitive high-explosive material

The other three candidates (ONTALITE, MCX-6002 and RXHT-80) were chosen for their sensitivity properties since they have been approved through literature, to be insensitive HE materials for different munitions (IMs) by passing the six-credit test for different impacts. The IM signatures are granted under the international standardisation in STANAG 4439 to avoid accidental initiation.

Generally, the sensitivity of an explosive is defined by the explosive's response to certain types of impact, friction, a spark or another influences. The insensitivity properties of an explosive material can be improved by embedding sensitive HE crystals in a polymeric matrix, as in the case of RXHT, or by combining the highly sensitive material into other relatively insensitive

materials at certain percentages, as in the case of (NTO-TNT) and MCX. Both methods were used in this study.

Nitrogen tetroxide (NTO), therefore, was used in this study as a base filling for the relatively sensitive explosives such as TNT and RDX, at a certain percentage to reduce their sensitivity. The energy released from an explosive material is a dependence factor for its sensitivity. In other words, the percentages used in a mixture are a constant balance of trade-offs between explosive energy output and material sensitivity. The mixture used in this study is found in various publications to be the optimum formulation for maximum performance with minimal sensitivity.

NTO (5-nitro-1,2,4-triazole-3-one [C2H2N4O3]) is a new energetic material with attractive characteristics and high performance, as listed in Table 3-5. It was developed as a potential replacement for RDX and other energetics in military munitions. It has a high reaction heat and is relatively less sensitive than RDX and TNT [69].

Table 3-5: NTO properties from the literature.

Characteristics	Values	Units
Molecular weight	130.06	g/mol
Melting temperature	270–271	^{o}C
Density	1.92	g/cc
Enthalpy of formation	–100.8	kJ/mol
Energy of formation	N/A	

ONTALITE (50-50) is a reference to mixing NTO and TNT explosive materials. The proposed mixture of ONTALITE at a 50**:**50 ratio was developed as a potential replacement for Comp-B. NTO-TNT is currently used in military applications as insensitive HE filling for various munitions, such as the 120 mm mortar bomb.

The MCX-6002 is a reference to mixing NTO, RDX and TNT at a 51**:**34**:**15 ratio. The proposed mixture of MCX-6002 was also developed as a potential replacement for Comp-B. MCX-6002 is currently used in military applications as insensitive HE filling for various munitions, such as 155 mm calibre artillery gun. Studies conducted on this mixture also considered it a preferable choice in the military field, as it exhibits high performance in its IM signature, as published in [68].

RXHT-80 is a reference to mixing 80% RDX with 20% synthetic rubbers to form what is known as a polymer-bonded explosive. This type of formulation was developed to reduce the sensitivity to accidental initiation of pure HE material such as RDX. This type of composition is approved in the literature as an insensitive explosive with high performance in various munitions applications and as a potential replacement for TNT. Five samples were, therefore, prepared for each formulation to accomplish the goals of this study.

Filling process

The filling process is a major concern in the selection of an explosive material. The considered samples were filled in two ways: by the melt-casting method and the cast-curing method (polymer-bonded explosives).

Since one of the main reasons for choosing TNT is its low melting point, it is preferable and available as a casting medium. Pure TNT melts at 80.4°C, which is much lower than its decomposition temperature of 300°C. It is also stable when molten for relatively long periods. Further, it is not affected by surrounding temperatures, and it can, therefore, be safely melted using steam heating. Other explosives such as RDX and NTO can be incorporated into TNT when molten, at a certain percentage to form the desired formulation, such as Comp-B, ONTALITE or MCX, as in our case.

The filling process of these mixtures began when TNT was heated to its melting point. The other explosives such as RDX or NTO were added at a certain percentage during the stirring process to form the desired formulation. For safety purposes, appropriate instruments were used for stirring the mixtures and casting the samples. After casting, the samples were left in controlled cooling processes to prevent cracking or de-bonding resulting from the contraction of the TNT. Once the filled samples were fully solidified and dimensionally stable, special tools were used for the cutting and machining processes.

In the case of RXHT, this formulation consisted of 80% pure RDX and 20% liquid polymer binder to reduce its sensitivity. This method is known as cast curing, and the explosive material in this formulation is known as a plastic-bonded explosive or a polymer-bonded explosive (PBXs) [66].

The curing process mainly depends on controlling the particle size of the explosive to achieve the highest possible percentage of explosive in the formulation. The filling process of the RXHT mixture began with mixing 80% RDX with 20% hydroxy-terminated polybutadiene HTPB (liquid polymer binder). The casting was performed under a vacuum, and the filling was agitated to remove any gas bubbles trapped in the mixture. The curing times were shortened using a slightly elevated temperature.

The explosive material in this formulation provides greater performance and reduced sensitivity relative to those produced using the normal melt-casting method. In contrast, the disadvantage of this method is the low density of the formulation after casting, as presented in Table 3-2, and this is because of the presence of cavities containing air.

Finally, after filling all samples were X-rayed and weighed as a part of quality control and quality assurance to ensure the densities and fillings did not contain serious flaws. The density of the explosive after filling must be close to its theoretical maximum density of formulation, which is a critical factor in the determination of the explosive performance. Appendix1 present a record and picture of the final solidification conditions of the test samples.

3.2 Detonation characteristics (expansion behaviour record)

As discussed in the previous chapter, according to the detonation theory, when a detonation wave passes through an explosive material filled in a cylindrical tube, the products of detonation accelerate the cylinder's material radially, fragmenting the tube material in an outward direction. The expansion behaviour for a casing material differs based on the type of explosive used.

In order to study the dependence of the natural fragmentation behaviour on the type of explosive material, the first part of this study was to characterise the expansion behaviour of the detonation products for different types of explosive in the same cylindrical configuration using the same assembly process, as illustrated in the next section.

3.2.1 Cylinder test

The expansion behaviour is a considerable factor when characterising explosive materials. The standard cylinder test, as discussed in the literature chapter, was developed along with several analytical models to characterise the expansion behaviour of the detonation products of an explosive material from the initial to the final stages of expansion. The initial movements of the cylinder material refer to P_{CJ}, whereas the final condition of the expansion behaviour refers to the final velocity related to the Gurney constant $\sqrt{2e}$.

The strain and the strain rate are the failure criteria that characterise the expansion behaviour depending on the expansion volume and the acceleration rate of the detonation products. The strain and the strain rate were addressed in the analytical models from the literature and are based on the radial displacement of the wall elements over time.

In this study, a test was designed that employs equipment, described in the following sections, to record the expansion history of the cylinder material to generate the relationship of wall displacement to time, which was the main purpose of this test. The displacement–time relation is used to extract the relation of velocity and acceleration to time through derivation. Our study focused on the acceleration time and its effects in the final distribution of fragments, as discussed in the next chapter.

3.2.1.1 **Cameras**

Two Imacon cameras were employed: one in streak mode to record wall displacement and the other in framing mode to record detonation development during the test. A high-speed video (HSV) camera was also employed for corroboration.

Streak camera

The streak camera is the leading tool available and is widely used in the explosive research field to record the expansion behaviour of an explosive being characterised. A streak camera record depends on the arrival time of the detonation front, the film width and the writing speed of the camera. The camera observes the detonation through a slit, which is focused on a point on the cylinder where it will begin recording. In order to capture the full detonation, this point must be far enough from the beginning and the end of detonation. This point is thus usually chosen to be at 2/3 of the cylinder length from the start of the cylinder. Timing is critical to capture the detonation front as well as to leave enough space on the film to record the expansion. Therefore, a calibration process was applied using an electric impulse to check the writing speed of the camera and to specify the strict width of the film. In addition, an illumination source is required in this test for visualisation. The characterisation of the timing of the back light is also critical, as will discuss later in this chapter. For these reasons, several tests were conducted to characterise the initiation system material (detonator, booster, velocity of detonation and light source).

For completion, the following points must be considered when recording an expansion history using a streak camera:

- The writing time of the events depends on the writing speed, which must be determined beforehand.
- The film width is also a critical factor in the analysis of the streak photograph and is calibrated through separate tests, and the film width must be determined for each photograph.
- The quality of the photograph depends on the width of the slit used, the distance to the object under consideration, the focus of the camera and the density of the light detected.

The photographs obtained and their analysis are discussed in the next chapter.

High-speed video and framing camera

High-speed framing camera are used to record the development of the detonation of the cylinder samples. An HSV camera was also available and was used at a speed of 200,000 frames/second. The pictures obtained from both camera is only used to investigate inconvenient event when happened.

3.2.1.2 Cylinder test setup

The test setup for the cylinder test was performed according to the arrangement of the equipment's illustrated in Figure 3-2.

- The framing camera, the streak camera and the HSV camera all used in protection room as shown in the right picture.
- The sample item (cylinder), flash source and back light have been arranged in the same line with the streak camera as shown in the left picture.
- The streak camera as the main method to record the expansion behaviour have been set to focus at the (2/3)L point of the cylinder item and the firing circlet of the sample are described in the following section.
- The BEW firing box has been used as a special firing for RP-83 detonator.

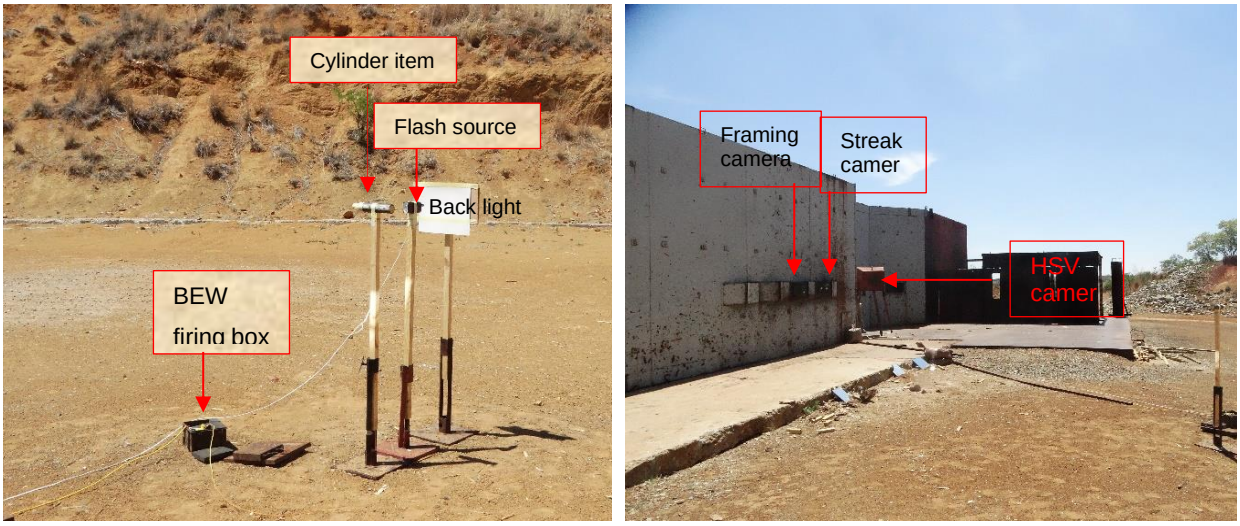

Figure 3-2: Photographs of the cylinder test setup.

3.2.1.3 Illumination and initiation circlet

In order to enhance the quality of the photographs used for analysis, Argon bombs are often used as a background illumination source for streak camera photography. In our case, a flash source

was employed as an alternative solution to the Argon bomb. The illumination time was characterised beforehand to synchronise the initiation of the cylinder item with the experiment. The illumination time was pre-set by using delay generators in the streak camera. The illumination intensity versus time recorded from the flash source every 20 µs is shown in Figure 3-3. The degree of intensity of the light is recorded relatively to the light occurrence of the flash during lightning.

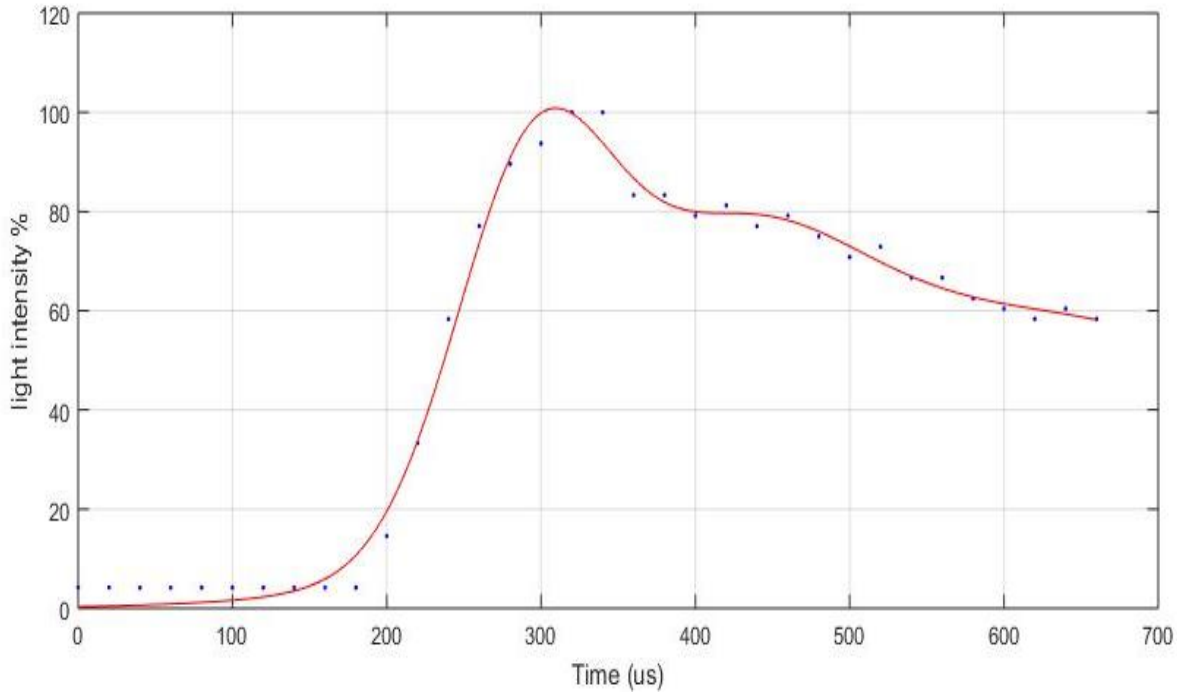

Figure 3-3: Light intensity versus time.

The test item must be initiated at a time when the illumination density is at a maximum as in Figure 3-3. The synchronisation of the cylinder to fit within the illumination time period required a fast-action exploding electric bridge wire detonator. The electronic circuit for the initiation after characterisation is shown in Figure 3-4.

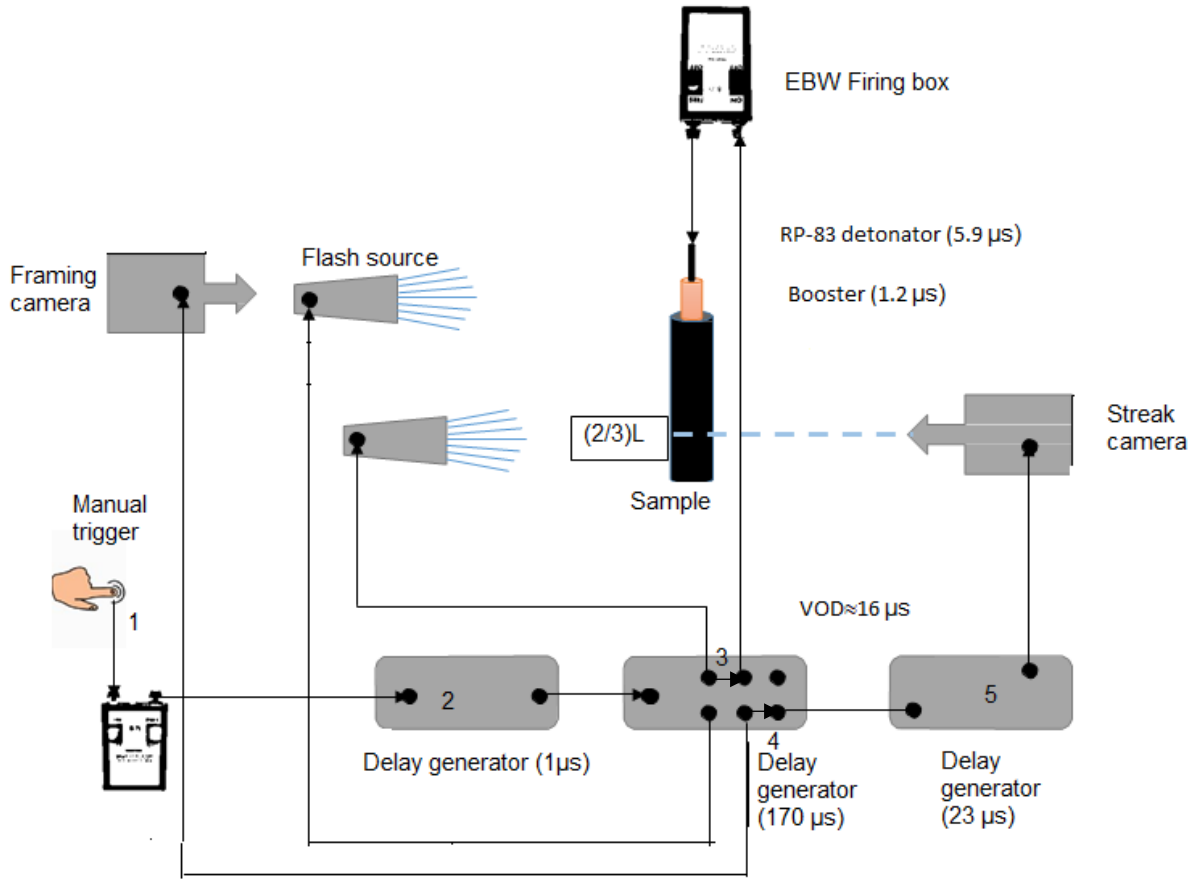

Figure 3-4: Schematic of the initiation system layout and the test setup.

After characterizing the time for each component of the initiation system (detonator and booster), the illumination source and the detonation, the final layout of the initiation circlet was arranged as follows:

1. An initiation signal is sent manually from the first exploder to the first delay generator.
2. The signal is delayed approximately 1 µs before it is released again for de-bounce (to reorganize the trigger pulse).
3. The signal is sent from the first delay generator to another delay generator waiting for the flash source to amplify the back light.
4. After 170 µs of waiting for the light to be amplified, a signal is sent from the second delay generator to the electric bridge wire exploder to initiate the test sample through the RP-83 detonator.
5. By measuring the signal time taken from the detonator to the 2/3 point on the cylinder item (5.9 µs +1.2 µs + velocity of detonation), a signal is released again from the second to the third and last delay generator to trigger the streak camera to begin recording.

The main output of this test is a streak photograph presenting the expansion behaviour of the cylinder under the effect of the detonation products to be analysed, as illustrated in the next chapter.

3.3 Fragmentation characteristics (arena test)

The distribution of the fragmentation caused by the interaction between a detonation load and an inert casing material is complex and considered as a natural event that can be characterised statistically. The first part of this study, as previously described, was to characterise the interaction between a detonation wave and the inert material from the first to the final stages of the expansion. The second part of this study was to characterise the fragmentation results from this interaction in terms of final velocities, masses, numbers and spatial dispersion. The fragments were accordingly captured for characterisation by using a catch-box technique designed for this study and by using an aluminium witness plate (AL plate) with an HSV camera to characterise fragment velocities.

The following information was obtained from this test:

- Fragment velocity distribution per 5° sector.
- Fragment mass distribution per 5° sector.
- The number of fragments per 5° sector.

The arena test can be used to obtain this information in a standard way. It is an international standard used to characterise the fragmentation of symmetrical warheads in the manufacturing field. The International Test Operations Procedure (ITOP-4-2-813) documents were developed for such a test [70]. The arena test discussed in the (ITOP-4-2-813) documents is used as a guideline in our study, as described here.

3.3.1 Arena test

A static fragmentation test of HE munitions is widely used in the military filed to characterise fragmentation in terms of mass, shape, velocity, fragments spatial distribution and other fragmentation characteristics to evaluate the performance of a fragmentation warhead as part of the qualification and development process.

The typical arena used for munitions is designed to capture the fragments horizontally from the nose to the rear of the warhead; it is circular or rectangular arena based on the specification and the type of munition under consideration. Approximately one half of the arena, or 180°, is lined

with catch boxes designed to capture fragments expelled from the munition upon detonation, and correction factors are then used to integrate for the entire body of the test item. The sample used in our case is symmetric and relatively small compared to military munitions, and one panel of wood was used vertically at a distance of R=1 m.

The test depends mainly on the dimensions of the capture boxes and the AL plates, as described in detail in the next section.

Capture box technique (soft recovery for fragment number and mass characterisation)

The arena fragmentation tests described in ITOP 4-2-813 assume that the warhead being tested is considered as a point source for fragments. This is done under the assumption that the arena is large enough that the warhead's relative dimensions are not significant in relation to the arena. Therefore, the test item must be centred in the arena and shaped into a rectangular or circular arena as standard in the ITOP document.

The capture boxes in our test have been designed to a rectangular arena and divided into sectors with defined size based on the projection angle of fragments. The capture box sectors sizes and the AL plate sectors are, therefore, determined with the centre of the sample item as the point source. Figure 3-5 illustrate the layout of the arena test designed for this study.

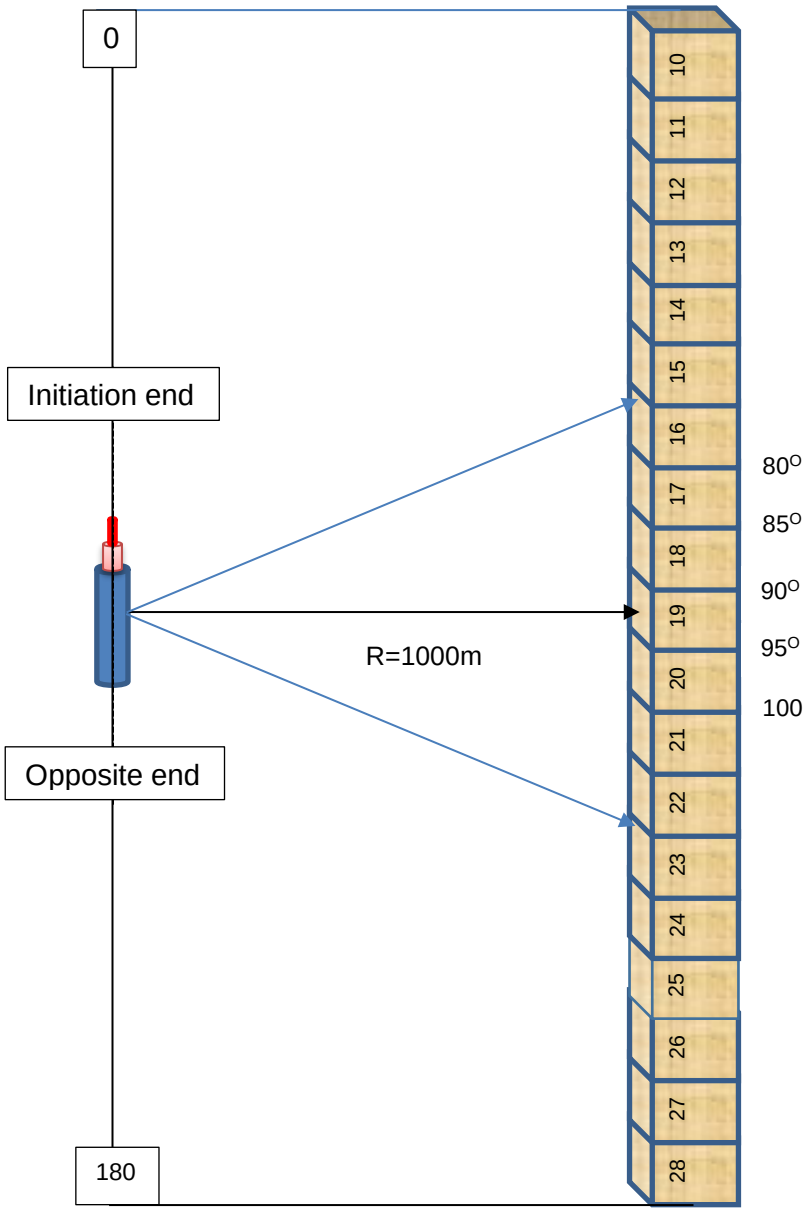

Figure 3-5: Catch box characterization.

The distance from the sample item to the capture box panel is R; the angle interval, or the angular polar zone from nose to base, is θ; and the azimuth angle, or the spray area around the sample, is φ. These are two the main criteria for this characterisation; the angular polar zone is used to determine the width of the sector and the azimuth angle is used for the determination of the correction factor.

In this test, the angular zone is designed to be a 5° angle (θ = 5°) to be determined from the initiation end to the opposite end (180°) of the sample item under consideration and this corresponding to the width of the sectors. The height of the sector is the determinative factor for the azimuth angle (φ angle), and vice versa, which is used to correct for 360° around the sample and is recommended to be close to 10°. Consequently, the width of a sector, in this case, would

be 352.6 mm. However, the greater the width, the more fragments are captured. In our test, therefore, we chose the width of a sector to be 450 mm, which helps to capture more fragments. Based on the amount of the explosive used on the sample item (< 0.45 kg), a distance R of 1 m was used between the test item and the catch box, which was proven from modelling predictions to have no blast effect or other secondary effects in this distance on the wooden boxes.

In accordance to ITOP documents, we covered the area from 45° to 135° with 19 polar zones perpendicular to the test item by adding 2.5° for each panel to provide average data for each interval. The sample item in this specification is aligned at 90° with the centre of the capture boxes, resulting in the centre of panel 19 representing 92.5° and corresponding to the centre of the item test. Figure 3-6 present an illustration of the dimensions between the centre of the sample item and the centre of the catch box corresponding to a triangular shape. A distance of 1 m represent the length of the triangle (R) in red colour and polar zone angle of 2.5° is used to determine the width of each sector. (H) in green colour represent the height of the sector corresponding to the azimuth angle, which used to calculate the correction factor (f).

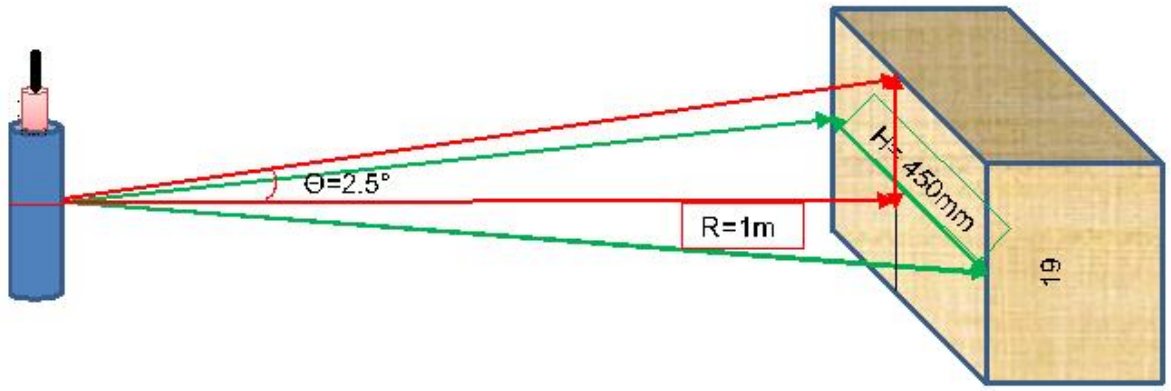

Figure 3-6: Dimensions for catch box characterization.

Correction factor (*f*)

As previously mentioned, the sample being tested is assumed to be the point source of fragments, and fragments are expelled away from this point uniformly in every direction. Under the listed assumptions and specifications, the recovery panels covering only a small section of the circumference of the warhead and the representative area of recovery.

In order to account for the possible number of fragments produced from the total mass, different scale factor can be used. The total number of fragments can be scaled by the collected mass or by the projection area or the projection angle of particular sector.

In accordance to ITOP document, the projection area of a particular sector is recommended. The total number of fragments in a circumferential sector are then obtained by scaling the number of fragments in that particular sector. In this case, the scale factor f can be obtained by calculating the representative projection area for each zone A_{panel} relative to the circumferential area A_{circ} to that zone:

$$f = \frac{A_{circ}}{A_{panal}} \qquad 3\text{-}1$$

In the cylindrical sample case, where no curvature and most of the fragments fall in the small angular zone between 70° and 120°, one correction factor would be sufficient and that can be calculated from the representative projection angle or the azimuth angle as mentioned (φ):

$$f = \frac{360}{\varphi} = \frac{360}{2\tan^{-1}(\frac{\mathrm{H}}{2\mathrm{R}})}. \qquad 3\text{-}2$$

Where:

$$\tan\frac{\vartheta}{2} = \frac{\mathrm{H}}{2\mathrm{R}}, \qquad 3\text{-}3$$

The correction factor value (f) therefore depends on the height of the box (H) and the distance between the sample and the catch box (R).

Catch boxes specification

The catch boxes used in this test were filled with 16 mm-thick pressboard cut to the size of each 5° section, with the centre of the sample considered as the source of the fragments and each board marked with its angle. In this test, eight layers of pressboard were used.

The capture box specification for this test was the following:

- Azimuth angle (2 x 12.680°) equal to H = 450 mm (height).
- Angular zone or polar zones (50°) from initiation end to opposite end (width).
- Catch box thickness (16 mm * 8) equal to 128 mm.
- Sectors numbered from10 to 28.
- 90° alignment with respect to the centre of the catch boxes.
- 1m radius (R= 1,000 mm), or the distance between the sample and the catch box.

The correction factor sometime can results to a total mass of fragments greater than the original mass of the body of the sample, which is illogical. Moreover, the correction factor is normally used to predict the lethality of warhead. For this study, the scale factor is more reasonable to be corrected through the mass of the collected fragments relative to the original mass of the body of the sample if needed. However, the original mass have been scaled in this study to extract the optimum value of μ in Mott distribution function as will discussed in next chapter.

Fragment characterisation procedure

The cumulative number of the collected fragments are the outputs of this characterisation, which can be obtained under the standard specification described here:

- After each test, the pressboard of each sector was burned separately, and the fragments were recovered.
- The fragments were also classified into different mass zones.
- The fragments were then weighed, counted and classified into the standard angular and mass zones.

The main output of this test was a characterisation of the captured fragments into their mass, number and angular zone, as presented in Table 3-6.

Table 3-6: Raw data of the fragment characterisation of the detonation of the test cylinder filled with ONTELIT, test number 1.

Mass Category (g)	075-080	080-085	085-090	090-095	095-100	100-105	N(m)	N(>m)
	Number of fragments per angular zone							
0.01 - 0.09	4	6	4	7	6	2	29	95
0.1 - 0.19	1	3	4	5	2	3	18	66
0.2 - 0.29	0	0	0	0	2	2	4	48
0.3 - 0.39	0	0	0	2	4	1	7	44
0.4 - 0.49	2	0	0	1	2	0	5	37
0.5 - 0.74	0	0	0	2	1	1	4	32
0.75 - 0.99	0	0	2	1	6	0	9	28
1 - 1.99	0	1	0	3	5	1	10	19
2 - 2.99	0	1	0	0	4	0	5	9
3 - 3.99	0	1	1	0	1	0	3	4
4 - 4.99	0	0	0	0	0	0	0	1
5 - 7.49	0	0	0	0	0	0	0	1
7.5 - 9.99	0	0	0	0	0	0	0	1
10 - 14.99	0	0	0	0	1	0	1	1
Sector Totals	7	12	11	21	34	10	95	

A minimum of three tests have been conducted for each type of explosive as recommended. The dependence of natural fragmentation characteristics on explosive parameters will be investigated through the cumulative number distribution of the collected fragments of the three tests. The average fragments mass of the collected fragments will be used as the critical parameters for this investigation. Mott distribution function will be used to extract the critical parameter (μ) for the average fragments mass. The optimization process used to extract the critical parameters (μ) is discussed in next chapter. Similar process have been followed to extract the critical parameters for all explosive material. In this study, the total number of the collected fragments of the three test is used. Table 3-7 presented the total and the cumulative number of the collected fragments of the three tests resulting from the detonation of ONTELIT.

Table 3-7: Total cumulative number of fragments of three tests of ONTELIT explosive.

Mass Category (g)	075-080	080-085	085-090	090-095	095-100	100-105	105-110	130-135	135-140	N(m)	N(>m)
	Number of fragments per angular zone										
0.01 - 0.09	4	10	10	21	26	3	0	0	1	74	241
0.1 - 0.19	1	5	6	12	7	6	1	0	0	38	167
0.2 - 0.29	0	2	2	3	6	2	0	0	0	15	129
0.3 - 0.39	0	1	0	4	6	2	0	1	0	13	114
0.4 - 0.49	3	1	0	3	4	1	2	0	0	14	101
0.5 - 0.74	0	2	3	4	6	3	0	0	0	18	87
0.75 - 0.99	0	0	2	2	7	2	0	0	0	13	69
1 - 1.99	0	2	6	5	13	2	0	0	0	28	56
2 - 2.99	0	4	0	2	5	1	0	0	0	12	28
3 - 3.99	0	2	2	0	3	0	0	0	0	7	16
4 - 4.99	0	0	2	0	1	1	0	0	0	4	9
5 - 7.49	0	0	0	2	0	0	0	0	0	2	5
7.5 - 9.99	0	0	0	0	0	0	0	0	0	0	3
10 - 14.99	0	0	0	1	1	0	0	0	0	2	3
15 - 19.99	0	0	0	0	0	0	0	0	0	0	1
20 - 29.99	0	0	0	1	0	0	0	0	0	1	1
Sector Totals	8	29	33	60	85	23	3	1	1	241	

All raw data have been attached in Appendix 2 in the same format to be analysed and discussed in the next chapter.

High-speed video camera technique (fragment velocity characterisation)

By following the same concepts of the catch box technique, the fragment velocities were determined per angular zone using AL plates and an HSV camera as described in this section.

Aluminium plates were used because they are illuminated when hit by fragments, and this illumination is then recognised by the record of the camera. The AL plates were allocated 1m away from the sample item in a 90° alignment with the centre of the sample item, as in the catch box specification. The HSV camera was located at a distance in protective glass behind the AL plates. A mirror was also placed approximately 2 m away from the sample item to indicate time zero from the initiation of the sample item, as illustrated in Table 3-7.

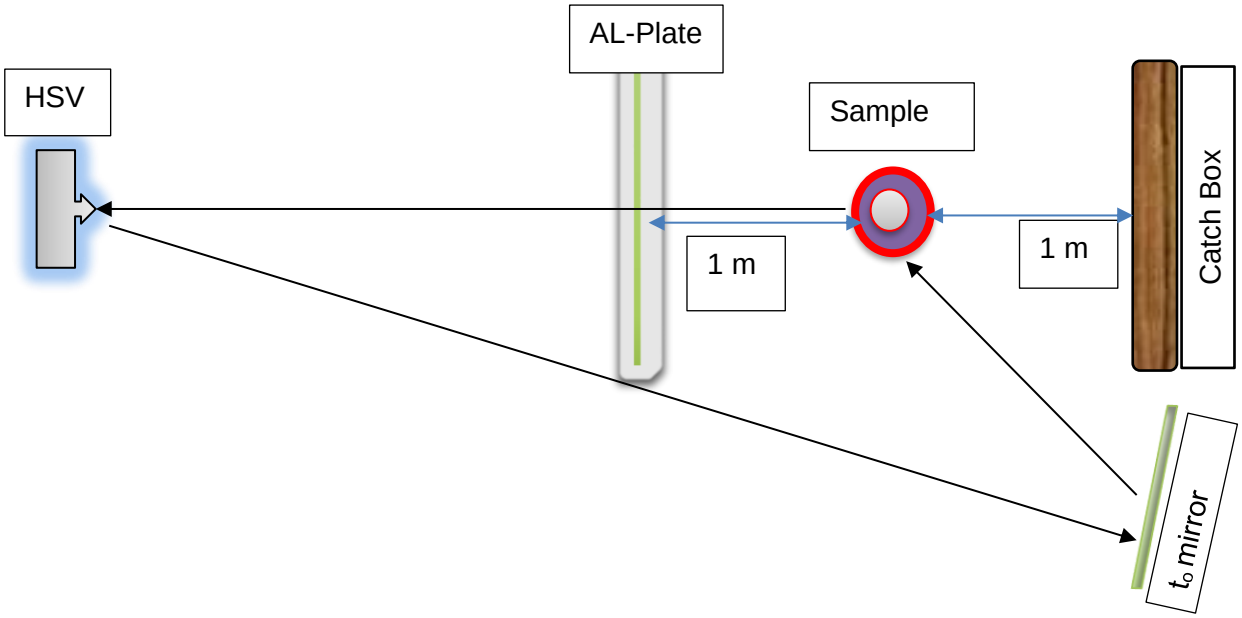

Figure 3-7: Fragmentation velocities layout from arena test.

The fragment velocity of each fragment in each angular zone could then be determined from time zero of the fragments captured from the t_o-mirror, the distance between the sample items and the AL plate, the dimensions of the AL plate and the speed of the camera. A simple numerical program in MATLAB was used for this calculation.

For fragment velocity determination, the following specifications were standard for this test:

- A distance of 1 m was used between each AL plate and the sample item.
- Each rectangular AL plate dimension was 1.25 m^2.
- 10 000 frames/s is recommended for the velocity calculation by the ITOP documents.
- By counting the frames and the number of fragments in each angular zone, the average velocity was obtained.

The main output of this test was the average velocity characterisation per angular zone for each formulation as presented in Table 3-8, and it was used to verify the streak results and for further analysis, as illustrated in the next chapter.

Table 3-8: Fragment velocities per sectors of ONTELIT, test number 2.

Sectors	Number of fragments	Average Distance	Average Velocity	Minimum Velocity	Maximum Velocity
Units		m	m/s	m/s	m/s
75 to 80	1	1.024	1164.3	1164.3	1164.3
80 to 85	9	1.009	1144.9	1007.1	1294.6
85 to 90	11	1.001	1256.9	1110.6	1358.1
90 to 95	11	1.001	1405.2	1260.3	1485.67
95 to 100	14	1.009	1450.7	1358.4	1540.1
100 to 105	10	1.024	1373.9	1238.4	1468.3
105 to 110	4	1.049	1189.4	1053.3	1355.3
110 to 115	0	1.082	0	0	0

An average fragments velocities of the three tests have been used. This part is the standard method used in an arena test to characterize the velocity of the fragments of a detonated bomb. This method has been included in this study only to verify the velocity extracted from the cylinder test and to the velocity calculated from Gurney model. The velocities extracted from these methods have been attached in the table of the cumulative number of fragments in Appendix 2.

The overall test setup for the arena test

A simple arena of catch boxes and AL plates was designed for fragment characterisation following the guidelines of the ITOP documents with the overall test setup. Figure 3-8 present a photographic illustration of the arena and the test setup used in this study. Two mild steel plates have been added to the configuration for further analysis of perforation, if needed.

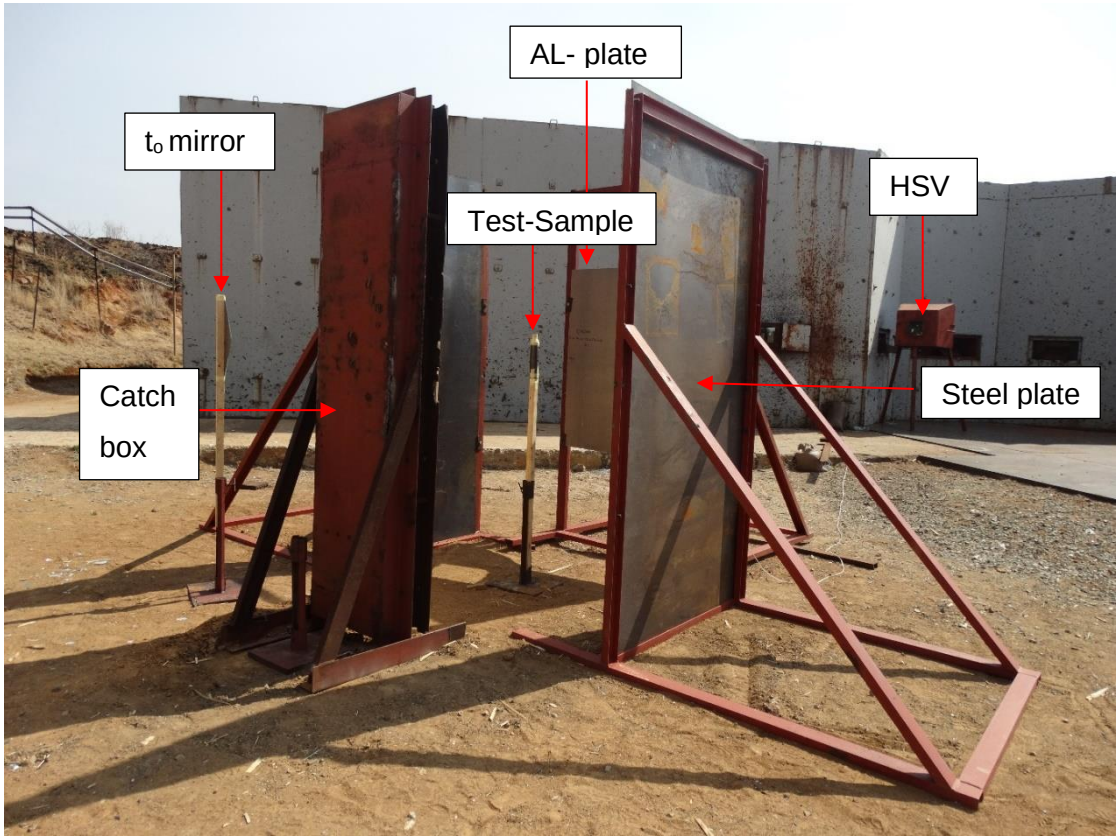

Figure 3-8: Photograph of the arena fragmentation test setup.

3.4 Overall test setup and procedures

The overall test setup was designed to simultaneously characterise the expansion behaviour of a cylinder and to characterise the fragments produced from the detonation of this cylinder. Figure 3-9 present a schematic illustration of the overall test setup designed for this study.

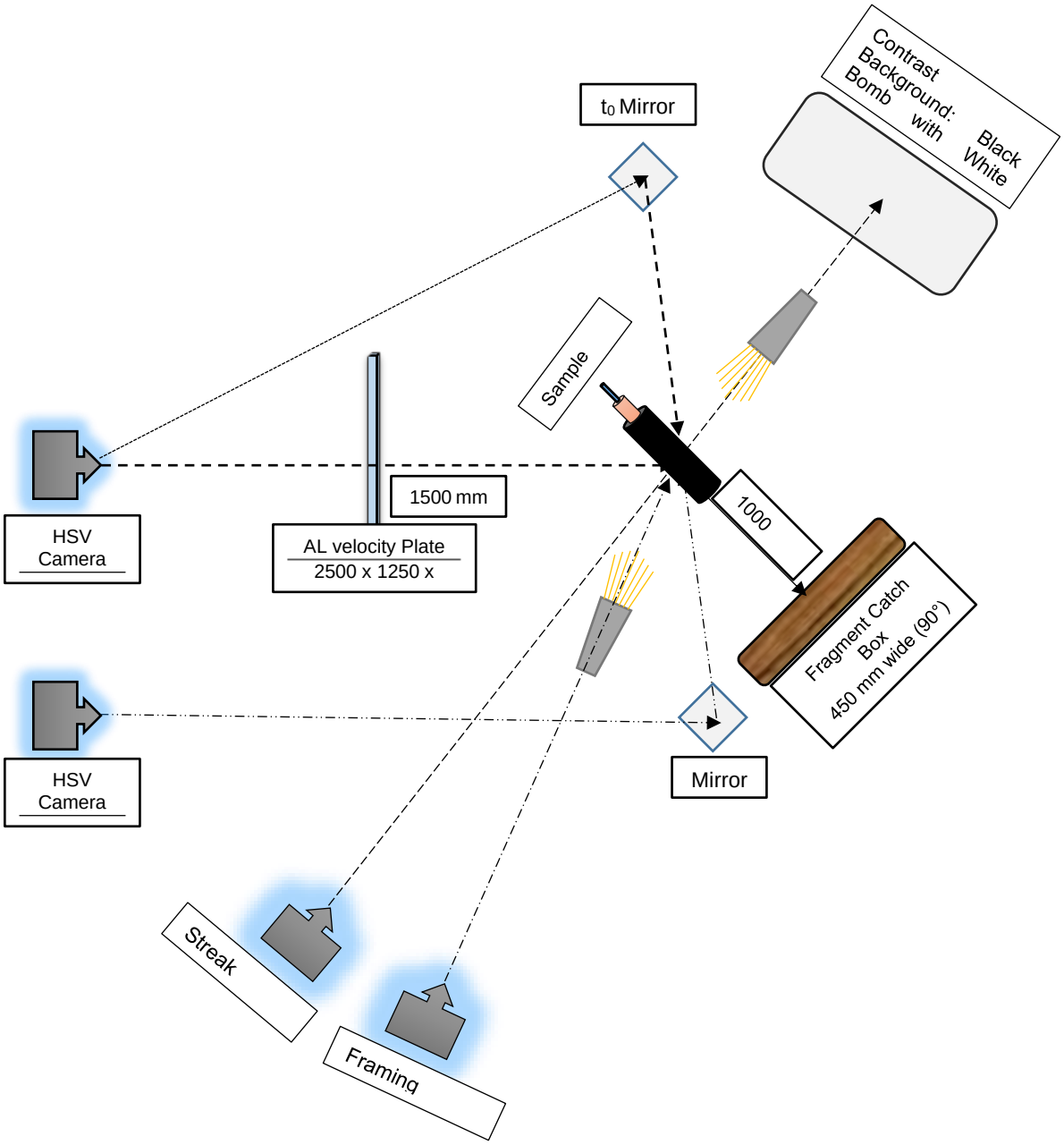

Figure 3-9: The overall test setup for both fragmentation and expansion characterisation

To guarantee more information and to generate reliable data in the same condition, six tests were planned for each type of explosive. However, for safety reasons, limited resources and company policy, the tests were conducted separately: three experiments for fragmentation characterisation and two for expansion characterisation with the same material.

In total, 25 tests were conducted for this study, and the results and the analysis of the data obtained are presented in the next chapters.

3.5 Conclusion

The methods used to gather the desired data to study the dependence of the natural fragmentation characteristics of a casing material on explosive parameters were conducted as presented in this chapter.

Twenty-five cylinder samples were prepared carefully for the aims of this study. The samples were made of alloy steel (EN19), fabricated and manufactured with specific dimensions to meet the requirements of this study. Five types of explosive were selected under certain limitations to achieve a wide range of strain and strain rates; these explosives were TNT, COMP-B, ONTELIT, MCX-6002 and RXHT-80.

A combination of two tests using available apparatuses was designed to generate specific data for use in our investigation. A high-speed streak camera was used to characterise expansion behaviour. An HSV camera was used in conjunction with AL plates for terminal velocity characterisation in different polar zones. A high-speed framing camera was used with the HSV camera for validation purposes. The catch box technique was employed to catch the fragments in different polar zones for fragment characterisation.

A brief description of the methods used was published under the title of "**The Dependence of Natural Fragmentation Characteristics of a Casing Material on Explosive Parameters**" in a SABO symposium [71]. The results and analysis of the data obtained are presented in the next chapters.

CHAPTER 4: ANALYSIS

The results obtained from the tests discussed in the previous chapter were used in an analytical procedure detailed herein to extract the optimum data, generate figures and investigate dependencies as outlined in the scope of this study.

The expansion behaviour of metal accelerated by the detonation products used to characterize the strain and the strain rate as the failure criteria of the material through the analysis of streak photography. In addition, the average fragment mass and the number distribution of the collected fragments were used in a correlational study between the explosive parameters and fragmentation characteristics.

4.1 Cylinder test analysis

The acceleration recording of a cylinder wall contains crucial information regarding the fragmentation process. The internal pressure is a major source of this acceleration behaviour, but other effects such as shock reverberation and heat of detonation may also affect the fragmentation.

A photograph is shown in Figure 4-1 of the recording of the expansion behaviour of the metal cylinder (in this case filled with ONTELIT) as captured by the high-speed camera described in the previous chapter.

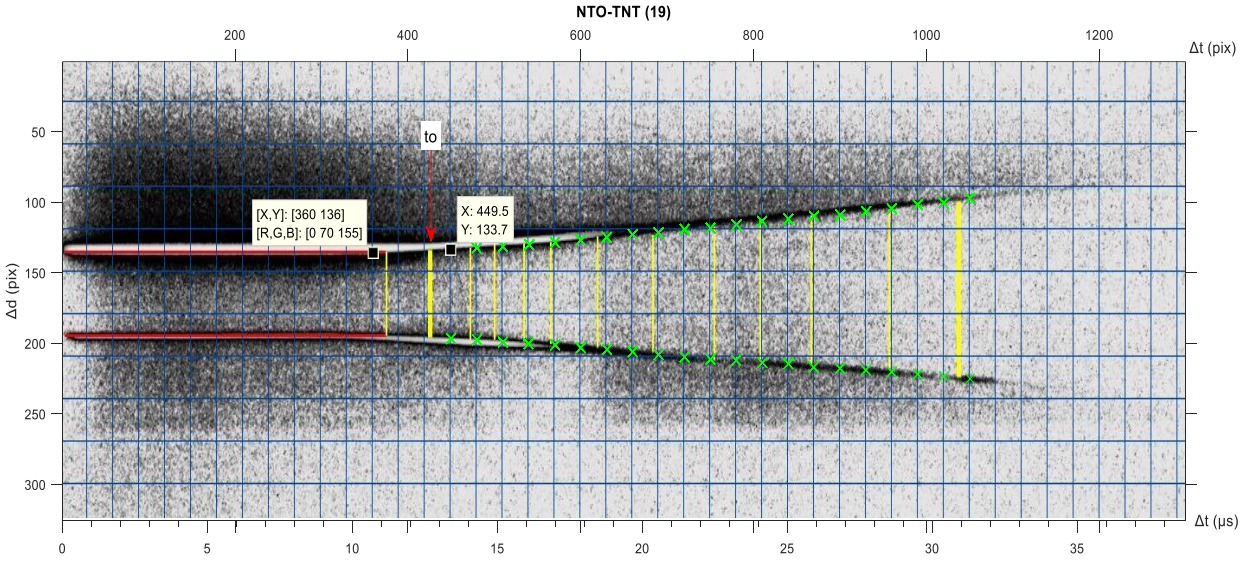

Figure 4-1: Discretisation process of the streak photograph of (ONTELIT).

The streak photograph we obtained recorded the tube diameter at a single cross-section of the cylinder wall during the acceleration process. This photograph represents the behaviour of the detonation products from initial to final expansion. The measurement position was chosen to approximate the steady-state expansion of any other position on the metal tube. The writing speed of the camera and original radius of the cylinder were the main parameters for the streak photograph analysis.

A simple numerical program was designed to discretise the horizontal axis and vertical axis of the photography obtained of the expansion behaviour as shown in Figure 4-1. The width, or horizontal-axis, of the photograph, represents the time extracted from the writing speed of the camera and the width of the camera slit. The height, or vertical-axis, of the photograph represents the expansion radius of the detonation product based on the initial diameter of the cylinder item.

An arbitrary initial point was chosen for the origin of the expansion of the tube. This point is assumed to coincide with the end of the reaction zone, or (P_{CJ}), and the beginning of the fragmentation process, (t_{o}). The appearance of smoke (manifesting as a blurred region in the streak record) indicates the end of the fragmentation process and represents the final velocity of the accelerated metal (v_f). The determination of the explosive expansion parameters relies on the determination of the initial and the final points.

The determination of the boundary condition in this study was crucial and could have affected the final results. For this reason, a fitting process employing an empirical equation of motion was applied, as described in the next section.

Fitting process

The final velocity and the acceleration time of the metal accelerated by the products of detonation are the main variables that characterise the effects of the explosive material under consideration. The two quantities are extracted from the analysis of the streak photograph obtained during the expansion of the cylinder item.

In order to achieve the optimum value of (t_{o}) and (v_f), a minimum of 20 points were placed on the obtained recording, beginning from the final point where the smoke began to appear (if it was observed) and ending (in a backward direction) with the point where the cylinder appears to have begun moving (t_{o}).

The data obtained from the streak photograph were initially obtained from raw data in pixel units, representing the horizontal -axis and vertical-axis, as listed in Table 4-1.

Table 4-1: Radial expansion data of ONTELIT in pixel units as taken from the streak photograph.

No	X1	X2	Y1	Y2	ΔXi	ΔYi
	pix	pix	pix	pix	pix	pix
1	449.5	449.9	133.7	196.8	9.7	63.1
2	479.7	479.9	132.5	197.6	39.8	65.0
3	510.0	509.9	131.4	199.2	69.9	67.7
4	540.3	539.5	130.2	200.4	99.9	70.1
5	570.4	570.4	128.6	201.2	130.4	72.6
6	600.0	600.0	127.0	203.2	160.0	76.2
7	630.0	630.4	124.9	204.5	190.2	79.5
8	660.0	660.1	122.9	206.1	220.0	83.1
9	690.1	690.1	121.7	208.1	250.1	86.4
10	720.1	720.1	119.3	209.7	280.1	90.4
11	750.1	750.1	118.4	211.4	310.1	92.9
12	780.1	779.7	116.0	212.2	339.9	96.1
13	809.7	810.2	113.6	213.8	370.0	100.2
14	840.2	840.2	112.0	214.6	400.2	102.6
15	869.8	869.4	109.9	217.0	429.6	107.1
16	900.2	899.8	109.1	217.9	460.0	108.7
17	930.3	929.8	106.7	219.1	490.1	112.3
18	959.9	959.9	104.7	220.3	519.9	115.6
19	989.9	989.9	101.8	221.9	549.9	120.0
20	1019.9	1020.3	100.6	223.5	580.1	122.9
21	1050.4	1050.3	97.3	225.2	610.3	127.8

A simple analytical process was applied to convert the horizontal -axis from pixels to μs, based on the writing speed of the camera and the camera slit width. Another process was applied to the vertical -axis to convert it from pixels to mm, based on the initial radius of the cylinder wall, as listed in Table 4-2.

Table 4-2: The radial expansion data processed for ONTELIT.

No	ΔX	Δd_2	r_o	Δt	Δr_m
	mm	mm	mm	μs	mm
1	0.54	50	25	0.29	0
2	2.24	51.53	25.76	1.18	0.84
3	3.93	53.70	26.85	2.08	2.03
4	5.61	55.61	27.81	2.97	3.07
5	7.32	57.54	28.77	3.88	4.11
6	8.99	60.44	30.22	4.76	5.66
7	10.68	63.01	31.50	5.66	7.03
8	12.36	65.90	32.95	6.55	8.56
9	14.05	68.47	34.23	7.45	9.92
10	15.74	71.69	35.84	8.34	11.60
11	17.42	73.62	36.81	9.24	12.61
12	19.10	76.19	38.09	10.12	13.95
13	20.79	79.41	39.70	11.02	15.62
14	22.49	81.33	40.66	11.92	16.62
15	24.14	84.87	42.43	12.80	18.45
16	25.85	86.16	43.08	13.70	19.11
17	27.54	89.05	44.52	14.60	20.60
18	29.21	91.62	45.81	15.48	21.93
19	30.90	95.16	47.58	16.38	23.74
20	32.60	97.41	48.70	17.28	24.89
21	34.30	101.27	50.63	18.18	26.87

For a better approximation, the change Δr_m from the outer radius r_o to the centre radius r_m, during expansion was used instead of the outer radius [72]:

$$\Delta r_m = F_m(t) = r_m - R_m = \sqrt{r_o^2 + \frac{R_i^2 - R_o^2}{2}} - \sqrt{\frac{R_i^2 + R_o^2}{2}} \qquad 4\text{-}1$$

where R_i, R_o and R_m are the radii of the inner, outer and mean circles at the initial position, respectively, and r_o and r_m are the radii of the outer and mean circles, respectively, at any time and position during the expansion of the hollow tube, as illustrated in Figure 4-2.

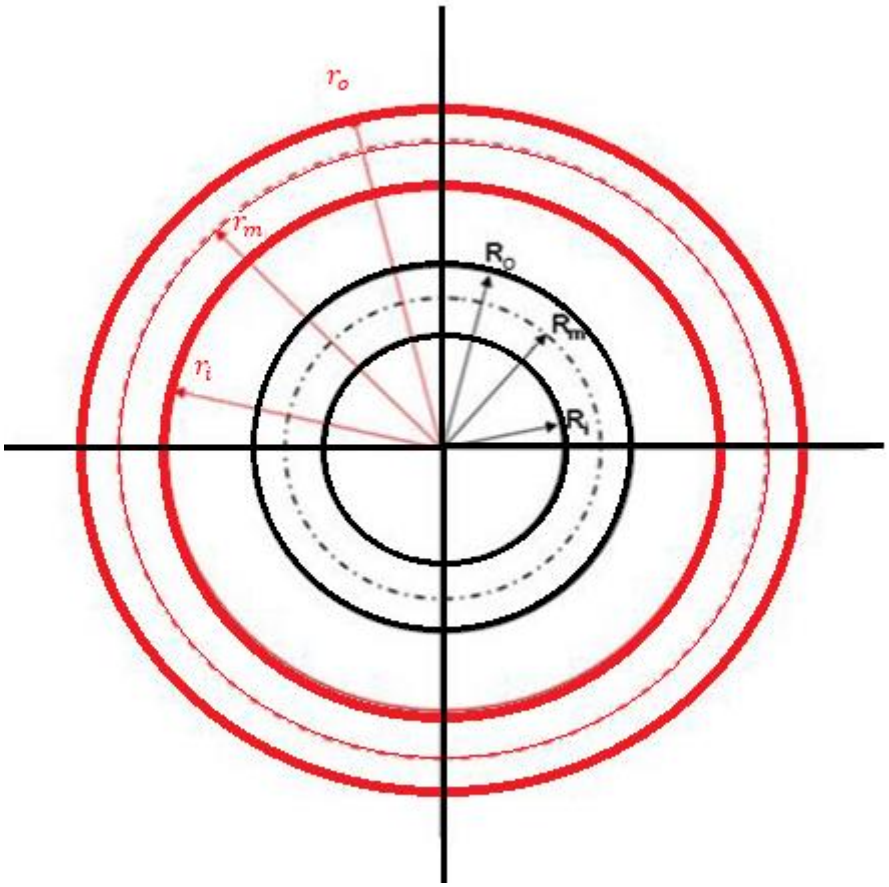

Figure 4-2: The schematic of a cross-section of the cylinder casing [72].

The data presented in Table 4-2 are the experimental data of the radial positions of the cylinder wall under acceleration at the corresponding discrete times. In order to simulate the cylinder's behaviour, an analytical approximation function was employed:

$$F(t) = \sum_{i=1}^{2} a_i\left[b_i t - \left(1 - e^{-b_i t}\right)\right] \qquad 4\text{-}2$$

where a_i and b_i (i = 1, 2) are numerical parameters to be optimised, and only one addend is used in this analysis. In the optimisation process applied to the experimental data, the optimum numerical parameters extracted for ONTELIT explosive are presented in Table 4-3.

Table 4-3: Equation of motion parameters for ONTELIT.

t_o	0.2	μs
a	1.578	mm/μs
b	0.55	1/μs

The fitting curve result of the optimisation procedure are illustrated in Figure 4-3.

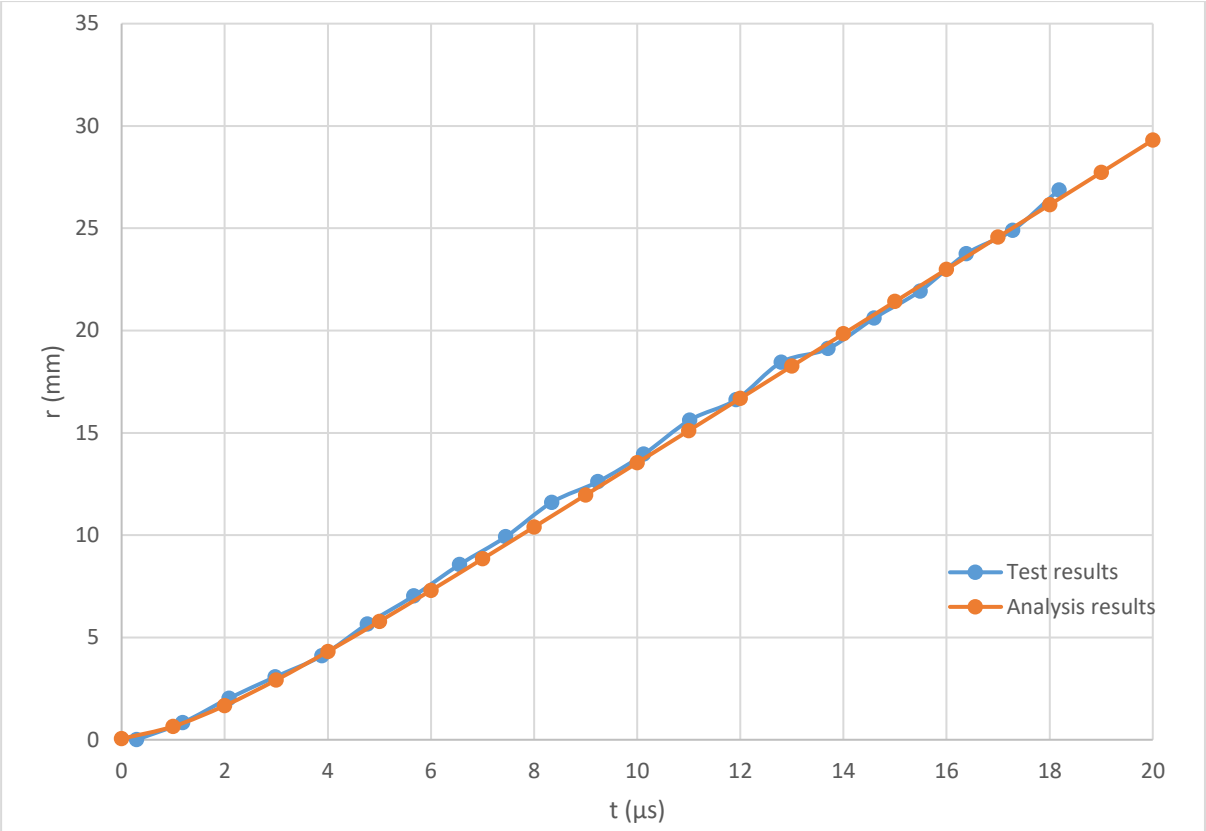

Figure 4-3: The radial position of the cylinder wall with respect to time for (ONTELIT).

The first and second derivatives of equation [4-2] gave gives the values of the apparent velocity and acceleration of the cylinder, respectively:

$$v_a = \frac{dF_c(t)}{dt} = \sum_{i=1}^{2} a_i\left(1 - e^{-b_i t}\right), \qquad 4\text{-}3$$

$$a_a = \frac{d^2F_c(t)}{dt^2} = \sum_{i=1}^{2} b_i a_i e^{-b_i t}. \qquad 4\text{-}4$$

The apparent velocity $v_a$corresponds to the radial velocity in Taylor model, which can be calculated in accordance to the grazing θ angle from the following equation:

$$v_a = D\ \tan\theta \qquad 4\text{-}5$$

Where; D is the detonation velocity.

By calculating (θ) from the previous equation, the Lagrangian values of the cylinder velocity (v) and acceleration (a) give the actual value of the velocity and acceleration from the following equations:

$$v = 2D\ sin\frac{\theta}{2}, \quad 4\text{-}6$$

$$a = a_a cos^3\theta. \quad 4\text{-}7$$

The values of the radial displacement, velocity and acceleration obtained from the analysis of the expansion behaviour of the cylinder wall under the effect of the detonation of ONTELIT are listed in Table 4-4.

Table 4-4: The radial expansion displacement, velocity and acceleration process for ONTELIT

No	Δt	Δr	v_a	a_a
	µs	mm	mm/µs	mm/µs^2
1.	0	0.047	0	0.8679
2.	1	0.651	0.667	0.5007
3.	2	1.667	1.052	0.2888
4.	3	2.921	1.274	0.1666
5.	4	4.312	1.403	0.0961
6.	5	5.782	1.477	0.0554
7.	6	7.298	1.519	0.0320
8.	7	8.840	1.544	0.0184
9.	8	10.394	1.558	0.0106
10.	9	11.963	1.566	0.0061
11.	10	13.534	1.571	0.0035
12.	11	15.108	1.574	0.0020
13.	12	16.684	1.575	0.0011
14.	13	18.261	1.576	0.0006
15.	14	19.838	1.577	0.0003
16.	15	21.415	1.577	0.0002
17.	16	22.993	1.577	0.0001
18.	17	24.571	1.577	7.55E-05
19.	18	26.149	1.577	4.35E-05
20.	19	27.727	1.577	2.51E-05
21.	20	29.305	1.577	1.45E-05

The apparent (observed) velocity and acceleration curve results from the generated data for ONTELIT are presented in Figure 4-4 and Figure 4-5.

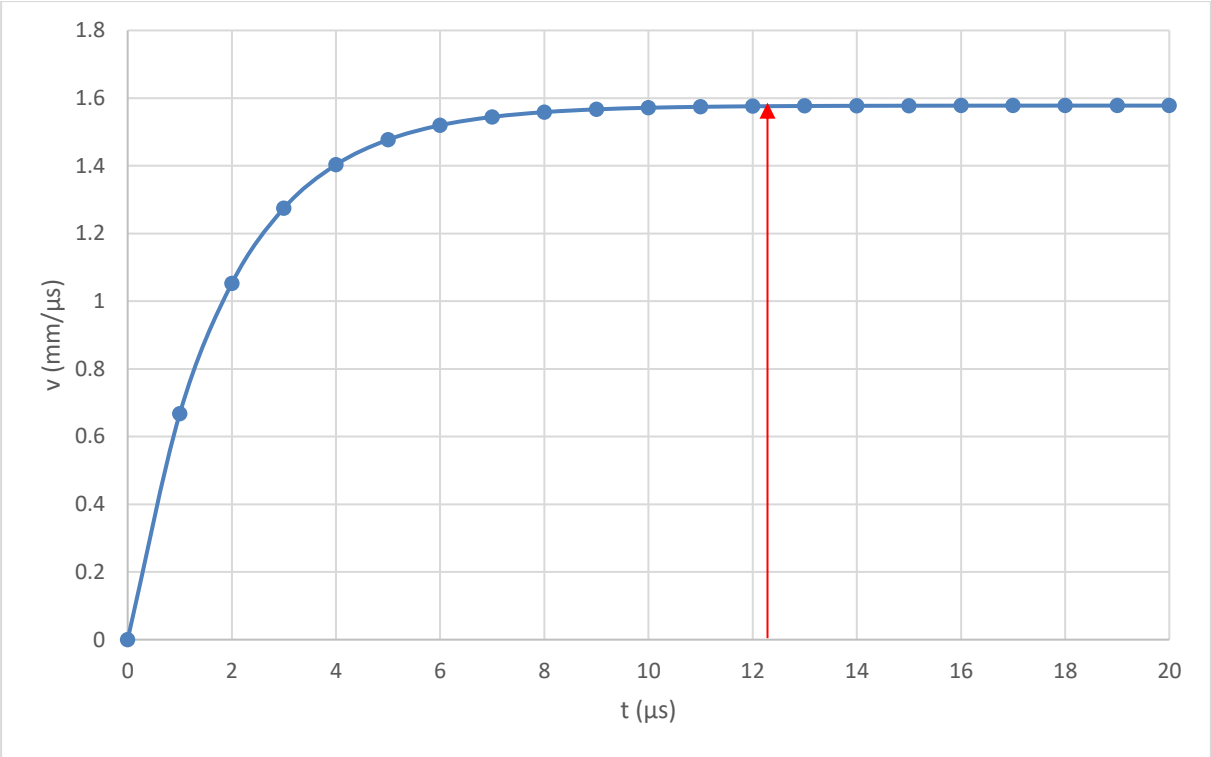

Figure 4-4: The radial expansion velocity of ONTELIT.

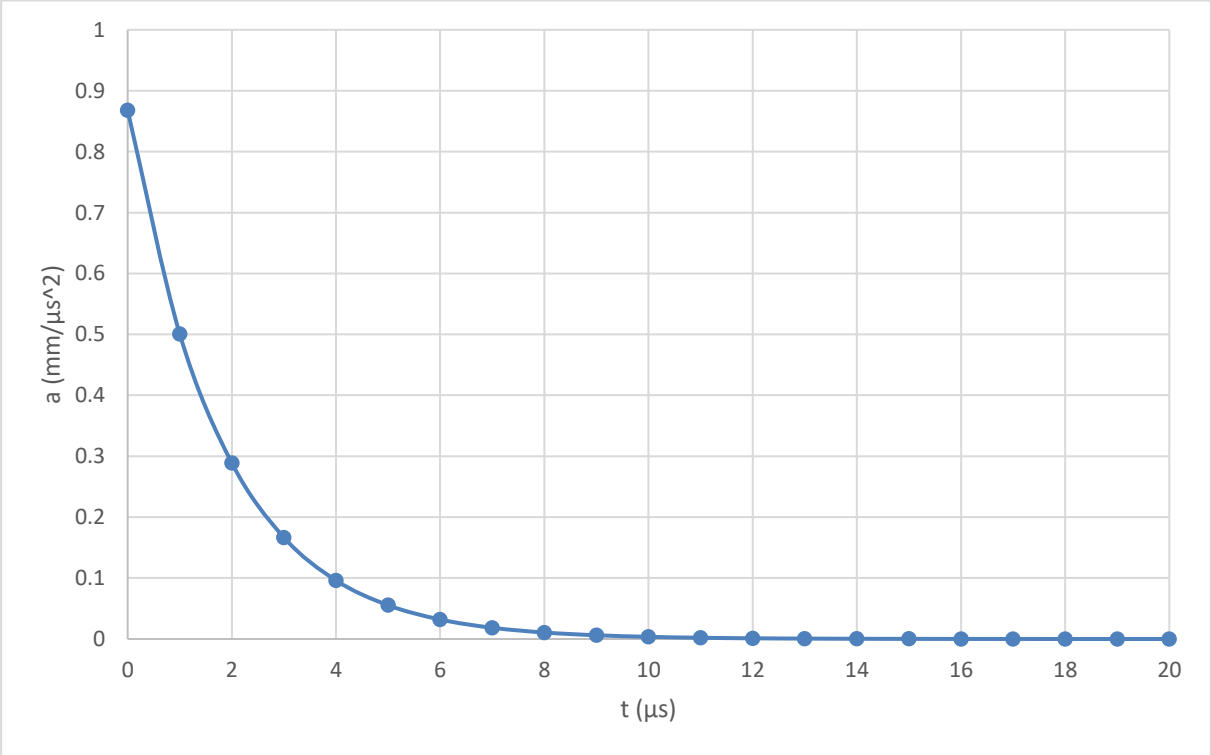

Figure 4-5: The radial acceleration behaviour of ONTELIT.

An optimisation procedure were applied to extract the optimum parameters for the empirical equation of motion of the expanded wall for all types of explosive. The numerical parameters obtained and the resulting curves for all the explosive types are referenced in Appendix 3.

The acceleration time Δt of the detonation product and the final velocity v_f achieved by the cylinder wall are the main explosive criteria for investigating the fragmentation behaviour. An additional analysis of the cylinder wall's actual velocity regarding the projection angle is added relative to the fragmentation results by the end of this chapter.

4.2 Strain rate characterisation

The characterisation of the acceleration time in this analysis is not sufficient to determine the actual time of fragmentation. Another characterisation was used based on previous studies [26,73] to determine the fragmentation time based on the effective strain of fragments.

The effective strain was measured through the effective thickness of fragments in the final shape:

$$\varepsilon_{tt} = -\ln\frac{t_f}{t_i}, \varepsilon_{\mathrm{tt}} = \text{-}\ln(\frac{\mathrm{t_f}}{\mathrm{t_i}}) \qquad \text{4-8}$$

where t_i is the initial fragment thickness (equal to 5 mm in this case), and t_f is the final fragment thickness measured from 75 samples, as presented in Appendix 2.

The effective thickness was, therefore, used to calculate the effective radius using:

$$r_f = r_i e^{\varepsilon_f} \qquad \text{4-9}$$

The effective radius was, therefore, used to determine the actual time of fragmentation from the equation of motion [4-2] presented previously.

In the case of ONTELIT, the average final thickness of 75 samples was 2.98 mm, the effective thickness was therefore 0.515 mm. From the effective strain of the fragments thickness, the effective radius of expansion was calculated to be $\Delta r_m = 16.85\ \mathrm{mm}$, and the effective strain based on the effective radius was equal to $r_f = 41.85\ \mathrm{mm}$. By substituting the effective radius value into the equation of motion equation (4-2), the effective fragmentation time for ONTELIT was equal to 12.16 µs. Figure 4-4 give an illustration of the actual time of fracture according to this model. In the same manner, the effective fragmentation times for other formulations were extracted and are presented in the next chapter for discussion.

4.3 Fragmentation analysis

The detonation of a cylinder produces an elliptical spatial fragment distribution around the symmetrical axis of the tube. The elliptical shape originates from the end effects of the cylinder, which are not in a steady-state. This study considers only the centre section where the steady-state applies, and the end effects are ignored. The expansion behaviour of the detonation products and the design of the cylinder item dictate the final distribution of the natural fragmentation. The capability of the test designed for this study is limited to catching only fragments produced from one side of the test item, as described in the previous chapter.

In order to rely on a reliable data, three tests were conducted for each type of explosive. As **the focus of this study**, the influence of explosive parameters extracted from cylinder tests is studied through the average fragments mass extracted from the cumulative number distribution of the collected fragments $N(>m)$ of the three tests. Since we are using a cumulative distribution function, the cumulative distribution in this study is characterised by adding the total numbers from each test and considering the result as the presentative final cumulative number for the three tests of the collected fragments.

Mott distribution function will be used in this study to extract the average fragment mass factor (μ) to be used as the critical parameter of the natural fragmentation characteristics. More detail on the characterisation of the cumulative number distribution is provided in the following section.

Fragment distribution per angular zone

The dispersion of the spatial distribution of the collected fragments characterised per angular zone and mass category are presented in raw data in Table 4-5. In order for the detonation products to have steady-state behaviour, this study focused on the fragments collected from the central section of the detonated sample.

Table 4-5: The fragment characterisation of ONTELIT, test 1.

Angular zone	070-075	075-080	080-085	085-090	090-095	095-100	100-105	105-110	…
Mass Category (g)	Number of fragments per angular zone								
0.01 - 0.09	0	4	6	4	7	6	2	0	
0.1 - 0.19	0	1	3	4	5	2	3	0	
0.2 - 0.29	0	0	0	0	0	2	2	0	
0.3 - 0.39	0	0	0	0	2	4	1	0	
0.4 - 0.49	0	2	0	0	1	2	0	0	
0.5 - 0.74	0	0	0	0	2	1	1	0	
0.75 - 0.99	0	0	0	2	1	6	0	0	
1 - 1.99	0	0	1	0	3	5	1	0	
2 - 2.99	0	0	1	0	0	4	0	0	
3 - 3.99	0	0	1	1	0	1	0	0	
4 - 4.99	0	0	0	0	0	0	0	0	
5 - 7.49	0	0	0	0	0	0	0	0	
7.5 - 9.99	0	0	0	0	0	0	0	0	
10 - 14.99	0	0	0	0	0	1	0	0	
15 - 19.99	0	0	0	0	0	0	0	0	
20 - 29.99	0	0	0	0	0	0	0	0	
Sector Totals	0	7	12	11	21	34	10	0	

The distribution of the fragments per angular zone from a detonated cylinder filled with NTO-TNT is presented in Figure 4-6.

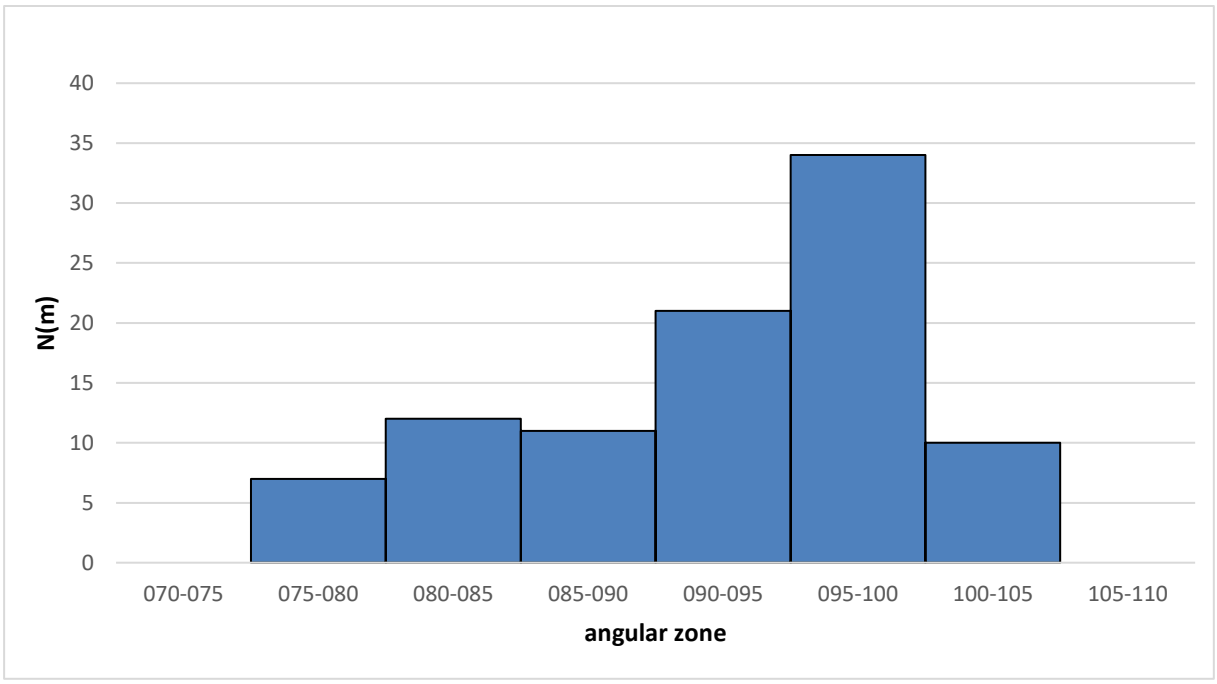

Figure 4-6: The fragment distribution per angular zone of ONTELIT; test 1.

From the combined ONTELIT tests, the final fragment distribution per angle is shown in Figure 4-7.

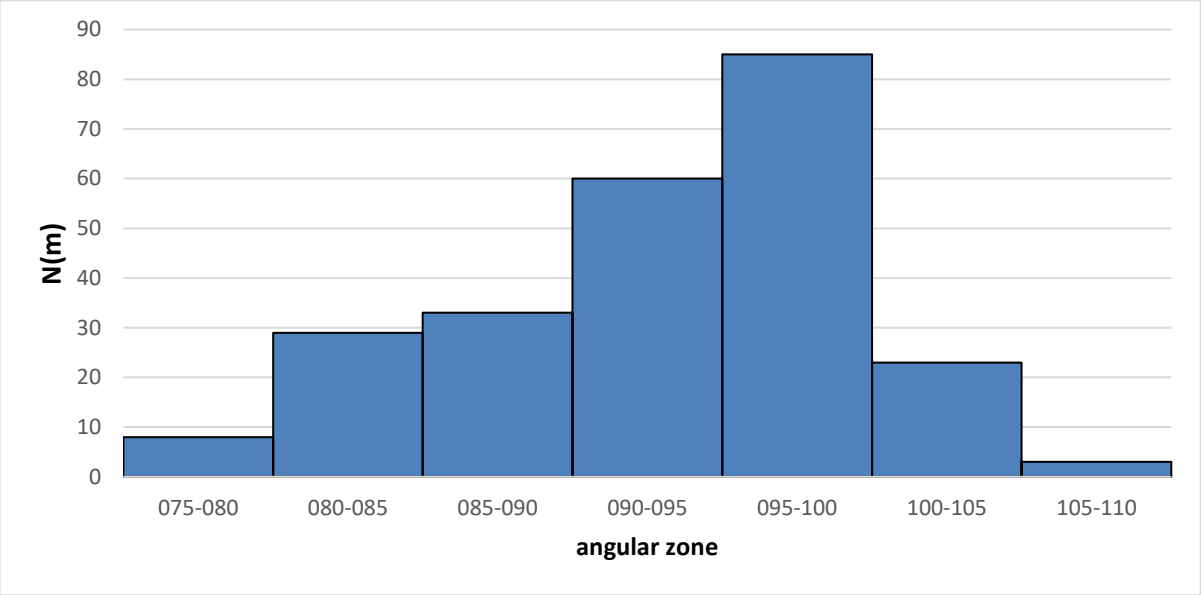

Figure 4-7: The fragment distribution per angular zone with respect to the total number of fragment tests (1 + 2 + 3) for ONTELIT.

It is clear from the fragments distribution in the two figures that most of the fragments lay in the angle between 90-100, which is displayed through Taylor model explained below.

According to the theory of explosives, the fragments released from a cylinder item expand under the effects of the products of detonation, and the projection angle of the fragments rely on the velocity of the detonation wave and the velocity of the products of detonation, or the Gurney velocity. Based on the Taylor model, Table 4-6 presents the expected production angle for each type of explosive.

Table 4-6: Production angles based on the Taylor model.

Explosive	Detonation Velocity (m/s)	Fragment Velocity (m/s)	Taylor Angle (º)
TNT	6940	1352	11.18
Comp B	7920	1594	11.55
NTO-TNT	7370	1360	10.59
MCX-6002	7970	1398	10.06
RXHT-80	7860	1365	9.96

Table 4-7: The total number of fragments per angular zone.

	065-070	070-075	075-080	080-085	085-090	090-095	095-100	100-105	105-110	110-115	115-120	120-125	125-130	130-135	135-140	
	Number of fragments per angular zone															N(m)
TNT	0	0	0	7	10	28	87	18	0	0	0	1	0	0	0	151
MCX-6002	0	3	17	15	50	53	112	81	0	0	0	0	4	0	3	338
Comp-B	2	3	12	16	31	73	122	12	7	3	0	1	1	3	2	288
NTO-TNT	0	0	8	29	33	60	85	23	3	0	0	0	0	1	1	243
RXHT-80	0	1	1	18	17	35	54	11	11	0	0	0	0	0	0	148
TNT	0%	0%	0%	5%	7%	19%	58%	12%	0%	0%	0%	1%	0%	0%	0%	99%
MCX-6002	0%	1%	5%	4%	15%	16%	33%	24%	0%	0%	0%	0%	1%	0%	1%	92%
Comp-B	1%	1%	4%	6%	11%	25%	42%	4%	2%	1%	0%	0%	0%	1%	1%	91%
ONTELIT	0%	0%	3%	12%	14%	25%	35%	9%	1%	0%	0%	0%	0%	0%	0%	96%
RXHT-80	0%	1%	1%	12%	11%	24%	36%	7%	7%	0%	0%	0%	0%	0%	0%	99%

The expected sector angle for maximum fragment yield is, therefore, between 95° and 100°, as shown in Table 4-7. In order to account for most fragments, the range of the production angle is extended to between 75° and 110°, which is approximately >95% of the total number of the collected fragments. The collected fragments from this area are assumed to be the result of steady-state detonation behaviour.

Fragment distribution with respect to the cumulative number

The first method of characterisation was built using only the fragments captured from only one orientation of the cylinder item. All the fragments collected from the three tests add to the total number of fragments. as a function of fragment mass.

Table 4-8 present the number of the collected fragments from the three test of ONTELIT and final cumulative number distribution of fragments as a function of fragment mass.

Table 4-8: The fragment characterisation for ONTELIT.

Mass Category (g)	Mass (g)	ONTELIT 1	ONTELIT 2	ONTELIT 3	N(m)	N(>m)
0.01 - 0.09	0.01	29	20	25	74	240
0.1 - 0.19	0.1	18	7	13	38	166
0.2 - 0.29	0.2	4	6	5	15	128
0.3 - 0.39	0.3	7	5	1	13	113
0.4 - 0.49	0.4	5	2	7	14	100
0.5 - 0.74	0.5	4	8	6	18	86
0.75 - 0.99	0.75	9	0	4	13	68
1 - 1.99	1	10	13	5	28	55
2 - 2.99	2	5	4	3	12	27
3 - 3.99	3	3	1	3	7	15
4 - 4.99	4	0	3	1	4	8
5 - 7.49	5	0	1	1	2	4
7.5 - 9.99	7.5	0	0	0	0	2
10 - 14.99	10	1	1	0	2	2

The cumulative number distribution of the three tests under this characterisation behave exponentially, as shown in Figure 4-8.

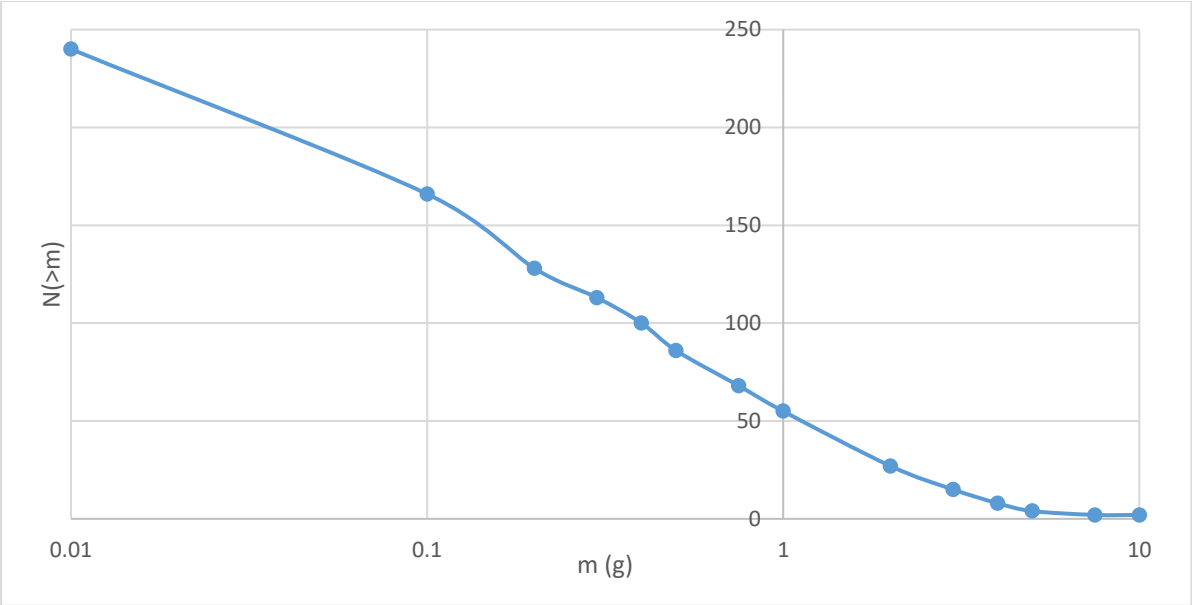

Figure 4-8: The cumulative distribution number for ONTELIT.

The final cumulative number distribution for all explosives under the first method of characterisation is presented in Table 4-9.

Table 4-9: The cumulative number distribution of the collected fragments for all explosives material.

Mass Category (g)	TNT	COMP-B	ONTELIT	MCX	RXHT
0.01 - 0.09	149	273	240	328	146
0.1 - 0.19	101	191	166	207	132
0.2 - 0.29	83	142	128	160	106
0.3 - 0.39	76	119	113	137	99
0.4 - 0.49	69	105	100	124	89
0.5 - 0.74	65	94	86	102	82
0.75 - 0.99	52	77	68	82	67
1 - 1.99	46	60	55	62	59
2 - 2.99	30	27	27	34	35
3 - 3.99	19	16	15	22	20
4 - 4.99	15	8	8	15	10
5 - 7.49	10	5	4	10	9
7.5 - 9.99	4	2	2	4	6
10 - 14.99	2	0	2	4	5

Figure 4-9 illustrate the cumulative number distribution of fragments produced from different explosive material. The figures of the cumulative number distribution of fragments have been

presented in a logarithmic scale to illuminate the effect of the explosive parameters on the small fragments size.

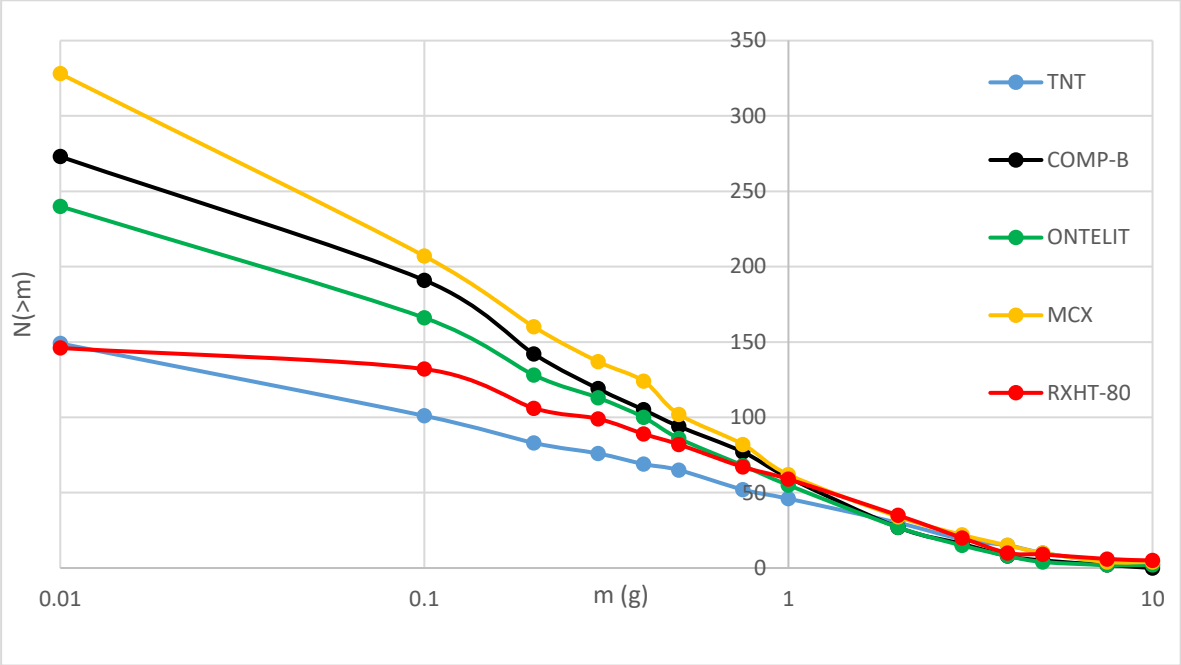

Figure 4-9: The cumulative number distribution for all explosives.

Optimization procedure to extract fragmentation parameters

The natural fragmentation characteristics will be investigated through the cumulative number distribution of the collected fragments. In order to improve the prediction in the fragmentation analysis, a measurable parameter must be in place. For the completion of this study, the test results optioned will be used to extract the critical parameters of one of the existing cumulative distribution function. Thus, Mott model have been employed for this study as an available tool to simulate the fragments distribution behaviour.

$$N(>m) = N_0 e^{-\left(\frac{m}{\mu}\right)^{\beta}} \qquad 4\text{-}10$$

Where; $N(>m)$ is the cumulative number of the collected fragments and their mass is bigger than m, and m is the fragments mass for each group. β is the Mott constant set to be equal to 0.5 under Mott consideration where (C/M < 2) for this study. N_0 is the initial fragments distribution related to μ factor under the following equation:

$$N_0 = \frac{M_0}{2\mu} \qquad 4\text{-}11$$

Where 2μ is the average fragments mass $\bar{m}$.

M_0 is the total mass of the casing material or the initial fragments mass. Since the fragments is only collected from one side of the casing material in this experiment, the total mass of the collected fragments used in this optimization process to extract the optimum value of μ as represented in the following Mott equation.

The mass of the collected fragments therefore is included in the final form of Mott equation:

$$N(>m) = \frac{M_0}{2\mu} e^{-\left(\frac{m}{\mu}\right)^{\beta}} \qquad 4\text{-}12$$

Since β factor was set to be equal 0.5 and M_0 is manually determined from the collected fragments, the distribution factor μ is the only parameter left to be optimized.

The Chi square test χ^2 is also employed for this process to extract the optimum value of μ on the following form:

$$\chi^2 = \sum \frac{(O_i - E_i)^2}{E_i} \qquad 4\text{-}13$$

Where O_i present the theoretical value of the cumulative number of the natural fragmentation distribution under Mott model. E_i present the test results or the cumulative number of the natural fragmentation distribution from experimental results.

Based on Chi square test theory, the lower the value of χ^2 the closest the theoretical value to the test results. Solver analysis is an available tool in Excel program employed for this study to extract the minimum value χ^2 by changing μ to the optimum value.

Mott model therefore simulate the natural fragmentation behaviour of the test results with the optimum parameters. The data obtained from this analysis is presented in Table 4-10.

Table 4-10: Mott distribution parameters for all explosive parameters.

	Mo	No	μ	$\bar{m}$	β	χ^2
	(g)			(g)		
TNT	207.78	154	0.67	1.34	0.5	3.68
COMP-B	201.14	330	0.30	0.60	0.5	2.46
ONTELIT	225.06	278	0.40	0.81	0.5	10.88
MCX	261.96	353	0.37	0.74	0.5	6.34
RXHT-80	241.44	185	0.65	1.30	0.5	8.48

The deviation between the theoretical value and the test value of ONTELIT is the highest among the other explosive, which is still low. Figure 4-10 present a comparison between the test results and theoretical results of the natural fragments distribution of (ONTELIT).

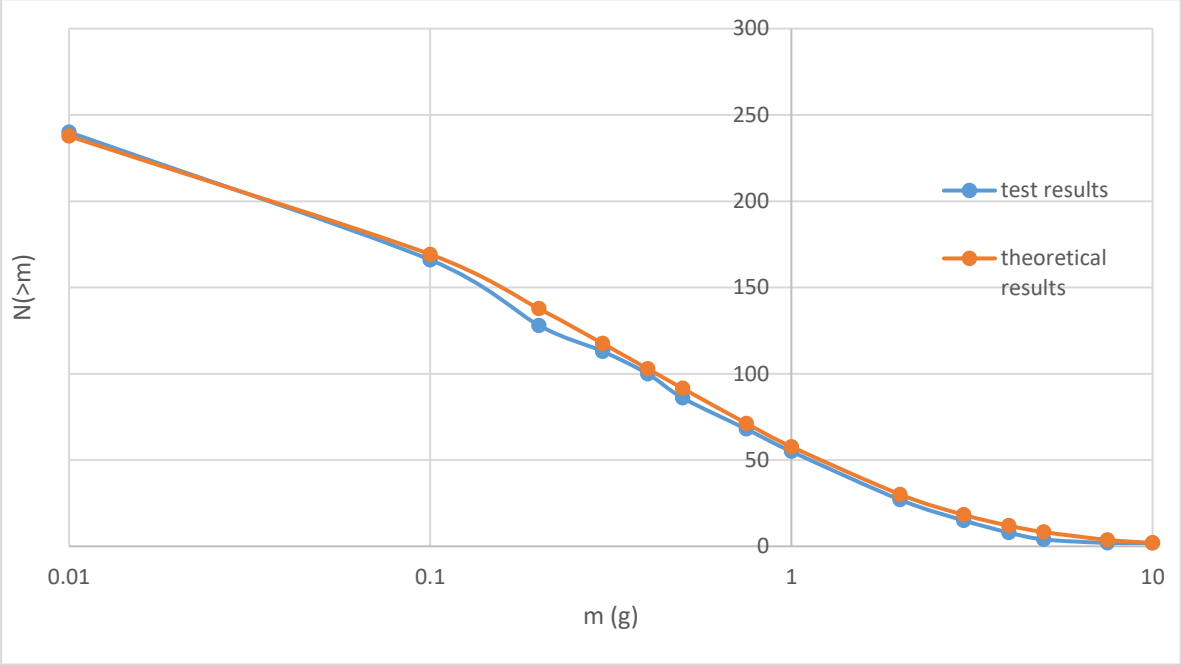

Figure 4-10: The theoretical distribution value vs the test results value of ONTELIT.

Figure 4-11 illustrate the theoretical cumulative number of the fragments obtained from the distribution function of Mott for all explosive material.

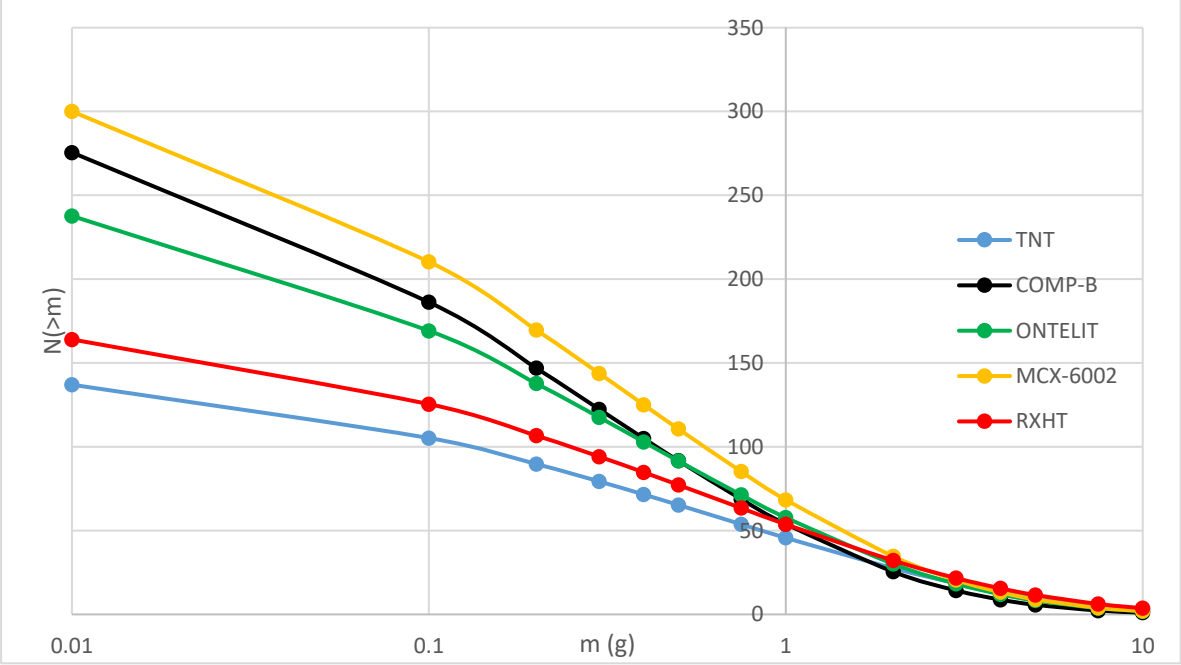

Figure 4-11: The cumulative number of fragments under Mott distribution function of all explosive material.

The μ factor in Mott model is the only distribution factor used to indicate the dependence of natural fragmentation characteristics on explosive parameters. It is clear from the trends of the fragments distribution that explosive material tends to affect the fragments in the small size range (e.g.<1 g). μ factor reflect the size and the number of the fragments that can produce from detonation. An inverse relationship between μ factor and the cumulative number of the produced fragments $N(>m)$, where a small value of (μ) indicate a high number of fragments will produce. The determination of μ value depends on the number and the mass of the collected fragments. Thus, the distribution factor obtained for Comp-B indicate a high number of a fragments compare to the produced fragments from MCX-6002 even with the high number that reflected on the cumulative distribution Figure 4-11. MCX-6002 produced higher number of fragments than Comp-B only in the small range of mass (i.e., <1 g). This is because the total mass of the collected fragments from MCX-6002 (M_o) is higher that the total mass of the collected fragments from Comp-B (M_o). In total, for the same total mass of the same body, Comp-B tends to produce higher number of fragments than the number of fragments that can be produced by MCX-6002.

4.4 Conclusion

An analysis of the results from two well established test methods – namely, the cylinder test and the arena test – was used to obtain the required data for this study. This chapter has discussed the analytical procedure that was followed to generate the optimum parameters based on the capabilities and the tools available, whether from the literature or from experimental resources.

A variation of the well known cylinder test was used to extract the required data on explosive behaviour for investigating the dependence of natural fragmentation behaviour on explosive parameters. In addition, physical recovery data from arena test experiments were used to extract the required parameters for natural fragmentation behaviour.

The final velocity approached under the expansion process of the detonation products and the acceleration time of the fragmentation process were generated from the cylinder test. On the other hand, the cumulative number distribution of the natural fragmentation and the relative empirical parameters controlling the distribution were the required data obtained through the arena test.

An example of one type of explosive, NTO-TNT, was provided to illustrate the process followed systematically to generate the required data. The same process was applied for the other explosive materials, and the results are shown in the Annexures.

A correlational study between the explosive parameters and the fragmentation parameters is discussed in the next chapter in an attempt to achieve a simple explosive–fragmentation model as the core of this analysis.

CHAPTER 5: DISCUSSION

The dependence of the natural fragmentation characteristics on explosive parameters is investigated using the parameters extracted from the analysis described in the previous chapter. Other critical explosive parameters are employed from the literature base on the availability of data and the density of the explosive, as presented in Table 5-1.

Table 5-1: Explosive parameters extracted from the literature [5, 65, 66, 67 and 68].

	ρ_o	M/C	D	P_{CJ}	$\sqrt{2e}$
Units	g/cc		(mm/μs)	(GPa)	(mm/μs)
1. TNT	1.59	2.78	6.86	19.57	2.31
2. Comp-B	1.67	2.70	7.95	26.30	2.68
3. ONTELIT	1.71	2.63	7.37	22.60	2.48
4. MCX-6002	1.79	2.44	7.97	27.22	2.86
5. RXHT-80	1.50	2.94	7.68	22.20	2.58

The explosive parameters (Chapman–Jouguet pressure P_{CJ} and Gurney constant $\sqrt{2e}$) were approximated relative to the casing material mass *M* and explosive material mass *C* . These values were measured manually based on the mass and the volume of the cylinder sample.

From the perspective of the explosive characterisation, the fragmentation process is the result of the expansion behaviour of the detonation products from the initial point to the final point of expansion. The initial point is the pressure known as Chapman–Jouguet pressure P_{CJ}. The initial pressure value is related to the change in detonation velocity on the x-axis and the polytropic constant γ:

$$P_{CJ} = \rho_o \frac{D^2}{\gamma + 1}, \qquad 5\text{-}1$$

The final point in the expansion process is known as the Gurney velocity (v_G) where the kinetic energy of the fragments is considered. The Gurney velocity (v_G) is the result of the expansion behaviour of the accelerated metal under the effects of the detonation products in the radial direction as a function relative to the value of the metal to explosive mass ratio (*M*/*C*):

$$v_G = \frac{\sqrt{2e}}{\sqrt{(\frac{M}{C} + \frac{1}{2})}}. \qquad 5\text{-}2$$

Accordingly, the initial pressure of the detonation products, manifested by P_{CJ}, and the final velocity of the expanded metal, manifested by $\sqrt{2e}$, are the beginning and end state conditions of the processes that dictate the fragmentation.

According to the literature research, the dependence of the natural fragmentation characteristics on P_{CJ} has been verified through several studies, such as the Gold model. In addition, the dependence of the detonation velocity *D* on the Gurney velocity has been approached through the Cooper model.

For the same casing material and different explosives, the fragmentation process based on these models is assumed to occur at the same level of expansion volume (e.g., $V/Vo \approx 3$), as approached in different models such as the Pearson model. Implicitly, this assumption means accepting that the metal will always fragment at a fixed value of strain, and that the acceleration time will dictate the final velocity.

The fragmentation process is involved within the expansion process, which cannot be easily observed by the optical method used to indicate the end of the fragmentation process. In addition, other explosive parameters should contribute to the process through heat or shock reverberation at different acceleration times.

However, the expansion process for the same casing material depends on the properties of the products of detonation, which dictate the effective strain, the effective strain rate and the fragment characteristics. The point of discussion, therefore, is to characterise the fragmentation process through the effective strain and the effective strain rate for different types of explosive from the expansion test to investigate the dependence of the natural fragment characteristics, in their final form, on the explosive parameters. The required values obtained for this study are provided in the next section.

5.1 Explosive parameters from cylinder test analysis

The explosive parameters extracted from the analysis of the expansion behaviour of the test cylinders filled with different types of explosive, and explained in the previous chapter, are listed in Table 5-2.

Table 5-2: Explosive parameters extracted from test analysis.

	ε_{tt}	r_f	Δt	v_a	θ	v_f	V/V_o
	$-\ln(\frac{t_f}{t_i})$	$r_i e^{\varepsilon_f}$	EOM	EOM	$\tan^{-1}(\frac{v_a}{D})$	$2Dsin\frac{\theta}{2}$	$(\varepsilon_{tt}+1)^2$
Units		mm	µs	mm/µs		mm/µs	
TNT	0.475	40.22	13.52	1.27	10.42	1.25	2.17
Comp-B	0.667	48.74	15.77	1.69	11.64	1.66	2.78
ONTELIT	0.515	41.85	12.16	1.59	11.83	1.57	2.29
MCX-6002	0.565	44.01	12.59	1.69	11.63	1.66	2.45
RXHT-80	0.471	40.03	13.20	1.30	9.32	1.28	2.16

The data presented in Table 5-2 describe the effective strain based on the effective thickness of the collected fragments after detonation (ε_{tt}). From the effective strain, the effective radius (r_f) was extracted, and this was also used to predict the expansion volume of the cylinder wall, the volume fraction (V/V_o).

The effective time of the fragmentation process (Δt) was extracted from the empirical equation of motion (EOM) relative to the effective radius (r_f) as discussed in the previous chapter. The effective time of the fragmentation process (Δt) was used relative to the effective strain to extract the final velocity at fracture (v_f).

The data listed in Table 5-3 illustrate the expansion behaviour of a cylinder wall under the effects of the detonation products of TNT at different stages. As presented in the table, the expansion process underwent different stages until it reached a consistent value of velocity, presenting the final fragment velocity that was used to extract the Gurney constant $\sqrt{2e}$. The data highlighted in yellow are the explosive parameters at failure extracted from the effective thickness of the collected fragments relative to the equation of motion parameters, which are used to present the curves in Figure 5-1. Based on the model exist by considering the point of fracture at constant strain equivalent to ($V/V_o \approx 3$) this corresponds to 21 µs of the acceleration time of TNT.

Table 5-3: Fragmentation process of TNT at different stages.

ε_{tt}	Δt	Δr_c	r_f	ε_r	v_a	θ	v_f	V/Vo
Units	µs	mm	mm		mm/µs		mm/µs	
	5	4.639	29.63	0.170	1.102	9.07	1.092	1.369
	10	10.75	35.76	0.357	1.251	10.28	1.236	1.844
0.475	13.52	15.22	40.22	0.475	1.269	10.42	1.253	2.177
	15	17.10	42.10	0.521	1.271	10.44	1.255	2.313
	20	23.47	48.47	0.662	1.274	10.46	1.258	2.762
	21	24.74	51.98	0.732	1.274	10.46	1.258	3.000

Figure 5-1 illustrate the differences in the acceleration time of the fragmentation process extracted from the effective thickness at fracture of the explosives.

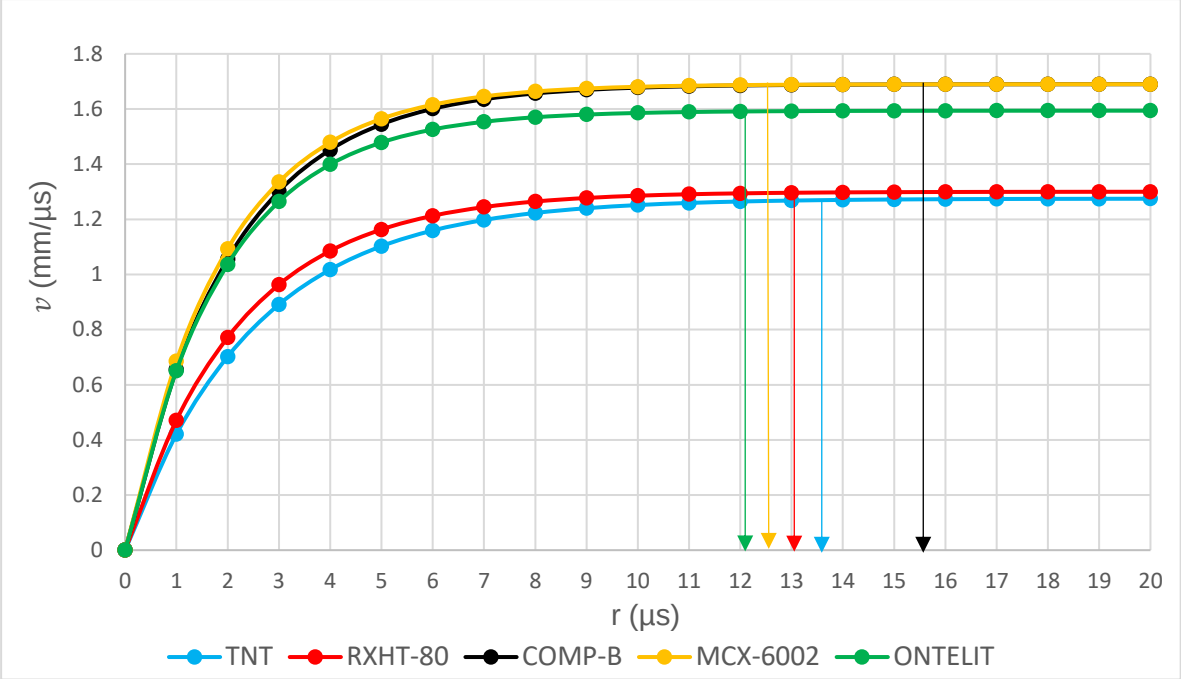

Figure 5-1: Expansion velocities from cylinder test analysis for different explosives.

The point at which the fracture takes place and the final velocity at this point of fracture cannot be readily determined. The final velocity based on the expansion behaviour on Figure 5-1 can be considered at any point after 10 µs.

In this study, the data presented in Table 5-2 are considered as the final velocities at full detonation. Figure 5-1 reveals that the final velocities and the acceleration time of Comp-B and MCX-6002 materials is the highest among other explosive material. Based on the data obtained in this study and from literature, MCX-6002 and Comp-B have almost the same value of P_{CJ} and the same value of final velocity of expansion v_f but with different acceleration times before fracture as extracted in this study. The fragmentation process of the Comp-B material displays the highest acceleration time, equal to 15.77 µs, and the acceleration time of MCX-6002 material is equal to 12.59 µs with different about 3 µs. The ONTELIT material has the lowest acceleration time among the explosives, equal to 12.16 µs. The variation in the acceleration time is a result of the change in the expansion level caused by the detonation products and the fragmentation process.

The metal in Comp-B's case endured the strain for a longer time due to its slow expansion, whereas the expansion of the metal of MCX-6002's case increased rapidly. In other words, the energy was released more rapidly by the detonation of MCX-6002 than by the detonation of Comp-B, which released energy slowly; this resulted in the same final velocity but a different strain and strain rate for these explosives.

Regarding the expansion process, some of the explosive materials, such as TNT, expanded for a longer time when compared to the other explosive materials such as the ONTELIT composition. Although TNT fractured at the lowest volume fraction, due to its slow expansion, the metal endured the strain for a longer time compared to ONTELIT expansion. However, the final velocity of the ONTELIT was still higher than that of TNT because the rapidity of the expansion and the internal pressure of ONTELIT were also higher.

Moreover, TNT expanded for a longer time but had a lower volume fraction than RXHT-80, which expanded for a shorter time but had a higher volume fraction because of its internal energy, which resulted in the same effective strain rate. The effect of these parameters on the final fragment shape is discussed in detail in the following section.

5.2 The fragmentation distribution factor as a function of explosive parameters

For fragmentation modelling, all the explosive parameters were considered from the initial to final stages of expansion: the initial pressure (P_{CJ}), the final velocity (v_f) and the acceleration time of detonation products (Δt) as extracted in the previous section. In this part of the discussion, the cumulative distribution factor of fragments μ have been used to draw the relation between of the natural fragmentation characteristics and the explosive parameters.

Generally, the explosive parameters of most of the explosive material have been related through literature to the equivalence value of TNT. Consequently, the explosive parameters of the explosive material used in this study have been normalized to the value of TNT by dividing their explosive parameters by the value of TNT.

The dependence of natural fragmentation characteristics on explosive parameters was investigated through the parameters listed in Table 5-4, where the acceleration time included in this study.

Table 5-4: The fragmentation distribution factors relative to explosive parameters.

	μ	$\bar{m}$	P_{CJ}	Δt	$I = \Delta t X P_{CJ}$	v_f
Units		(g)	(GPa)	(μs)	(GPa.μs)	(mm/μs)
TNT	0.67	1.34	19.60	13.52	265.07	1.25
Comp-B	0.30	0.61	26.30	15.77	414.77	1.66
ONTELIT	0.40	0.81	22.60	12.16	274.83	1.56
MCX-6002	0.37	0.74	27.22	12.59	342.78	1.66
RXHT-80	0.65	1.30	22.20	13.20	293.08	1.28

5.2.1 Initial pressure effect (P_{CJ})

The dependence of the natural fragments characteristics on the initial pressure (P_{CJ}) is investigated through the value listed in Table 5-5.

Table 5-5: The distribution factors in relation to P_{CJ}.

	μ	$\bar{m}$	Normalised	P_{CJ}	Normalised
Units		(g)		(GPa)	
TNT	0.67	1.34	1.00	19.60	1.00
COMP-B	0.30	0.61	0.45	26.30	1.34
ONTELIT	0.40	0.81	0.60	22.60	1.15
MCX-6002	0.37	0.74	0.55	27.22	1.38
RXHT-80	0.65	1.30	0.97	22.20	1.13

The trend line of the relation in Figure 5-2 illustrate the dependence of the natural fragmentation characteristic on the initial pressure of the explosive material used in this study.

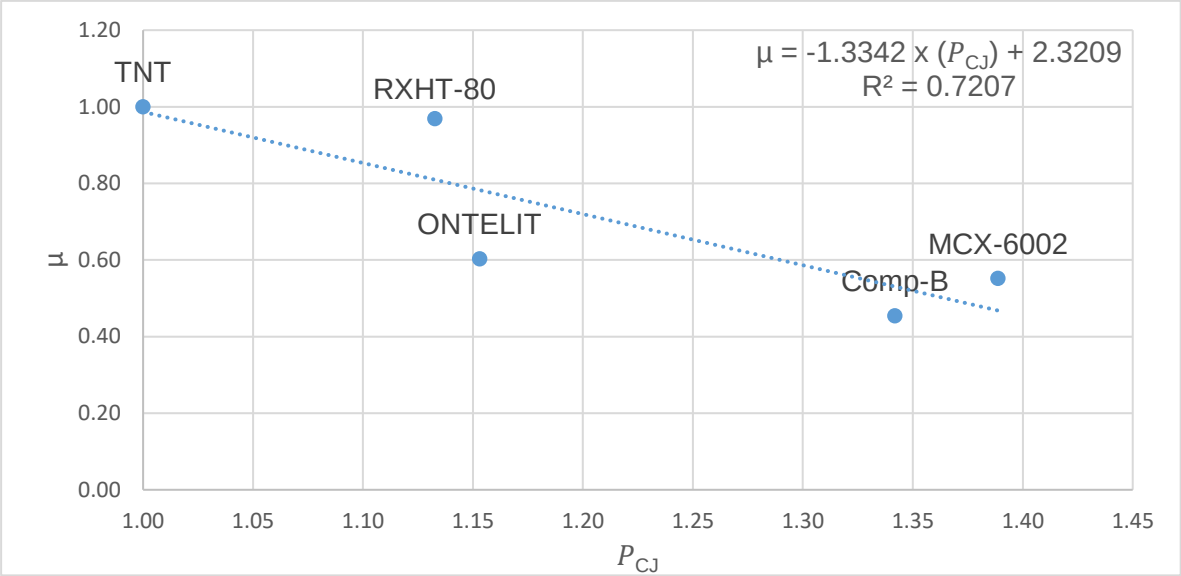

Figure 5-2: The dependence of natural fragmentation characteristics on P_{CJ}.

An inverse relationship have been revealed between the initial pressure factor (P_{CJ}) of the detonation products and average mass factor (μ) of the collected fragments, where the increase of the initial pressure results to decrease in the average fragments mass and more fragments will produce. An increase of the initial pressure to about 40% will decrease the average fragments mass to about the half (50%) of the fragments produced by TNT.

The initial pressure factor P_{CJ} is the indicating factor for the potential amount of energy in the explosive. As expected, the more powerful the explosive, the higher the expected shattering of

the casing material and the more fragments will produce, which is reflected in the trend of the line in Figure 5-2. Nevertheless, the data are scattered, which indicates that there are other criteria that may play a critical role in the relation. The acceleration time of the detonation products may play a critical role as the indicating explosive factor of the expansion behaviour. The next step, therefore, was to include the acceleration time in combination with the initial pressure, as illustrated in the next section.

5.2.2 Explosive impulse (I) effect

Considering the acceleration time Δt combined with the initial pressure factor P_{CJ} in terms of the detonation impulse (I) of the detonation products may reflect a variation in the relation between the distribution factor and the explosive parameters, where we expected that the higher the impulse, the more damage would occur to the casing material. The explosive and the fragmentation parameters for this analysis are listed in Table 5-6.

Table 5-6: The distribution factor in relation to detonation impulse (I).

	μ	$\bar{m}$	Normalised	I	Normalised
Units		(g)		(GPa.μs)	
TNT	0.67	1.34	1.00	265.08	1.000
Comp-B	0.30	0.61	0.45	414.78	1.565
ONTELIT	0.40	0.81	0.60	274.84	1.037
MCX-6002	0.37	0.74	0.55	342.78	1.293
RXHT-80	0.65	1.30	0.97	293.08	1.106

Figure 5-3 illustrate the dependence of the natural fragmentation characteristics on the impulse of different explosive material.

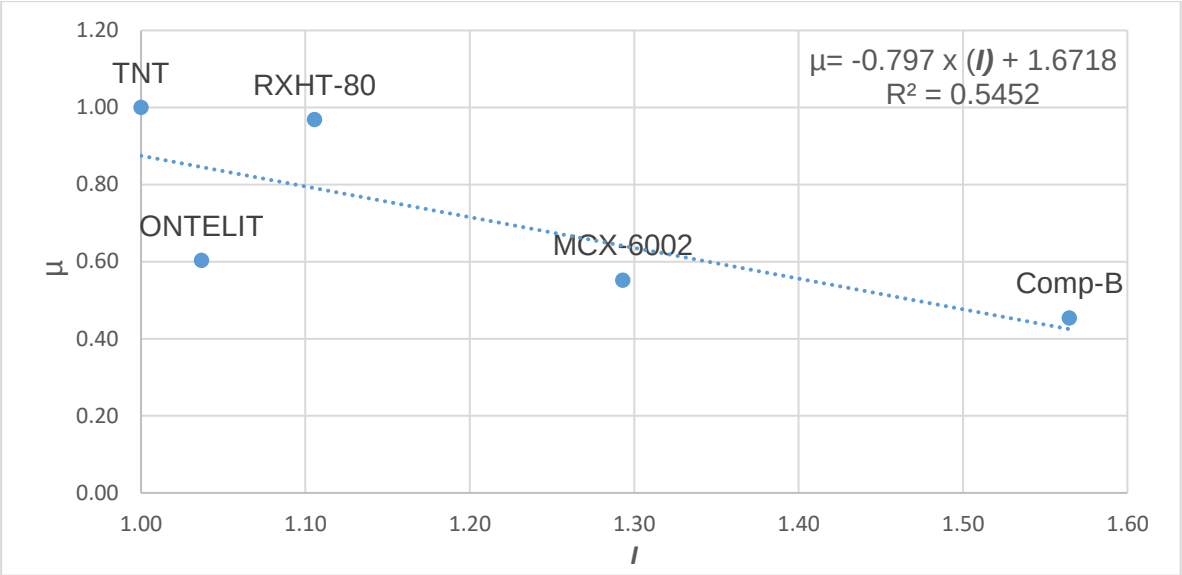

Figure 5-3: The dependence of natural fragmentation characteristics on detonation impulse (*I*).

Explosive material with high acceleration time such as in the case of Comp-B tends to produce higher number of fragments compare to the number of fragments produced by MCX-6002, which have almost the same initial pressure. The impulse of the detonation products have been considered in this case to evaluate the variation in the relation between the distribution factor and the initial pressure of the detonation products. Even though, there was no real improvement in the relationship under this consideration.

The amount of energy transferred from an explosive to the metal is reflected through the expansion behaviour of the detonation products by the mean of the kinetic energy transferred to the metal, or Gurney energy in our case. In addition, the P_{CJ} value employed from the literature is approximated based on the density of the filling, which is not accurate and which may affect the final analysis. Therefore, the final velocity would be the optimum explosive parameters extracted from test result to complete this analysis.

The next step was to study the dependence of the fragment characterisation on the final velocity, where the final velocity is the indicating factor of the amount of energy transferred to the metal before fracture.

5.2.3 Final velocity (v_f) effect

The evaluation parameters to study the dependence of the natural fragmentation on the explosive parameters through the final velocity v_f of the expanded metal accelerated under the effect of the detonation products is listed in Table 5-7 as obtained from the cylinder test.

Table 5-7: The distribution factor in relation to the final velocity of expansion v_f.

	μ	$\bar{m}$	Normalised	v_f	Normalised
Units		(g)		(mm/μs)	
TNT	0.67	1.34	1	1.25	1
Comp-B	0.3	0.61	0.45	1.66	1.33
ONTELIT	0.4	0.81	0.60	1.57	1.25
MCX-6002	0.37	0.74	0.55	1.66	1.33
RXHT-80	0.65	1.3	0.97	1.28	1.02

Figure 5-4 illustrate the dependence of the natural fragments distribution through (μ) factor on the final expansion velocity (v_f).

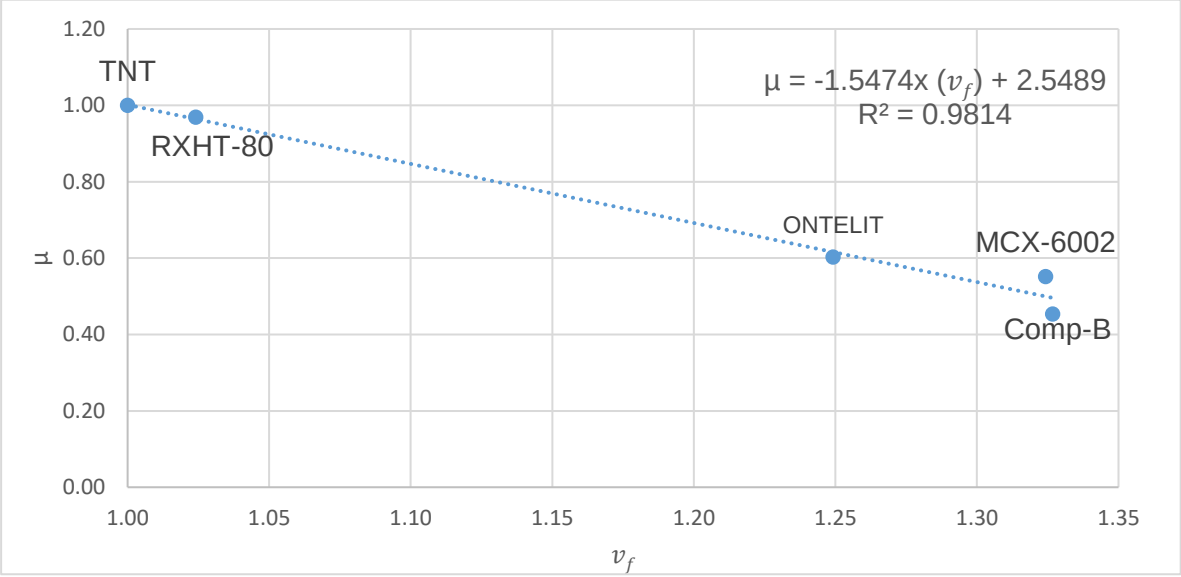

Figure 5-4: The dependence of natural fragmentation characteristics on the final velocity of expansion (v_f).

The final velocity is the representative value of the effective amount of energy transferred to the metal. The natural fragmentation characteristics depend strongly on the final velocity, as presented in Figure 5-4. An improvement in the relation was made by correlating the effective velocity at fracture extracted from the effective strain of collected fragments with the statistical distribution factor μ.

Even with the small scattering in this relation, this proved a clear picture of the dependency of the fragment characteristics on the expansion behaviour of the detonation products. The final velocity had been extracted from the analysis of the streak photograph of the detonation products. The acceleration time have been extracted in correlation to the effective strain obtained from the

effective thickness of the collected fragments. The small scatter in the relation maybe because the difference in the acceleration time between MCX-6002 and Comp-B.

The effective amount of energy transferred to a metal is the significant factor in characterising the fragments generated from the detonation of an explosive material. The effective amount of energy is better reflected in the collected fragments than the expansion behaviour analysed photographically or the initial pressure of explosive.

5.3 Discussion

An investigative study has been pursued to develop a simple model to explain the dependence of the natural fragmentation characteristics on explosive parameters.

Firstly, experimental data were generated using the famous cylinder test to extract the required explosive parameters, as well as to characterise the natural fragmentation distribution. The fragments collected from the detonation of a cylinder tube each filled with one of five types of explosives (TNT, Comp-B, ONTELIT, MCX-6002 and RXHR-80), were used to extract the effective strain from the effective thickness as well as to extract the statistical distribution factor of the cumulative number distribution.

The expansion of the detonation products for the representative explosives was characterised through streak photography to extract the parameters of the empirical equation of motion used to obtain the volume and the velocity of the metal case during expansion.

The effective velocity at fracture was the main criteria that was extracted from the correlation between the effective thickness of the collected fragments and the empirical equation of motion parameters of the detonation products. In contrast, the statistical distribution factors of the cumulative number distribution were the main criteria that were extracted from the collected fragments to characterise the natural fragment distribution.

Finally, a correlation analysis was applied to the data obtained from the literature and from the test results to study the dependence of the explosive parameters on the natural fragmentation distribution through the cumulative distribution factors.

Fragment characteristics relative to expansion behaviour

The collected fragments from the detonation of a cylinder item filled with a type of explosive, were characterised as described in the previous chapter. The distribution factor μ is the natural fragmentation parameter used to study the effect of detonation behaviour on fragments distribution. The distribution factor μ reflected the characteristics of the collected fragments based on their mass (0.01 g-15 g). The cumulative number distribution $N(>m)$ of the fragments produced from the detonation of different type of explosive depends on the distribution factor (μ). An inverse relationship between the cumulative number distribution $N(>m)$ and the distribution factor (μ), where the smaller the value of (μ) the higher the number of fragments is predicted.

The distribution factor (μ) in this study have been characterized through the total number and the total mass of the collected fragments. The distribution factor of the total fragments product from Comp-B is the lowest, which produced high number of total fragments. Explosive material however, tends to affect the fragments characteristics on the small range of mass (<1g). As a result, the MCX-6002 explosive tended to produce the highest number of small fragments and a relatively low number of larger fragments. These phenomena have been discussed in detail as below.

The dependence of natural fragmentation characteristics on explosive parameters is better reflected through the effective energy at fracture, which can be indicated through the final velocity of expansion. Gurney energy normally used through literature to represent the effective energy at fracture.

In the case of two type of explosive have the same final velocity base on the data obtained from the expansion behaviour, the acceleration time from the effective strain of the collected fragments is the crucial parameter to characterize fragmentation.

The linear relationship between the fragmentation characteristics and the explosive parameters obtained through this analysis is very sensitives and strongly depends on the time at fracture. The dependency of the natural fragmentation characteristics on the acceleration time is clear in the case of MCX-6002 and Comp-B.

Comp-B had almost the same initial pressure factor as MCX-6002 and the same final velocity as a result. The detonation product in the Comp-B case accelerated the metal tube for a longer time, approximately 15 μs, but this was the highest acceleration rate among the explosives. This high rate of acceleration expanded the metal into the highest level of strain and total small distribution factor μ. In contrast, MCX-6002 produced higher number of only small fragments compare to

Comp-B. This means that a detonation with a lower acceleration time and a faster detonation rate generates a higher number of small fragments.

An interpretation of this is that the expansion of the cylinder for MCX-6002 occurred faster than the expansion process in the detonation of Comp-B, and that if did not expand efficiently, which did not allow for a proper perforation of the fragments in MCX-6002. In other words, the expansion process occurred over a longer time in the case of Comp-B and resulted in the highest volume fraction, which allowed for more cracking in the outer surface of the tube.

The detonation of MCX-6002 generated a high number of small fragments, known as seed fragments, with a low number of large fragments, known as principal fragments. In contrast, in the case of Comp-B, the fragmentation process occurred over a longer period of expansion, which allowed for more cracks in the outer surface and the proper perforation of fragments from the outer to the inner surface of the cylinder wall.

From the literature, the other difference in these cases is the joint point between the interior and exterior cracks, known as the coalescence of the crack at failure. If we consider two types of seed fragment B' and B". B' is a result of a shear crack from the inner surface of the wall, and B" is a result of a sharp rupture from the outer surface of the wall. The coalescence or the shear crack for MCX-6002 was higher (or deeper in the cylinder wall) because of the accelerating time of detonation products is lower. The detonation products in MCX-6002 accelerated faster than the detonation products of Comp-B, which resulted in less available time for fragmentation and that accelerated the share-band formation. This behaviour resulted in a high number of seed fragments of type B' in the interior surface and a low number of large fragments. This may also cause a waste of the mass of the casing material. In contrast, in the case of Comp-B, the detonation products occurred slower compared to MCX-6002, which allowed for more compression on the cylinder wall, and the joint point or the coalescence, as a result, occurred thinner. Another consideration was the reflected wave from the external surface of the cylinder wall during expansion, which creates a better environment for fragmenting by introducing new dislocations in the microstructure. A higher acceleration time of the detonation products allows the reflected wave to occur, which results in more cracks in the outer surface and a majority of seed fragments of type B" as was in the case for Comp-B.

The model approach

The dependence of natural fragmentation characteristics on explosive parameters had been studied through different stages, starting from the initial point of expansion (C–J pressure employed from the literature) and the final point of expansion (the effective velocity obtained experimentally).

The natural fragmentation characteristics depended on the explosive parameters such as (P_{CJ} and the Gurney energy). The initial pressure showed a good relationship with the distribution factors μ, as shown in Figure 5-2. Extracting Gurney velocity at a fixed value of strain will show almost the same relation as that obtained from the initial pressure. The distribution factor of natural fragments is strongly depended on the explosive parameters at the moment of fracture, as shown in Figure 5-4.

In attempting to combine the acceleration time and the initial pressure in terms of impulse, a correlation study showed no real improvements in the relationship between the impulse of the detonation products and the fragment distribution factor, as shown in Figure 5-3.

The final velocity obtained from the experiment showed a very good improvement in the relation between the fragment distribution factor and the explosive parameters. However, the methods used to extract the final velocity did not reflect the real time of the fracture, and the velocity was sometimes extracted from a fixed strain. Therefore, the effective strain and the effective time of fracture were used in a combination study to include all expansion processes from initial to final stages of expansion and to study the dependence of the natural fragmentation factors on the explosive parameters. The acceleration time of the fragmentation process was the dominant parameters in the determination of the fragments characteristics, such as in the case of Comp-B and MCX-6002, where both have almost the same initial pressure and the same final velocity, but different acceleration time. This study found that, the acceleration time of the detonation products is not only the dominant parameter dictated the fragmentation process, the acceleration time is also play a principle role in the fragmentation characteristic. In the case of two types of explosive with the same explosive parameters, this study found that, the lower the acceleration time of the detonation products the higher the number of the small fragments was generated (i.e. <1 g). In addition, the higher the acceleration time of the detonation products the higher the number of the total fragments was generated.

CHAPTER 6: CONCLUSION

The dependence of the natural fragmentation characteristics on explosive parameters had been studied using empirical parameters. The cylinder test, in combination with an arena test, were used to characterise the expansion behaviour as well as the natural fragmentation distribution. The tests designed for this characterisation were used to extract the empirical fragmentation distribution parameters and the empirical explosive parameters required for this study.

Thus, a cylindrical case fabricated from alloy steel (EN19), and filled with different types of explosive (TNT, Comp-B, ONTELIT, MCX-6002 and RXHT-80), was explosively driven to fragmentation in order to determine the effective strain and the effective strain rate of this material.

The strain and the strain rate were considered over time as the material parameters that dictate fragmentation characteristics. The effective strain and the effective strain rate are a result of the expansion behaviour of the detonation products. The expansion behaviour of the detonation products from the initial to final stages of expansion determines the explosive parameters. Different explosive parameters contribute to the fragmentation process, such as the initial pressure and the final velocity of the expansion behaviour. The explosive parameters were addressed in the fragmentation characteristics using the final velocity in the strain rate models. In addition, the dependence of the natural fragmentation characteristics on the initial pressure was considered through different studies. Other explosive parameters in the expansion process between the two stages can lead to different expansion processes with the same final velocity, such as the heat and shock reverberation of the detonation products. This study, therefore, included all the explosive parameters from the initial to the final stages of expansion using the acceleration time of the detonation products between two stages.

The effective strain was extracted relative to the effective thickness of the collected fragments, whereas the effective strain rate was extracted from the analysis of the streak photography of the expanded metal under the effect of the detonation product load. The effective strain rate was, therefore, determined through the acceleration time of the detonation product relative to the effective strain. Furthermore, the empirical natural fragmentation parameters were extracted from the cumulative number distribution of the collected fragments. In order to find the optimum model and to include the explosive parameters and the material parameters in one model, the following were attempted.

Firstly, the dependence of the natural fragmentation distribution on the initial pressure was investigated.

Secondly, the acceleration time was combined with the initial pressure in terms of impulse. The dependence of the natural fragmentation on the impulse of the detonation products was studied through the empirical distribution factor of the cumulative distribution.

Finally, the dependence of the natural fragmentation distribution on the final velocity was investigated. The acceleration time was combined with the effective strain to study the dependence of the natural fragmentation characteristics on the effective velocity at fracture.

The results of this investigation showed a correlation between the explosive parameters (P_{CJ} and the effective velocity at fracture v_f) in different fragmentation mass regimes. It also showed that effective velocity at fracture correlates closely with the total distribution of fragments. The effective velocity at fracture did not reflect the effect of the explosive parameters on the small fragments group (<1 g).

The Gurney velocity is an explosive parameter that is used to predict the fragment size; it is attributed to the energy deposited into the casing. However, not only do explosive parameters affect the fragment size, but acceleration time is also a critical factor in the fragmentation process.

The effect of the acceleration time of the detonation product have been discussed in detail in the case of MCX-6002 and Comp-B. Looking to the case of MCX-6002 and Comp-B, they both had the same energy but different fragmentation times and therefore different strain rates. The detonation products of MCX-6002 was faster than Comp-B, which led to lower strain in the case of MCX-6002.

Therefore, considering the Gurney velocity or P_{CJ} as the only explosive parameters that dictate the fragmentation process can lead to ambiguous predictions. The strain rate, on the other hand, is a material parameter used to predict the fragmentation size distribution. The acceleration time of the detonation products used as an explosive parameter with the effective strain is the optimum way of achieving the effective strain rate to characterise the fragmentation process.

Future study:

Limited research have been performed on changes in fragmentation that occur in a specific material due to changing the explosive type. The detonation characteristics of the same explosive it also may affect the fragmentation characteristics. Another change on the fragmentation might occur when the detonation wave sweeps across the material at different angles.

CHAPTER 7: REFERENCES

[1] Türker, L., *Thermobaric and enhanced blast explosives (TBX and EBX),* Defence Technology, Vol.12, 2016, pp.423–445.

[2] Zecevic, B., Terzic, J., Razic, F. and Serdarevic-kadic, S., *Lethal Influence Factors of Natural and Preformed Fragmentation Projectiles*" DAAAM INTERNATIONAL SCIENTIFIC BOOK, 2015 pp. 219-234.

[3] Callister Jr, W. D. *Materials Science and Engineering*, 7th Edition, John Wiley & Sons Inc., USA, 2007.

[4] Johnson, G.R., Cook, W.H., *A constitutive model and data for metals subjected to large strains, high strain rates and high temperatures*, Proceedings, 7th International Symposium on Ballistics, The Hague, 1983.

[5] Cooper, P.W., *Explosives Engineering,* Wiley-VCH, New York, 1996.

[6] Jones, H. and Miller, A. R., *The Detonation of Solid Explosives*, Proc. Roy. Soc. London A, Vol.194, 1948.

[7] Wilkins, M.L., *The Equation of State of PBX 9404 and LXO4-01*, Lawrence Radiation Laboratory Technical Report, UCRL-7797, 1964, Livermore, USA.

[8] Lee, E., Horning, H.C and Kury, J.W, *Adiabatic Expansion of High Explosive Detonation Products*, Lawrence Radiation Laboratory Technical Report, UCRL-50422, 1968, Livermore, USA.

[9] Elek, P.M., Džingalašević, V.V., Jaramaz, S.S. and Micković, D.M., *Determination of Detonation Products Equation of State from Cylinder Test*: Analytical Model and Numerical Analysis, Thermal Science: Vol. 19, No. 1, 2015, pp. 35-48.

[10] Ugrčić, M., *Numerical Simulation of the Fragmentation Process of High Explosive Projectiles*, Scientific Technical Review, Vol. 63, No. 2, 2013, pp.47-57.

[11] Jackson, S.I., *Scaled Cylinder Test Experiments with Insensitive PBX 9502 Explosive*, In the Proceedings of the 15th International Symposium on Detonation, 2014, pp.1-10.

[12] Taylor, G.I., *The fragmentation of tubular bombs,* Scientific Papers of G. I. Taylor, Vol. III No. 44, Cambridge University Press, 1963, pp. 387-390.

[13] Al-Hassani, S. T. S., Hopkins, H. G., and Johnson, W., *A Note on the Fragmentation of Tubular Bombs***,** Int. J. mech. Sci; Pergamon Press. Vol. 11, 1969, pp. 545-549.

[14] Mott, N.F., *Fragmentation of shell cases*. Proceedings of the Society Royal. London A 189, 1947, pp.300-308.

[15] Kipp, M.E. and Grady, D.E., *Dynamic fracture growth and interaction in one dimension*, Journal of Mechanics and Physics of Solids, Vol. 33, No. 4, 1985, pp. 399-415.

[16] Tanapornraweekit G. and Kulsirikasem W., *An Effects of Material Properties of Warhead Casing on Natural Fragmentation Performance of High Explosive (HE) Warhead*, International Journal of Mathematical, Computational, Physical, Electrical and Computer Engineering Vol. 5, No. 11, 2011, pp.1770-1775.

[17] Jian-jun Zhu, Wei-bing Li, Xiao-ming Wang and Wen-bin Li**,** *Study on the Expansion and Fracture of a Cylindrical 50simnvb Steel Shell Under Different Tempering Temperatures,* 29TH International Symposium on Ballistics Edinburgh, Scotland, UK, 2016, pp. 1630-1640.

[18] Wei-bing Li, Wen-bin Li, Xiao-ming Wang, Chun Chen and Jian-jun Zhu, *Expansion and Fracture of Fragmenting Warhead Shells of Various Materials under a Cl-20 Explosive Charge* 29TH International Symposium on Ballistics Edinburgh, Scotland, UK, 2016, pp. 1631-1629.

[19] Carleone, J., *Tactical Missile Warheads,* Progress in Astronautics and Aeronautics,

Vol. 155, 1993.

[20] Grady, D.E. and Hightower, M.M., *Natural fragmentation of exploding cylinders*, International Conference on the Materials Effects of Shock-wave and High-strain-rate phenomena, 1990, pp.713-721.

[21] Hoggatt, C.R. and Recht, R.F., *Fracture behaviour of tubular bombs*, J. Appl. Phys.; Vol. 39, No. 3, 1968, pp.1856-1862.

[22] Loyd, R.M., *Conventional warhead systems physics and engineering design*, American Institute of Aeronautics and Astronautics, 1998.

[23] Pearson, J., *A fragmentation model for cylindrical warheads*, Technical Report NWC TP 7124. China Lake, California: Naval Weapons Center; December 1990.

[24] Johnson, G. R. and Cook, W. H., "*Fracture Characteristics of Three Metals Subjected to Various Strains, Strain Rates, Temperatures and Pressures.*" Engineering Fracture Mechanics Vol. 21, No.1, 1985, pp.31-48.

[25] Hancock, J. W. and Mackenzie, A. C., *On the mechanism of ductile failure in high-strength steels subjected to multi-axial stress-states*. J. Mech. Phys Solids Vol. 24, 1976, pp. 147-169.

[26] Goto, D.M., Becker, R. Orzechowski, T.J., Springer, H.K., Sunwoo, A.J. and Syn, C.K., *Investigation of the Fracture and Fragmentation of Explosively Driven Rings and Cylinders*, International Journal of Impact Engineering, Vol. 35, 2008, pp.1547-1556.

[27] Zecevic, O. B., Terzic, J. and Catovic, A., *Influence of warhead case material on natural fragmentation performances*, in 12th DAAAM International Symposium Vienna, Austria, 2004.

[28] Shahraini M. T., *Casing toughness effect on anti-air fragmentation warhead performance*, in 23rd International Symposium on Ballistics, Tarragona, Spain, 2007, pp. 209-213.

[29] Elek, P. and Jaramaz, S., *Fragment Mass Distribution of Naturally Fragmenting Warheads*, FME Transactions Vol.37, No. 3, 2009, pp. 129-135.

[30] Grady, D.E. and Kipp, M.E., *Geometric statistics and dynamic fragmentation*, Journal of Applied Physics, Vol. 58, No. 3, 1985, pp. 1210-1222.

[31] Elek, P. and Jaramaz, S., *Fragment size distribution in dynamic fragmentation,* Geometric probability approach, FME Transactions, Vol. 36, No. 2, 2008, pp. 59-65.

[32] Elek, P. and Jaramaz, S., *Dynamic fragmentation: Geometric approach*, Proceedings of the First International Congress of Serbian Society of Mechanics, Kopaonik, Serbia, 2007, pp. 647-652.

[33] Glenn, L.A., Gommerstadt, B.Y. and Chudnovsky, A., *A fracture mechanics model of fragmentation*, Journal of Applied Physics, Vol. 60, No. 3, 1986, pp.1224-1226.

[34] Mott, N.F. and Linfoot, E.H., *A theory of fragmentation*, British Ministry of Supply Report, AC 3348, 1943.

[35] Held, M., *Fragment mass distribution of HE projectile*, Propellants, Explosives, Pyrotechnics, Vol. 15, No. 6, 1990, pp. 254-260.

[36] Victor, A. C., "*Warhead Performance Calculations for Threat Hazard Assessment***"** Department of Defence Explosives Safety Seminar, Las Vegas, 1996.

[37] B. Zecevic, J. Terzic, A. Catovic, and S. Serdarevic-Kadic, *Characterization of distribution parameters of fragment mass and number for conventional projectiles*, New Trends in Research of Energetic Materials, Czech Republic, 2011.

[38] Strømsøe, E. and Ingebrigtsen, K.O., *A modification of the Mott formula for prediction of the fragment size distribution*, Propellants, Explosives, Pyrotechnics, Vol. 12, No. 5, 1987, pp. 175-178.

[39] Magis, S.F., *Material Selection for Naturally Fragmenting Munitions*, NWL TM 13/67, 1967.

[40] Gurney, R.W. and Sarmousakis, J. N., *The mass distribution of fragments from bombs, shell and grenades*, US Army Ballistic Research Laboratory Report BRL 448, Aberdeen Proving Ground, MD, 1944.

[41] Elek, P. and Jaramaz, S., *Modeling of fragmentation of rapidly expanding cylinders,* Theoret. Appl. Mech., Vol.32, No.2, Belgrade 2005, pp. 113-130.

[42] Grady, D., *Investigation of Explosively Driven Fragmentation of Metals-Two-Dimensional Fracture and Fragmentation of Metal Shells***,** Progress Report II, February 1,2003.

[43] Gold, V. M., Baker, E. L. Poulos, W. J. and Fuchs, B. E., *PAFRAG Modeling of Performance of Explosive Fragmentation Munitions*, Int. J. Imp. Engng, Vol. 33, 2006, pp. 294-304.

[44] Gold V. M. and Wu, Y., *An Effect of Explosive Detonation Pressures on Fragmentation Characteristics of Explosive Fragmentation Munitions*, Picatinny Arsenal, 2009.

[45] Gold, V.M. "*Fragmentation model for large L/D (Length over Diameter) explosive fragmentation warheads*". Defence Technology, Vol.13, pp.300-309, 2017.

[46] Gurney, R.W., *The initial velocity of fragments from bombs, shells and grenades,* Army Ballistic Research Laboratory Report No. 405, 1943.

[47]Kennedy J.E., *Gurney energy of explosives: estimation of the velocity and impulse imparted to driven metal*, Sandia National Laboratories, Report No. SC-RR-70-790, 1970.

[48]Sućeska, M., *Test Methods for Explosives*, 1st edition, Springer-Verlag, New York, 1995.

[49] Frem, D., *Estimating the metal acceleration ability of high explosives*, Defence Technology, 2019.

[50] Arnold, N., Estermann, M. and Koch, A., *A Simple Relation between the Detonation Velocity of an Explosive and its Gurney Energy*, Propellants, Explosives, Pyrotechnics, 2002, pp. 365 – 368.

[51]Zukas, J. A. and Walters, W. P., *Explosive Effects and Applications,* Springer-Verlag, 2003.

[52] Taylor, G.I., *Analysis of the explosion of a long cylindrical bomb detonated at one end*, Cambridge University Press, Vol. 3, No. 30, 1963, pp. 277-286.

[53] Randers-Pehrson, G., *An Improved Equation of Calculating Fragment Projection Angles*, Proceedings of the 2nd International Symposium on Ballistics, Daytona Beach, 1976.

[54] Hennequin, E., "*Influence of Edge Effects on the Initial Velocities of Fragments from a Warhead*", Proceedings of the 9th International Symposium on Ballistics, Shrivenham, 1986.

[55] König, P.J., "*A Correction for the Ejection Angles of Fragments from Cylindrical Warheads*, Propellants and Explosives, Pyrotechnics Vol. 12, 1987, p.154.

[56] Smit, G.J.F. Mostert, F.J. and du Plessis, J.P., *A Novel Approach to The Multidimensional Nature of Velocities of Fragments Originating From Convex Shaped Warheads*", 19th International Symposium of Ballistics, Interlaken, Switzerland, 2001, pp. 655-661.

[57] Polk, J. F., *Determination of Equation of State of Explosive Detonation Products from the Cylinder Expansion Test*" Technical report ARBRL-TR-02571, Ballistic Research Laboratory, Aberdeen Proving Ground, Md., USA, 1984.

[58] Lee E, Horning H.C and Kury J.W, *Adiabatic Expansion of High Explosive Detonation Products*, Lawrence Radiation Laboratory Technical Report, Livermore, USA, UCRL-50422, 1968.

[59] Catanach R., Hill L., Harry H., Aragon E. and Murk D., *Cylinder Test Specification*, Los Alamos National Laboratory, USA, 1999.

[60] EMĠR, T., *Design and Development of a Cylinder Expansion Test Setup for Determination of Equation of State Parameters of Various Explosives*, Master Degree Thesis. 2014.

[61] Hornberg, H., *Determination of fume state parameters from expansion measurements of metal tube*, Propellants, Explosives, Pyrotechnics, Vol.11, No. 1,1986, pp. 23-31.

[62] Lan, I.-F., et al., "*An improved simple method of deducing JWL parameters from cylinder expansion test*", Propellants, Explosives, Pyrotechnics, Vol. 18, No. 1, 1993, pp. 18-24.

[63] Hill, L.G., *Detonation products equation-of-state directly from the cylinder test*, Proceedings 21st International Symposium on Shock Waves, Great Keppel Island, Australia, 1997, pp. 1-6.

[64] Souers P.C., Garza R., Hornig H., Lauderbach L., Owens C., and Vitello P., *Metal Angle Correction in the Cylinder Test*, Propellants, Explosives and Pyrotechnics, Vol. 36, No. 1, 2011, pp. 9-15.

[65] Akhavan, J., *The Chemistry of Explosives*, Royal Society of Chemistry, 2011.

[66] *Agrawal, J.P., High Energy Materials***,** Propellants, Explosives and Pyrotechnics, 2010.

[67] Kinney, G. F. and Graham, K. J., *Explosive Shocks in Air,* Springer Science+Business Media, LLC, 1985.

[68] Prytz, A. K., Ødegårdstuen, G. and Heiberg, O.M., *IM assessment for a state of the art 155mm HE round*, Insensitive Munitions & Energetic Materials Technology Symposium, Rome, Italy, 2015.

[69] Spyckerelle, C., Songy, C. and Eck, G., *IM Melt Cast Compositions based on NTO*, Insensitive Munitions & Energetic Materials Technology symposium, 2010.

[70] International test operation procedure, *Static Testing of High-Explosive Munition for Obtaining Fragment Spatial Distribution*, 4-2-813, 1990.

[71] Alqarni, S.A., Mostert**,** F.J., Wichers, Benade, J.G., *The Dependence of Natural Fragmentation Characteristics of a Casing Material on Explosive Parameters***,** the South African Ballistic Organization, 2018.

[72] Esen, S. Nyberg, U. Arai, H. and Ouchterlony, F., *Determination of the Energetic Characteristics of Commercial Explosives with the Cylinder Expansion Test Technique*, Swebrec, Sweden, 2005.

[73] Minzu Liang, Xiangyu Li and Fangyun Lu, *Effects of Strain Rate on Fragmentation Performance of Dynamic Fracture and Fragmentation of Notched Cylinders*, 29TH INTERNATIONAL SYMPOSIUM ON BALLISTICS EDINBURGH, SCOTLAND, UK, 2016, pp. 1388-1402.

CHAPTER 8: APPENDICES

8.1 Appendix A

TEST SAMPLE:

Sample number	M	L	OD	t_o	ID	V_M	ρ_M	V_C	M_{Total}	C	ρ_o
Units	g	mm	mm	mm	mm	cc	g/cc	cc	g	g	g/cc
TNT 1	1105.5	200.1	50.0	5.1	39.9	142.9	7.7	250.5	1497.8	392.3	1.6
TNT 2	1095.4	199.9	50.0	5.0	39.9	142.5	7.7	250.2	1490.4	395.0	1.6
TNT 3	1094.6	200.0	49.9	5.0	40.0	140.3	7.8	250.9	1488.5	393.9	1.6
TNT 4	1098.8	200.0	50.1	5.0	40.0	142.6	7.7	251.1	1492.5	393.7	1.6
TNT 5	1114.8	200.0	50.0	5.1	39.9	142.7	7.8	250.6	1517.4	402.6	1.6
Comb-B 1	1096.9	199.9	49.9	5.0	39.8	141.6	7.7	248.6	1523.0	426.1	1.7
Comb-B 2	1113.2	200.0	50.1	5.1	40.0	143.0	7.8	251.0	1532.7	419.5	1.7
Comb-B 3	1112.8	200.0	50.0	5.1	39.8	143.2	7.8	249.2	1518.6	405.8	1.6
Comb-B 4	1103.7	200.0	50.0	5.1	39.8	143.5	7.7	249.2	1522.4	418.7	1.7
Comb-B 5	1108.6	200.0	50.0	5.1	39.9	143.4	7.7	250.0	1512.3	403.7	1.6
ONTELIT 1	1097.1	199.8	50.0	5.1	39.9	142.6	7.7	250.2	1523.0	425.9	1.7
ONTELIT 2	1104.0	199.7	50.0	5.1	39.9	142.8	7.7	249.8	1526.5	422.5	1.7
ONTELIT 3	1088.7	200.0	50.0	5.0	40.0	142.3	7.6	250.8	1534.7	446.0	1.8
ONTELIT 4	1100.2	199.9	50.0	5.1	39.9	142.6	7.7	249.9	1537.3	437.1	1.7
ONTELIT 5	1103.4	200.0	50.1	5.0	40.0	142.5	7.7	251.3	1515.7	412.3	1.6
MCX-6002 1	1092.3	200.0	49.9	5.0	40.0	140.5	7.8	251.4	1535.4	443.1	1.8
MCX-6002 2	1104.9	199.9	50.1	5.1	39.8	144.9	7.6	248.9	1544.0	439.1	1.8
MCX-6002 3	1103.9	199.9	50.0	5.0	39.9	142.1	7.8	250.5	1544.5	440.6	1.8
MCX-6002 4	1098.8	199.9	50.0	5.1	39.9	143.1	7.7	249.6	1543.9	445.1	1.8
MCX-6002 5	1083.2	200.0	49.9	4.9	40.0	139.2	7.8	251.9	1556.5	473.3	1.9
RXHT-80 1	1098.2	199.9	50.0	5.0	39.9	141.7	7.7	250.3	1474.5	376.3	1.5
RXHT-80 2	1096.1	200.0	50.0	5.0	39.9	142.2	7.7	250.0	1472.3	376.2	1.5
RXHT-80 3	1086.1	200.1	49.9	5.0	39.8	142.1	7.6	249.0	1463.4	377.3	1.5
RXHT-80 4	1109.1	200.0	50.0	5.0	40.0	141.7	7.8	251.3	1484.1	375.0	1.5
RXHT-80 5	1109.3	200.0	50.1	5.1	40.0	142.8	7.8	250.7	1482.1	372.8	1.5
average	1100.7	199.9				142.3	7.7	250.2			

L : Length of the sample
OD: Outer diameter of the sample
ID: Inner diameter of the sample
t_o : Wall thickness of the sample
V_M : Volume of the cylindrical case
ρ_M : Density of the metal case
M_{Total}: Total mass of the sample
ρ_o : Density of the filling
* M: refer to cylinder metal.
* C: refer to explosive material.

Table 8-1: Gurney velocity from High-Speed-Velocity camera vs literature:

average	v_f	M	C	M/C	$\sqrt{2e}$ HSV	$\sqrt{2e}$ *Cooper
Units	mm/µs	g	g		mm/µs	mm/µs
TNT	1.374	1101.82	395.48	2.78	2.49	2.37
Comp-B	1.669	1107.04	414.76	2.67	2.97	2.66
ONTELIT	1.418	1098.68	428.76	2.56	2.48	2.68
MCX	1.448	1096.62	448.24	2.45	2.49	2.48
RXHT-80	1.398	1099.76	375.52	2.93	2.59	2.59

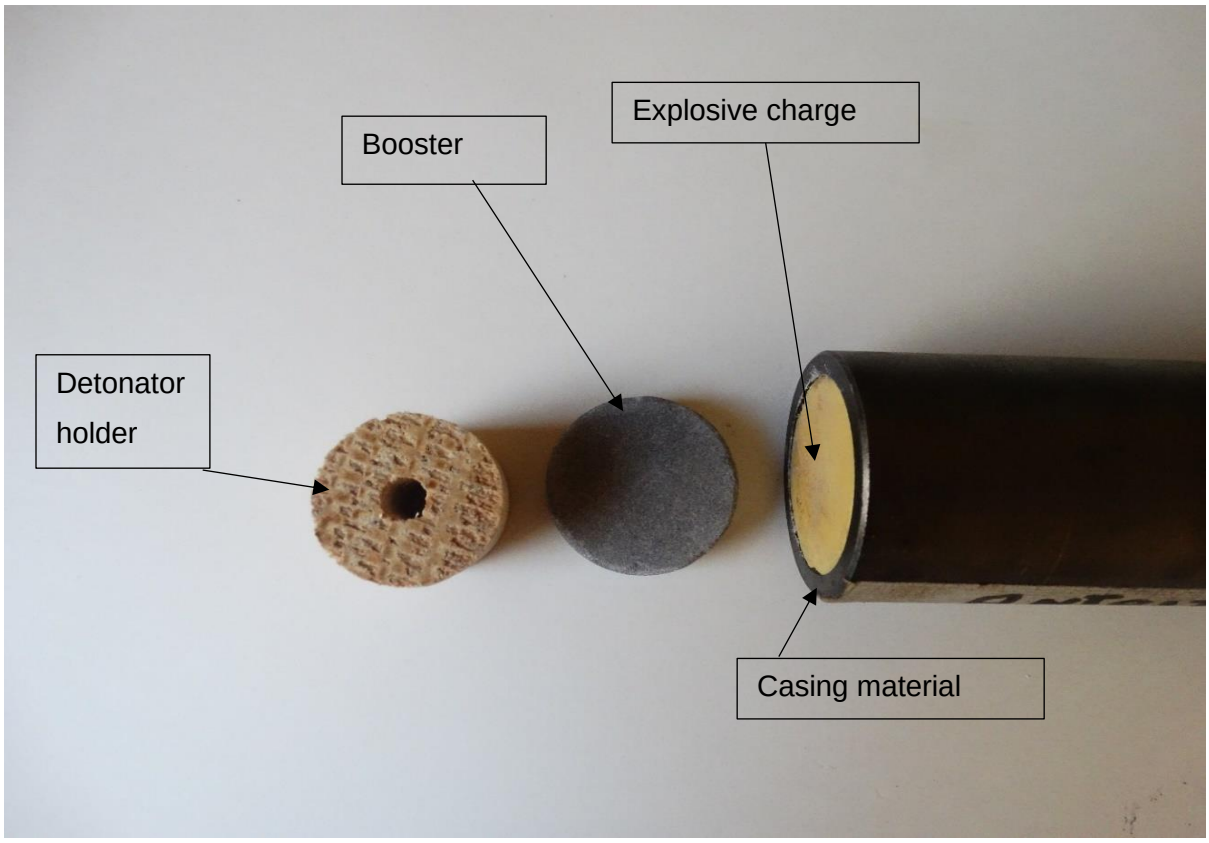

Figure 8-1: Test sample components.

8.2 Appendix B

Fragmentation characterization based on average of three tests.

Table 8-2: TNT mass, number and velocities distribution per angular zone.

No.Fragm/Sector.	080-085	085-090	090-095	095-100	100-105	120-125	N(m)	N(<m)
Mass Category (g)	Number of fragments per angular zone							
0.01 - 0.09	2	2	10	31	3	0	48	150
0.1 - 0.19	0	0	5	11	2	0	18	102
0.2 - 0.29	1	0	2	4	0	1	7	84
0.3 - 0.39	0	0	0	5	2	0	7	77
0.4 - 0.49	0	0	1	1	2	0	4	70
0.5 - 0.74	1	1	1	10	0	0	13	66
0.75 - 0.99	0	1	0	3	2	0	6	53
1 - 1.99	1	2	5	7	1	0	16	47
2 - 2.99	0	0	1	6	4	0	11	31
3 - 3.99	1	0	1	1	1	0	4	20
4 - 4.99	0	0	1	4	0	0	5	16
5 - 7.49	1	2	1	1	1	0	6	11
7.5 - 9.99	0	1	0	1	0	0	2	5
10 - 14.99	0	1	0	1	0	0	2	3
15 - 19.99	0	0	0	1	0	0	1	1
Sector Totals	7	10	28	87	18	1	150	
Fragments velocity (km/s)	1245	1292	1362	1386	1345	1345		

Table 8-3: Comp-B mass, number and velocities distribution per angular zone.

No.Fragm/Sector.	065-070	070-075	075-080	080-085	085-090	090-095	095-100	100-105	105-110	110-115	115-120	120-125	125-130	130-135	135-140	N(m)	N(>m)
Mass Category (g)	Number of fragments per angular zone																
0.01 - 0.09	0	0	3	3	9	19	41	3	4	1	0	0	0	1	0	82	273
0.1 - 0.19	2	1	2	3	8	11	24	1	0	1	0	0	1	2	1	49	191
0.2 - 0.29	0	0	1	0	5	4	12	0	1	0	0	0	0	0	1	23	142
0.3 - 0.39	0	0	0	1	1	6	5	0	1	1	0	1	0	0	0	14	119
0.4 - 0.49	0	0	0	1	1	4	5	0	0	0	0	0	0	0	0	11	105
0.5 - 0.74	0	1	0	2	1	5	7	2	0	0	0	0	0	0	0	17	94
0.75 - 0.99	0	1	2	3	0	6	5	1	0	0	0	0	0	0	0	17	77
1 - 1.99	0	0	4	2	4	5	14	3	1	0	0	0	0	0	0	33	60
2 - 2.99	0	0	0	0	0	6	3	2	0	0	0	0	0	0	0	11	27
3 - 3.99	0	0	0	1	0	3	4	0	0	0	0	0	0	0	0	8	16
4 - 4.99	0	0	0	0	1	0	2	0	0	0	0	0	0	0	0	3	8
5 - 7.49	0	0	0	0	0	3	0	0	0	0	0	0	0	0	0	3	5
7.5 - 9.99	0	0	0	0	1	1	0	0	0	0	0	0	0	0	0	2	2
10 - 14.99	0	0	0	0	0	0	0	0	0	0	0	0	0	0	0	0	0
15 - 19.99	0	0	0	0	0	0	0	0	0	0	0	0	0	0	0	0	0
Sector Totals	2	3	12	16	31	73	122	12	7	3	0	1	1	3	2	273	
Fragments velocity (km/s)				1479	1559	1674	1662	1514									

Table 8-4: NTO-TNT mass, number and velocities distribution per angular zone.

No.Fragm/Sector.	075-080	080-085	085-090	090-095	095-100	100-105	105-110	130-135	135-140	N(m)	N(>m)
Mass Category (g)	Number of fragments per angular zone										
0.01 - 0.09	4	10	10	21	26	3	0	0	1	74	241
0.1 - 0.19	1	5	6	12	7	6	1	0	0	38	167
0.2 - 0.29	0	2	2	3	6	2	0	0	0	15	129
0.3 - 0.39	0	1	0	4	6	2	0	1	0	13	114
0.4 - 0.49	3	1	0	3	4	1	2	0	0	14	101
0.5 - 0.74	0	2	3	4	6	3	0	0	0	18	87
0.75 - 0.99	0	0	2	2	7	2	0	0	0	13	69
1 - 1.99	0	2	6	5	13	2	0	0	0	28	56
2 - 2.99	0	4	0	2	5	1	0	0	0	12	28
3 - 3.99	0	2	2	0	3	0	0	0	0	7	16
4 - 4.99	0	0	2	0	1	1	0	0	0	4	9
5 - 7.49	0	0	0	2	0	0	0	0	0	2	5
7.5 - 9.99	0	0	0	0	0	0	0	0	0	0	3
10 - 14.99	0	0	0	1	1	0	0	0	0	2	3
15 - 19.99	0	0	0	0	0	0	0	0	0	0	1
20 - 29.99	0	0	0	1	0	0	0	0	0	1	1
Sector Totals	8	29	33	60	85	23	3	1	1	241	
Fragments velocity (km/s)		1190	1273	1411	1424	1346					

Table 8-5: MCX-6002: mass, number and velocities distribution per angular zone.

No.Fragm/Sector.	070-075	075-080	080-085	085-090	090-095	095-100	100-105	125-130	135-140	N(m)	N(>m)
Mass Category (g)	Number of fragments per angular zone										
0.01 - 0.09	2	4	3	8	20	45	41	3	1	121	328
0.1 - 0.19	0	2	4	7	11	13	10	1	1	47	207
0.2 - 0.29	1	0	2	5	3	7	6	0	1	23	160
0.3 - 0.39	0	3	0	3	1	1	5	0	0	13	137
0.4 - 0.49	0	1	3	4	4	7	3	0	0	22	124
0.5 - 0.74	0	2	1	3	3	8	3	0	0	20	102
0.75 - 0.99	0	0	1	6	5	4	4	0	0	20	82
1 - 1.99	0	3	1	6	2	10	6	0	0	28	62
2 - 2.99	0	1	0	6	0	4	1	0	0	12	34
3 - 3.99	0	0	0	0	1	5	1	0	0	7	22
4 - 4.99	0	0	0	1	3	1	0	0	0	5	15
5 - 7.49	0	0	0	1	0	4	1	0	0	6	10
7.5 - 9.99	0	0	0	0	0	0	0	0	0	0	4
10 - 14.99	0	1	0	0	0	3	0	0	0	4	4
15 - 19.99	0	0	0	0	0	0	0	0	0	0	0
Sector Totals	3	17	15	50	53	112	81	4	3	328	
Fragments velocity (km/s)			1246	1333	1424	1463	1396				

Table 8-6: RXHT-80 mass, number and velocities distribution per angular zone.

No.Fragm/Sector.	070-075	075-080	080-085	085-090	090-095	095-100	100-105	105-110	N(m)	N(>m)
Mass Category (g)	Number of fragments per angular zone									
0.01 - 0.09	0	0	1	3	3	6	0	1	14	147
0.1 - 0.19	0	0	6	3	6	7	0	4	26	133
0.2 - 0.29	0	0	0	2	2	1	2	0	7	107
0.3 - 0.39	0	0	1	2	1	4	1	1	10	100
0.4 - 0.49	0	0	0	0	3	3	1	0	7	90
0.5 - 0.74	1	0	2	2	4	5	1	1	15	83
0.75 - 0.99	0	0	1	1	4	2	0	0	8	68
1 - 1.99	0	0	5	2	4	10	2	1	24	60
2 - 2.99	0	0	2	0	2	7	2	2	15	36
3 - 3.99	0	1	0	1	2	4	2	0	10	21
4 - 4.99	0	0	0	0	0	1	0	0	1	11
5 - 7.49	0	0	0	1	0	1	0	1	3	10
7.5 - 9.99	0	0	0	0	1	0	0	0	1	7
10 - 14.99	0	0	0	0	3	2	0	0	5	6
15 - 19.99	0	0	0	0	0	1	0	0	1	1
Sector Totals	1	1	18	17	35	54	11	11	147	
Fragments velocity (km/s)			1249	1338	1382	1415	1400			

Table 8-7: Fragmentation thickness analysis.

		TNT			COMP-B			MCX			NTO-TNT			TXHT-80		
		SHOT-1	SHOT-2	SHOT-3	SHOT-1	SHOT-2	SHOT-3	SHOT-1	SHOT-2	SHOT-3	SHOT-1	SHOT-2	SHOT-3	SHOT-1	SHOT-2	SHOT
tf	mm															
	1	3.68	3.98	4.18	1.96	2.39	3.18	2.71	3.13	2.74	2.93	4.32	3.77	3.9	3.66	1.74
	2	2.49	1.77	2.27	1.33	2.8	2.56	3.03	2.32	3	2.69	3.29	3.65	2.57	2.33	2.73
(85-90)	3	3.81	2.55	4	2.33	2.6	3.53	1.89	1.78	1.99	3.3	1.98	3.83	2	2.62	1.83
	4	2.83	2.12	2.43	2.53	2.9	2.59	3.84	2.44	2.04	2.33	1.78	3.6	2.39	2.94	3.97
	5	4.01	3.68	2.79	2.56	1.6	3.51	3.06	3.56	3.85	2.32	3.81	3.44	2.17	2.56	2.69
	1	1.64	2.92	3.57	1.68	3.1	1.5	2.89	2.92	2.36	2.78	3.22	3.84	2.61	3.93	3.53
	2	2.04	3.58	3.1	1.7	3.9	2.37	3.47	2.68	2.56	2.81	2.79	3.91	3.16	3.87	3.74
(90-95)	3	1.97	2.32	2.52	1.77	2.11	2.86	3.51	3.75	2.24	2.98	2.39	3.75	2.05	2.6	4.75
	4	3.21	2.5	3.34	2.1	2.05	2.75	2.37	2.58	2.8	2.78	3.64	3.56	3.06	2.66	3.75
	5	3.77	3.87	2.16	3.19	1.84	1.93	3.29	3.09	2.24	2.73	3.02	3.78	3.42	3.13	4.04
	1	2.61	4.04	4.16	2.53	2.21	2.27	3.41	2.79	3.32	3.75	1.68	2.21	4.28	2.41	4.06
	2	2.14	4.3	3.81	3.54	3.31	2.41	2.75	3.95	3.77	2.69	2.06	1.97	3.18	2.9	2.93
(95-100)	3	3.78	3.89	3.91	3.35	1.79	2.91	2	1.69	3.23	2.14	3.7	2.67	3.94	3.1	2.69
	4	2.87	3.79	3.87	2.38	2.77	2.48	3.54	1.86	2.61	3.47	3.41	2.43	3.7	2.59	3.83
	5	2.47	3.73	2.62	3.07	2.67	1.51	2.12	2.32	3.71	2.27	3.61	2.22	3.75	2.32	3.1
	1	3.46	2.7	3.97	2.53	2.99	2.71	3.19	2.4	2.44	2.6	2.23	2.02	3.79	2.95	2.93
	2	3.83	4.06	3.34	2.61	3.67	3.43	3.3	2.38	3.77	2.8	3.82	2.23	2.26	3.68	3.23
(100-105)	3	3.54	2.33	2.27	3.74	2.37	1.89	3.06	2.47	3.83	3.85	4.23	2.93	3.12	3.56	2.51
	4	2.47	2.98	2.04	3.47	2.65	2	2.5	1.98	3.84	2.81	1.97	2.21	2.61	3.85	2.49
	5	2.61	2.69	3.08	2.96	1.88	2.57	3.01	2.48	2.56	3.11	3.79	3.3	3.71	3.68	3.79
		2.96	3.19	3.17	2.5665	2.58	2.548	2.947	2.628	2.945	2.857	3.037	3.066	3.0835	3.067	3.21
	mean			3.107			2.5648			2.840			2.9866			3.12
	SD			0.738			0.6215			0.616			0.6916			0.679
	εtt			0.475			0.6675			0.565			0.515			0.47
	rf			40.22			48.736			44.01			41.852			40.03
	eps			0.549			0.7708			0.653			0.5949			0.543

8.3 Appendix C

Streak photographic results and analysis

TNT-1:

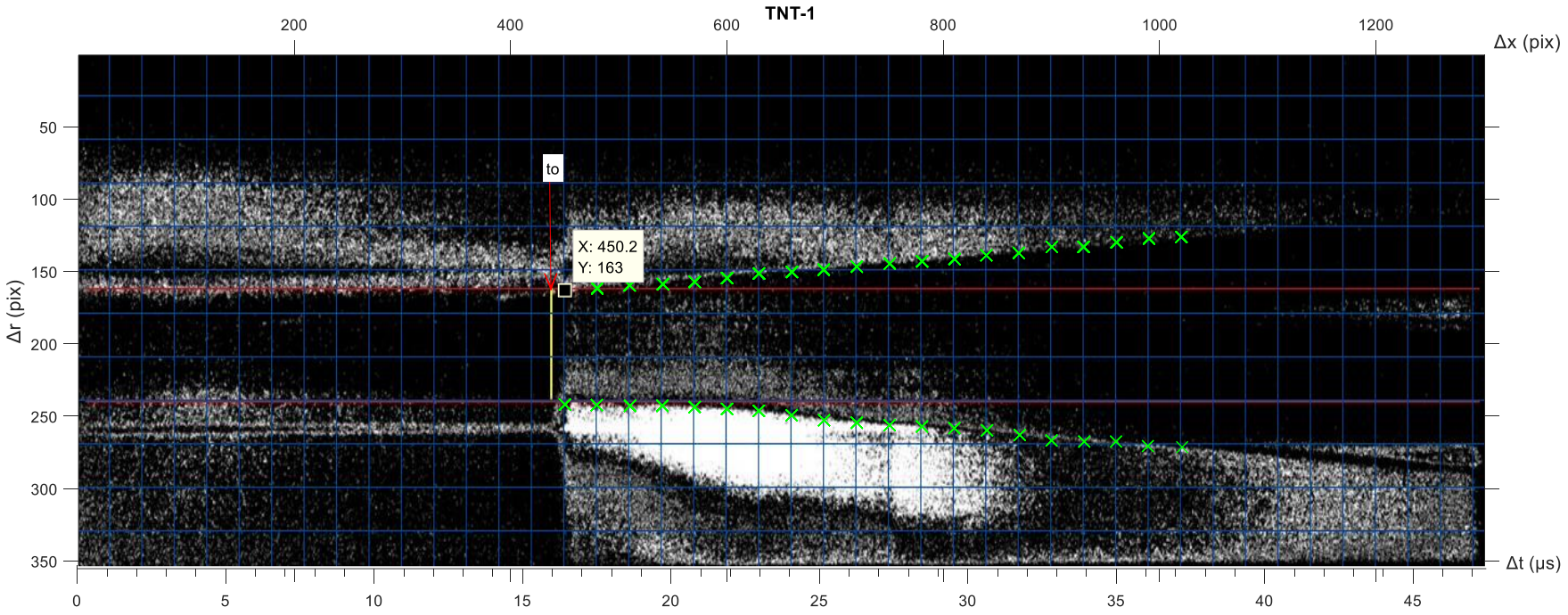

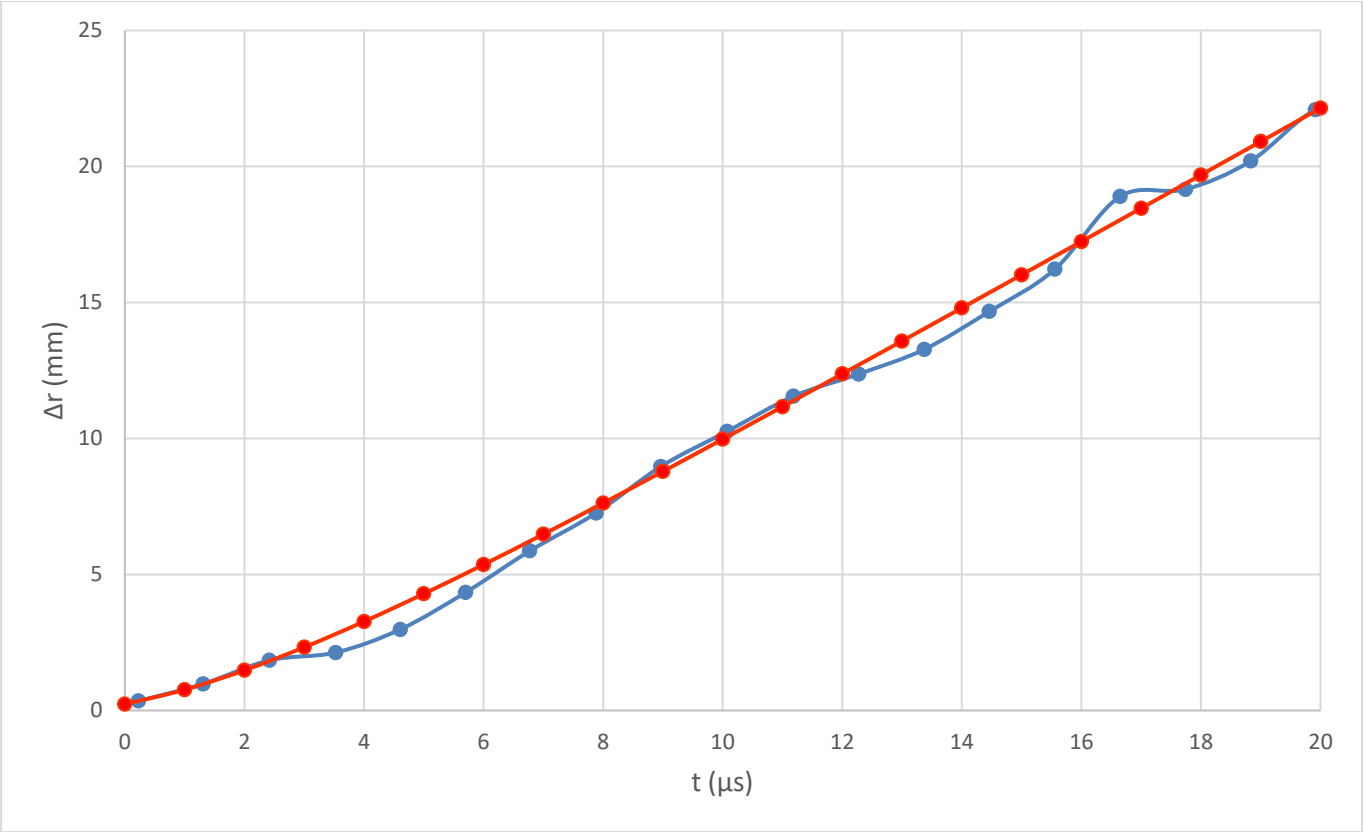

Figure 8-2: The radial position of the cylinder wall with respect to time for (TNT-1)

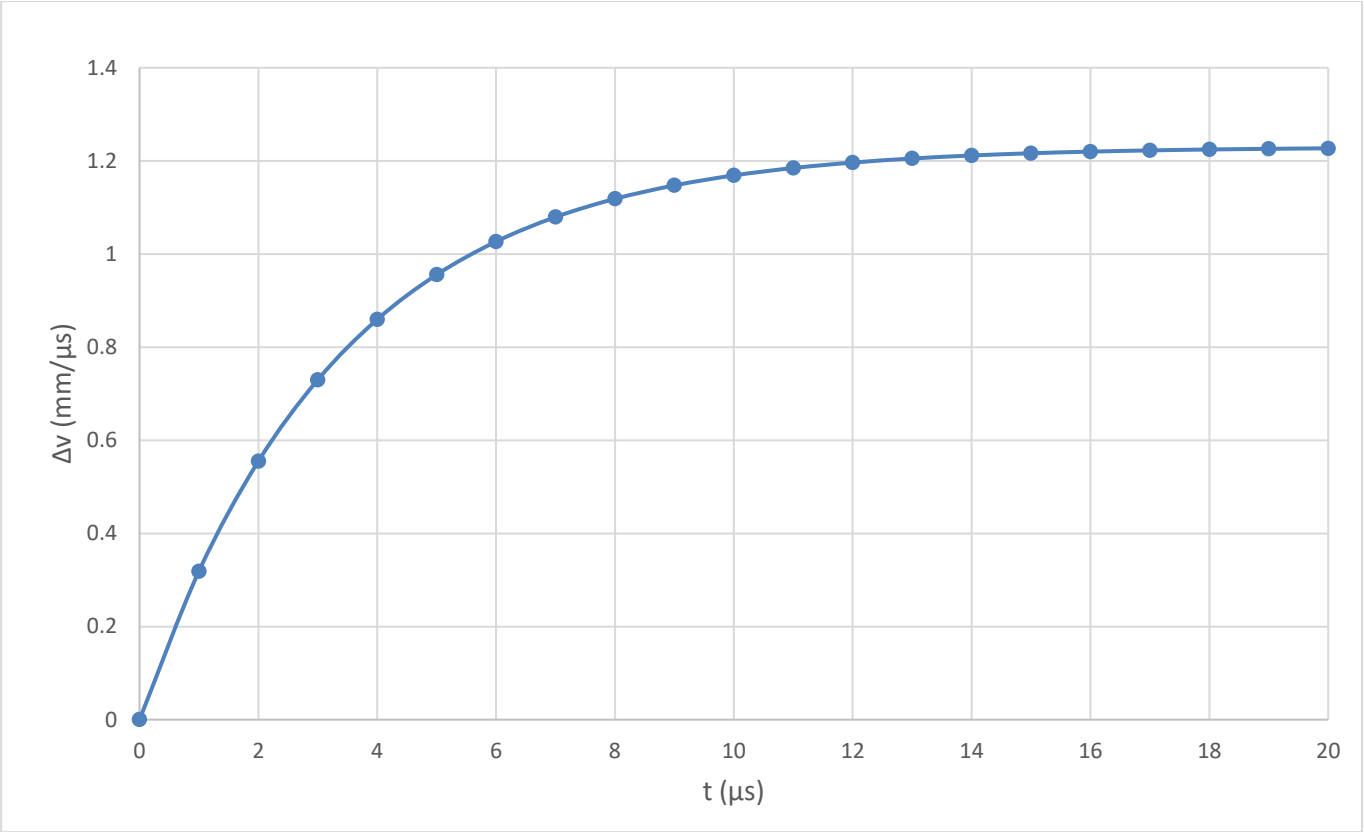

Figure 8-3: The radial expansion velocity of (TNT-1).

TNT-2:

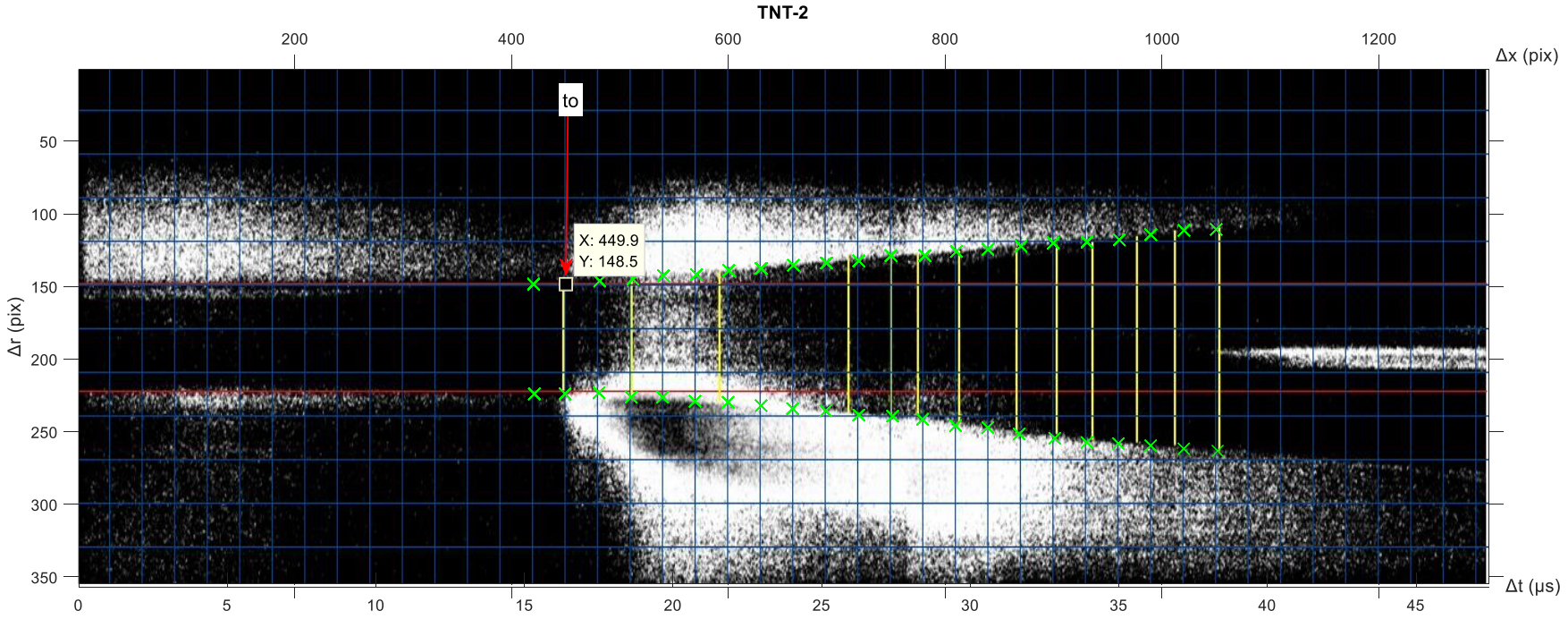
TNT-2
200
400
600
800
1000
1200
Δx (pix)
to
X: 449.9
Y: 148.5
50
100
150
200
250
300
350
Δr (pix)
0
5
10
15
20
25
30
35
40
45
Δt (μs)

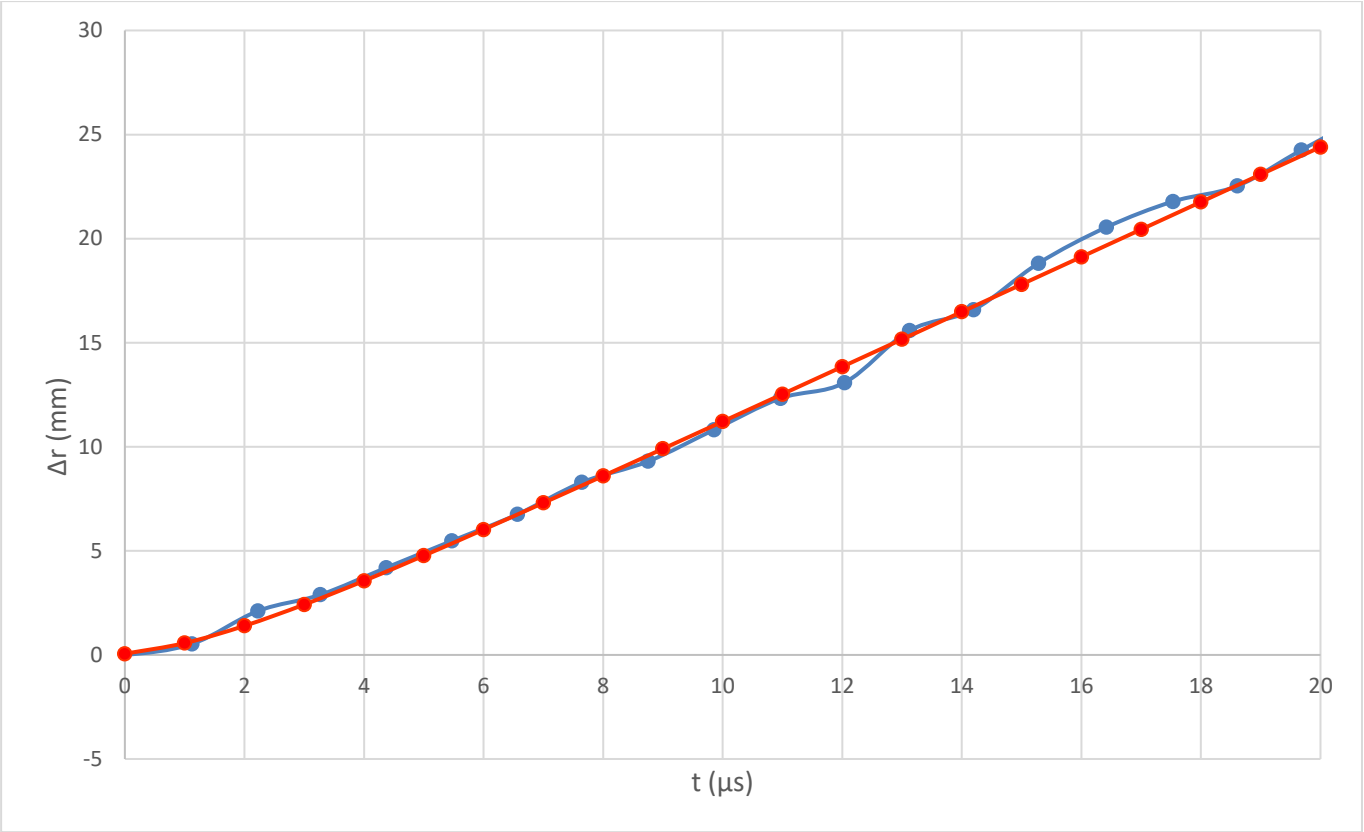

Figure 8-4: The radial position of the cylinder wall with respect to time for (TNT-2).

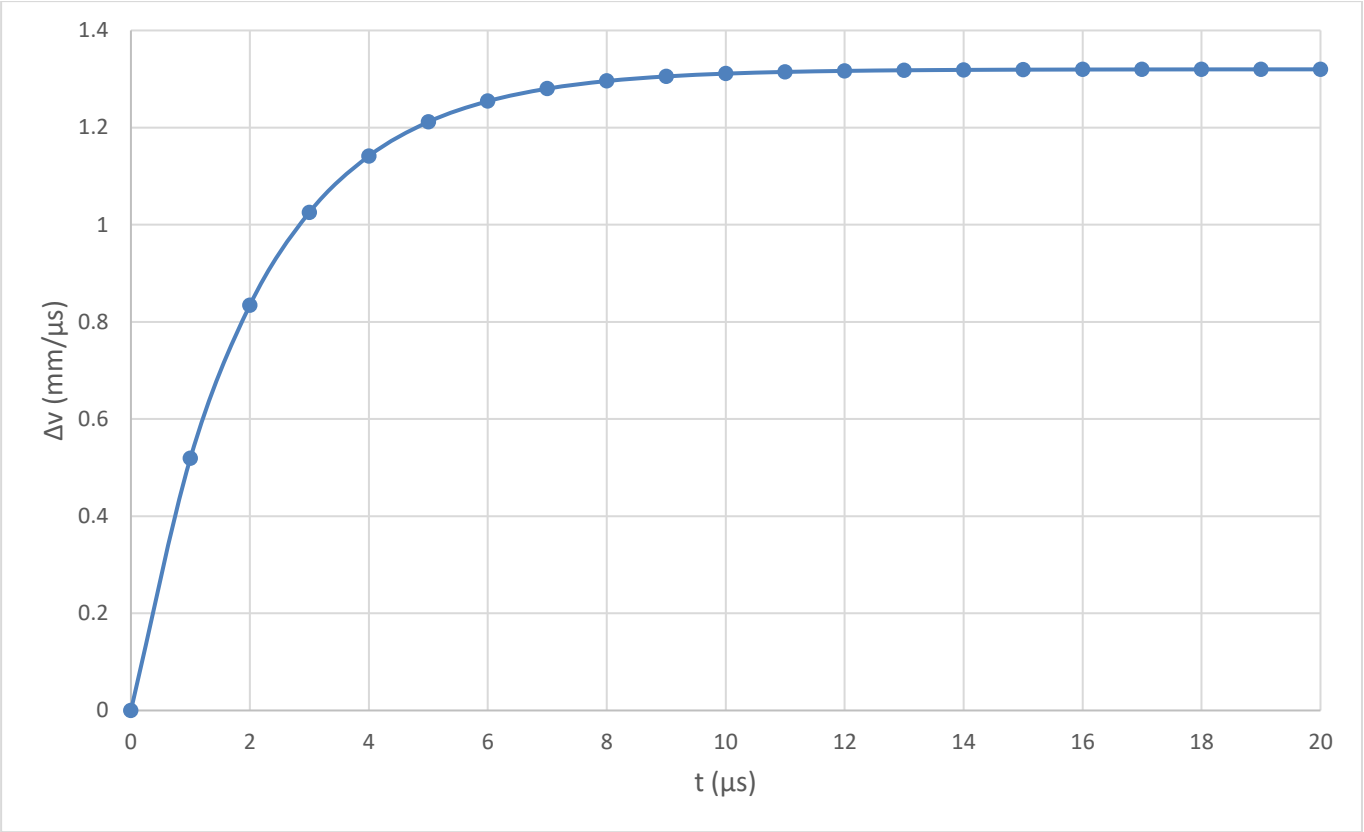

Figure 8-5: The radial expansion velocity of (TNT-2).

Comp-B-1:

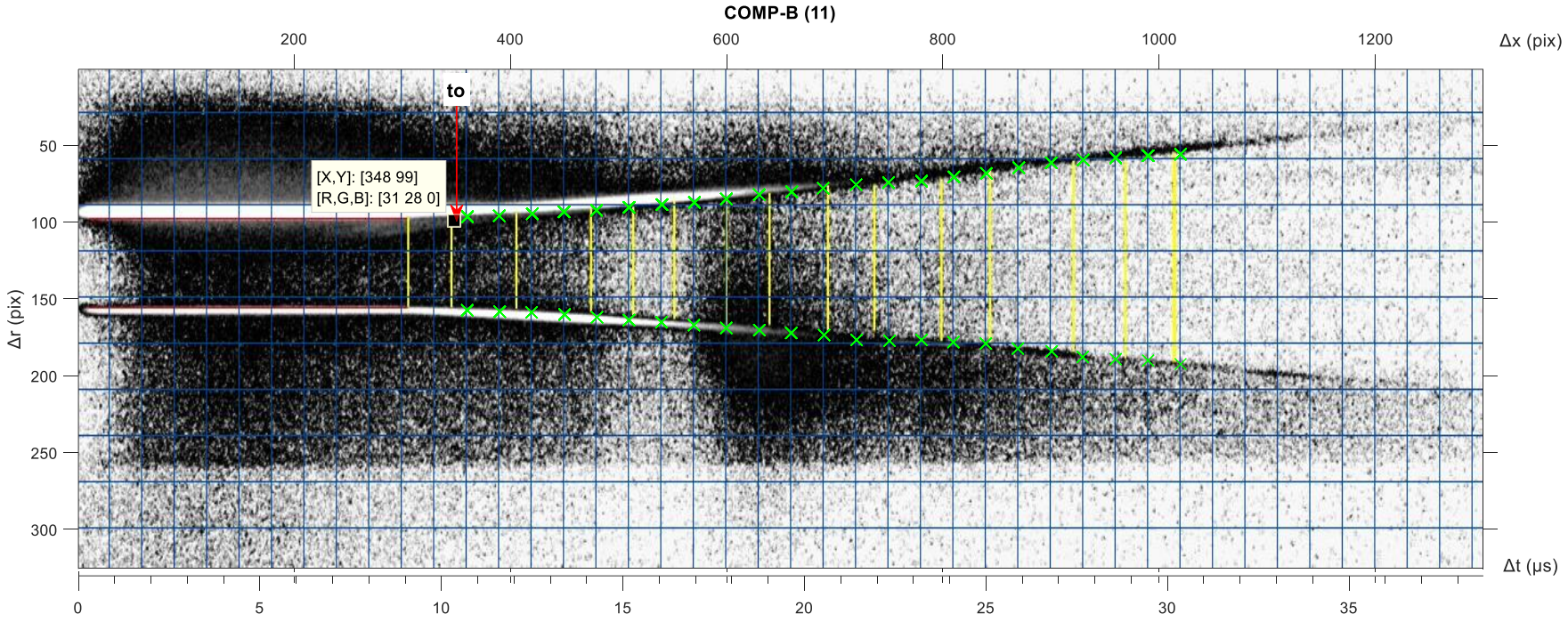
COMP-B (11)
200
400
600
800
1000
1200
Δx (pix)
to
[X,Y]: [348 99]
[R,G,B]: [31 28 0]
50
100
150
200
250
300
Δr (pix)
0
5
10
15
20
25
30
35
Δt (μs)

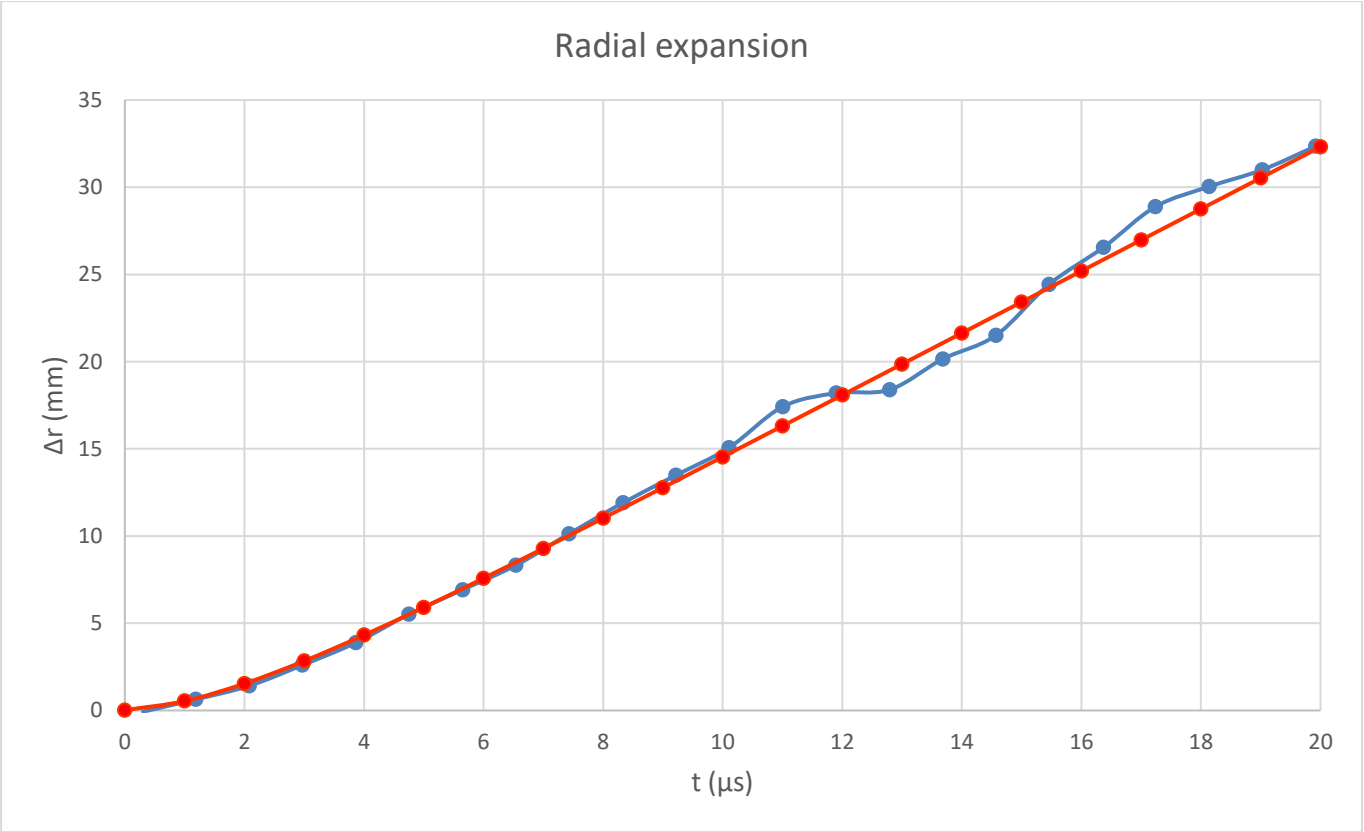

Figure 8-6: The radial position of the cylinder wall with respect to time for (Comp-B -1).

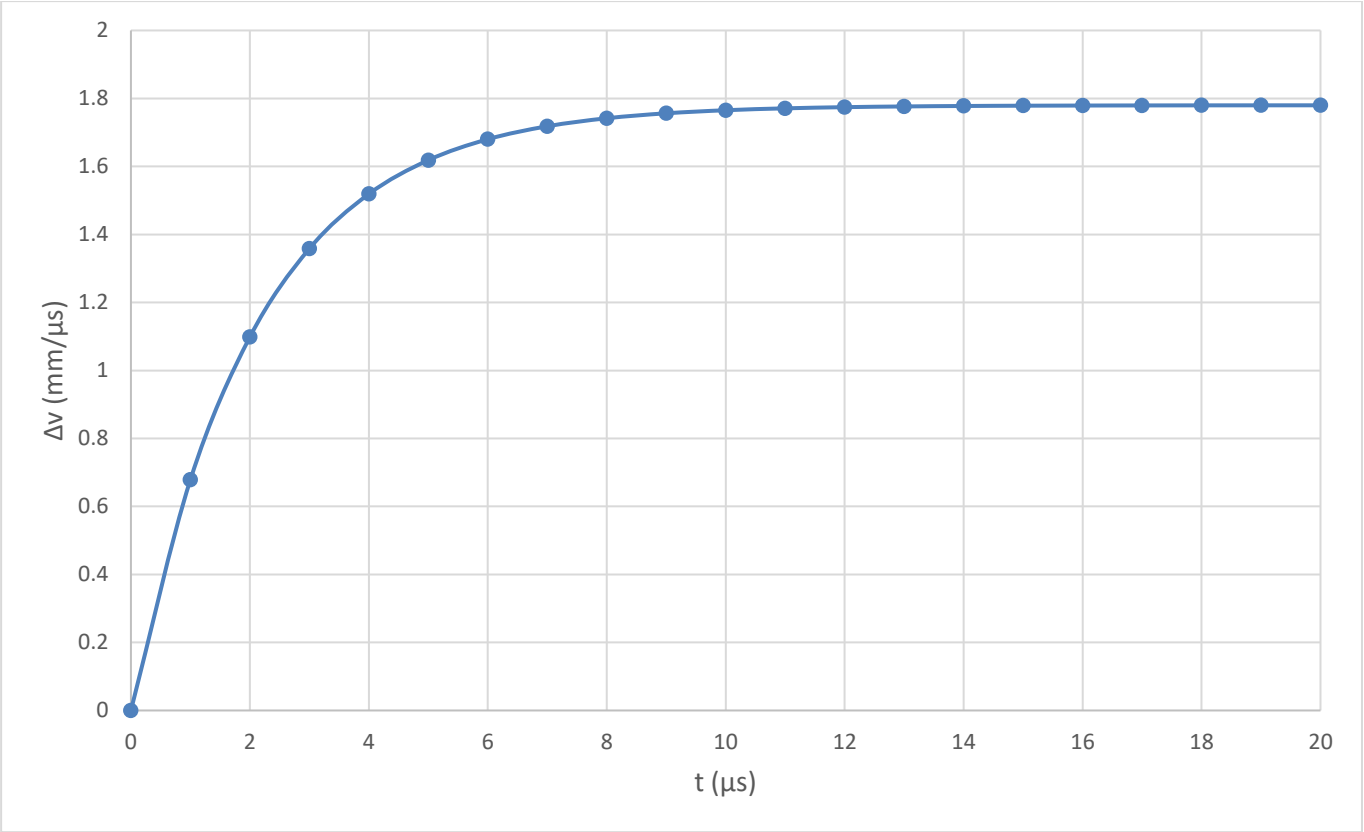

Figure 8-7: The radial expansion velocity of (Comp-B-1).

Comp-B-2:

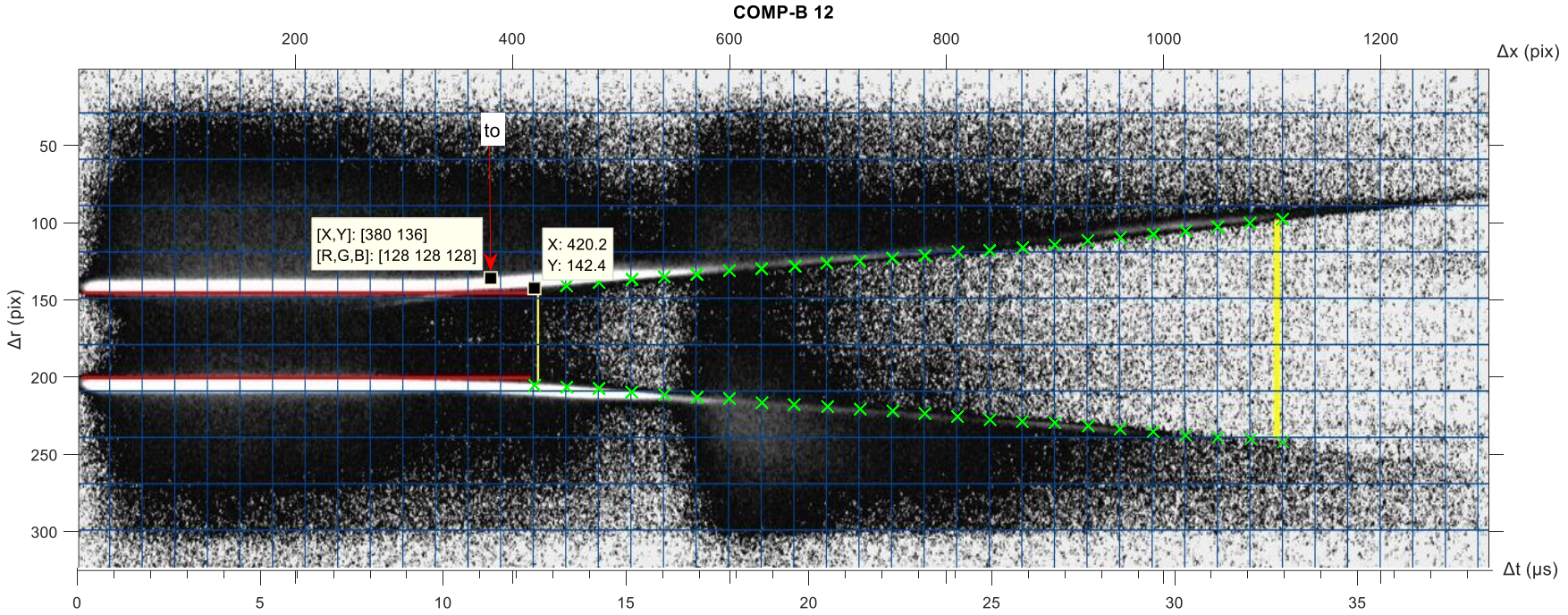
COMP-B 12
200
400
600
800
1000
1200
Δx (pix)
50
100
150
200
250
300
Δr (pix)
to
[X,Y]: [380 136]
[R,G,B]: [128 128 128]
X: 420.2
Y: 142.4
0
5
10
15
20
25
30
35
Δt (μs)

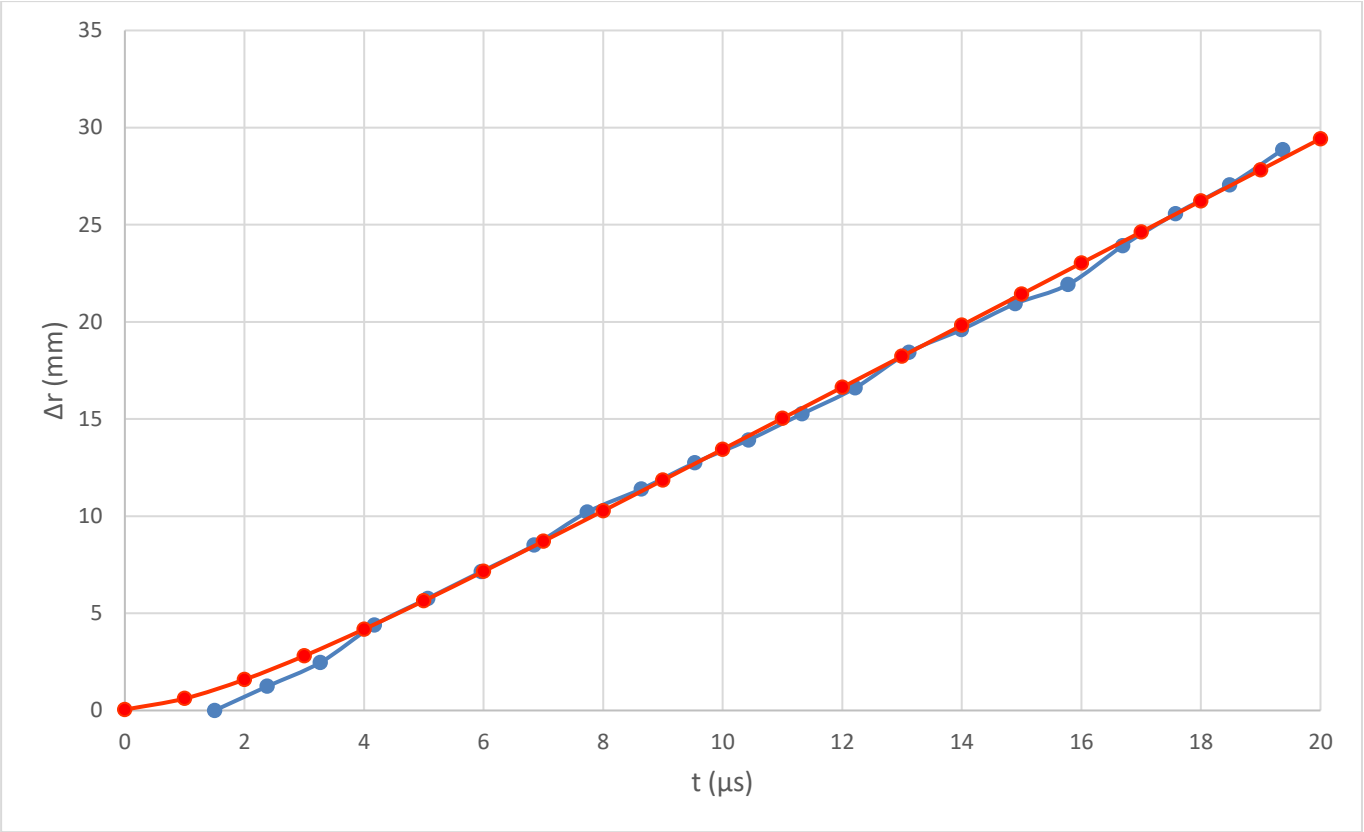

Figure 8-8: The radial position of the cylinder wall with respect to time for (Comp-B -2).

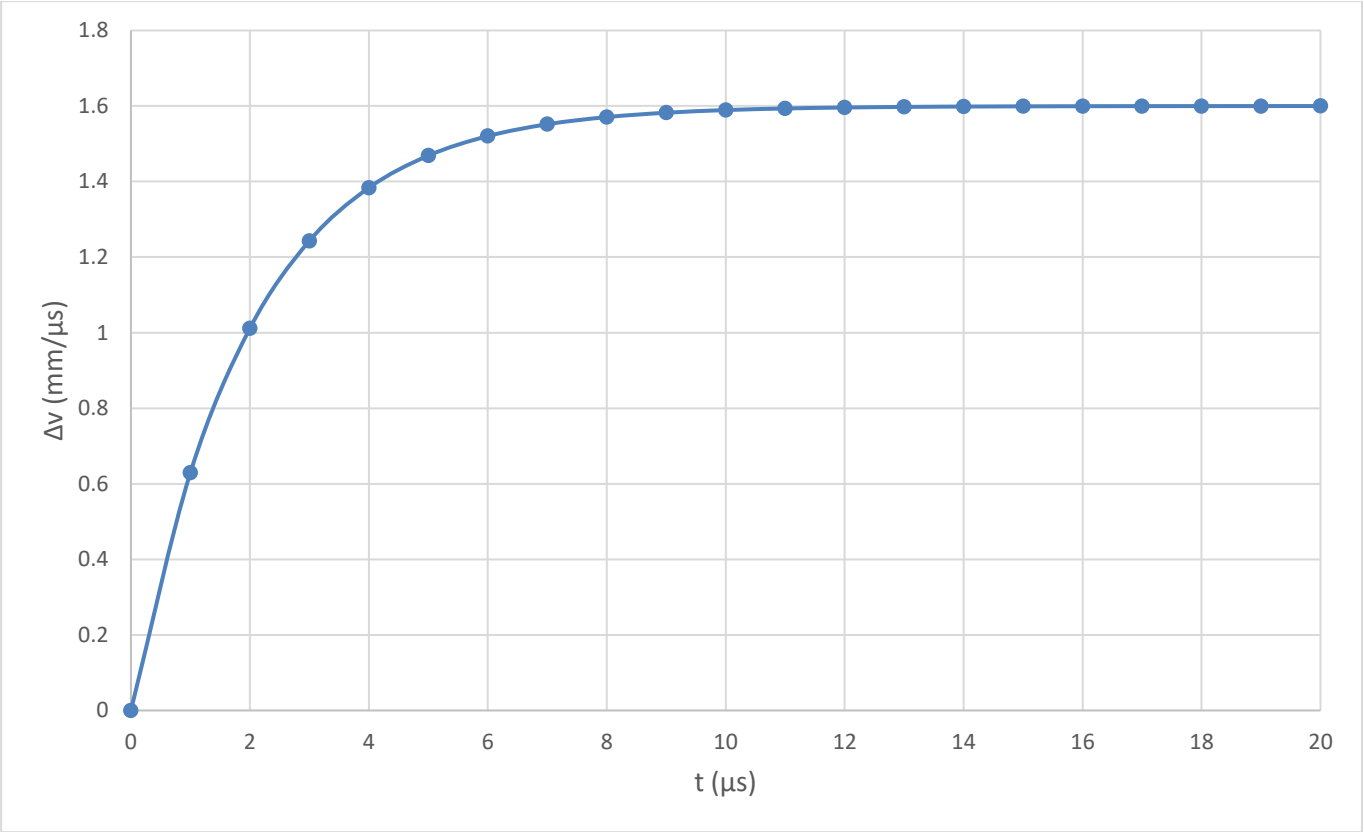

Figure 8-9: The radial expansion velocity of (Comp-B-2).

ONTELIT -1:

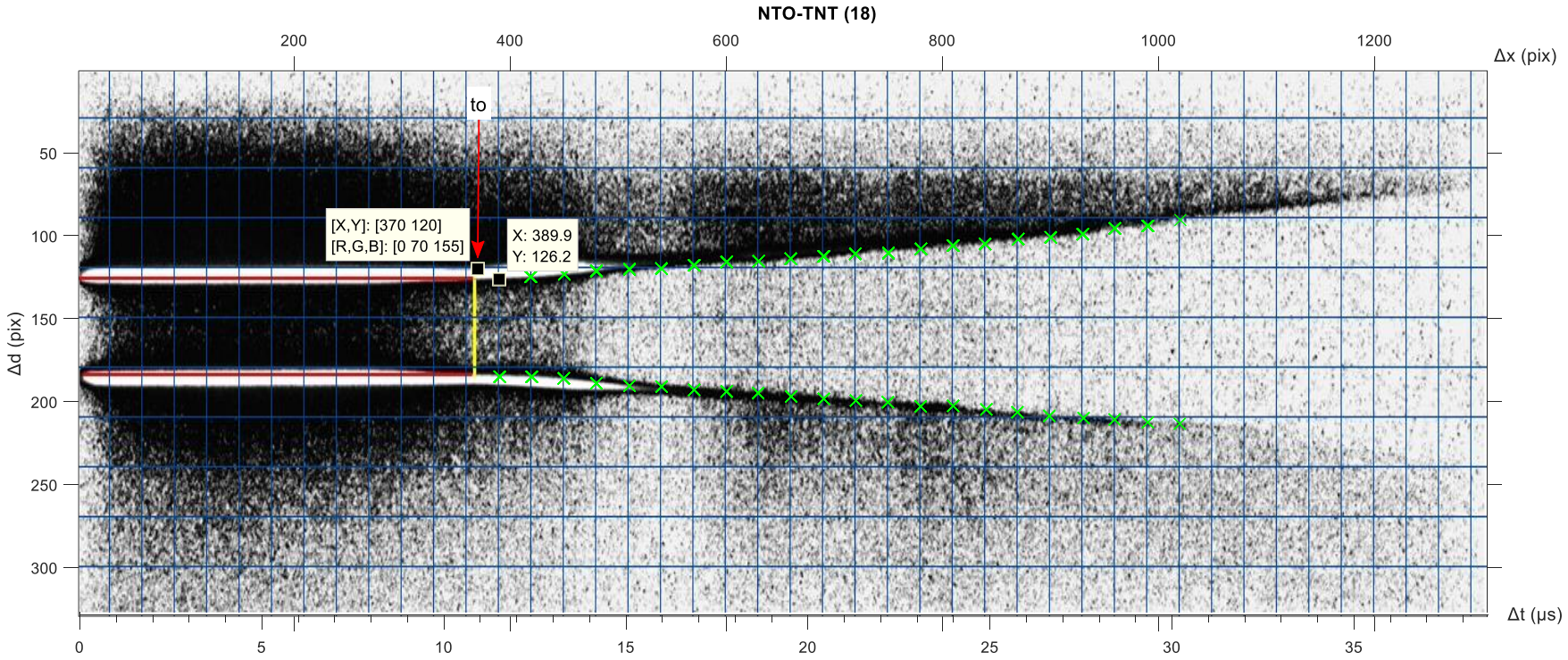
NTO-TNT (18)
200
400
600
800
1000
1200
Δx (pix)
to
50
100
150
200
250
300
Δd (pix)
[X,Y]: [370 120]
[R,G,B]: [0 70 155]
X: 389.9
Y: 126.2
0
5
10
15
20
25
30
35
Δt (μs)

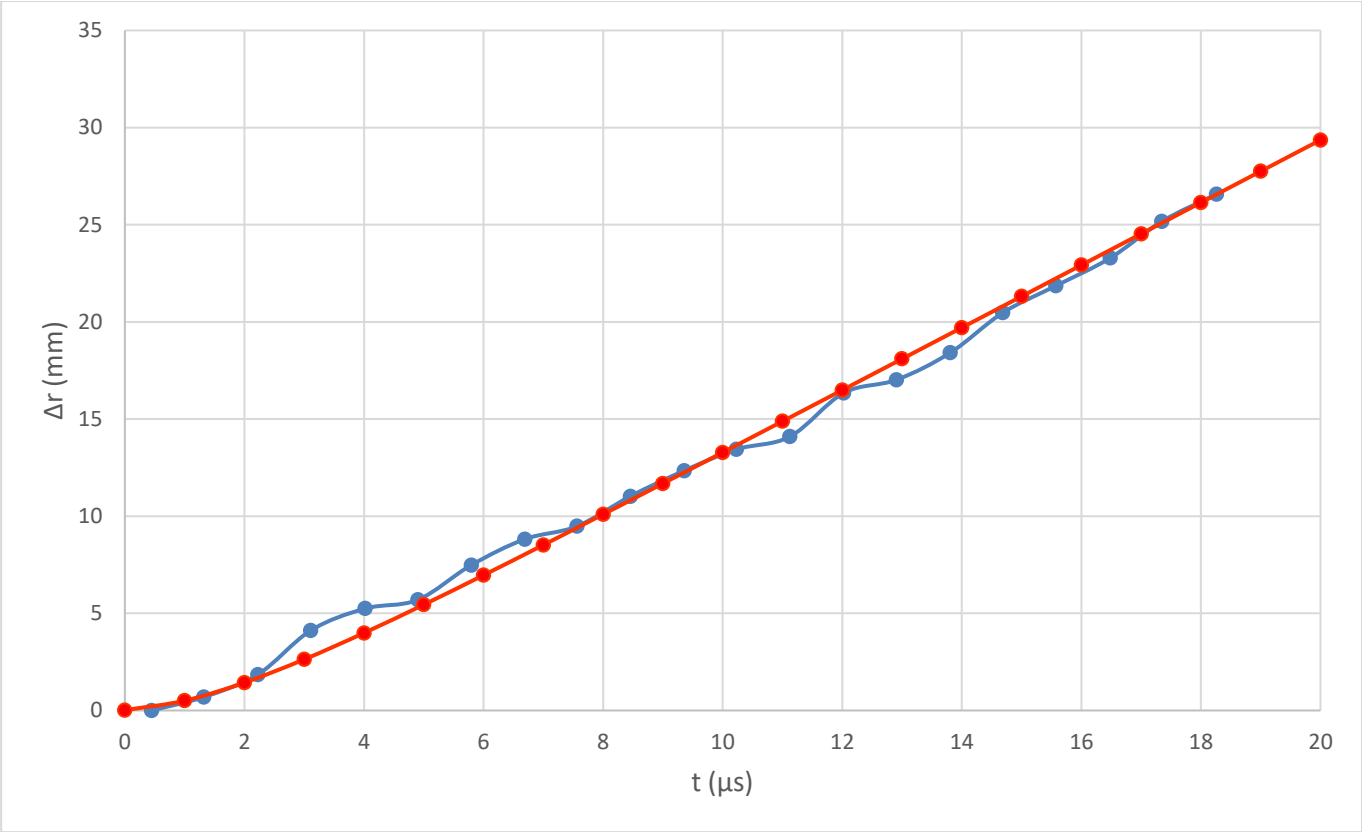

Figure 8-10: The radial position of the cylinder wall with respect to time for (ONTELIT -1).

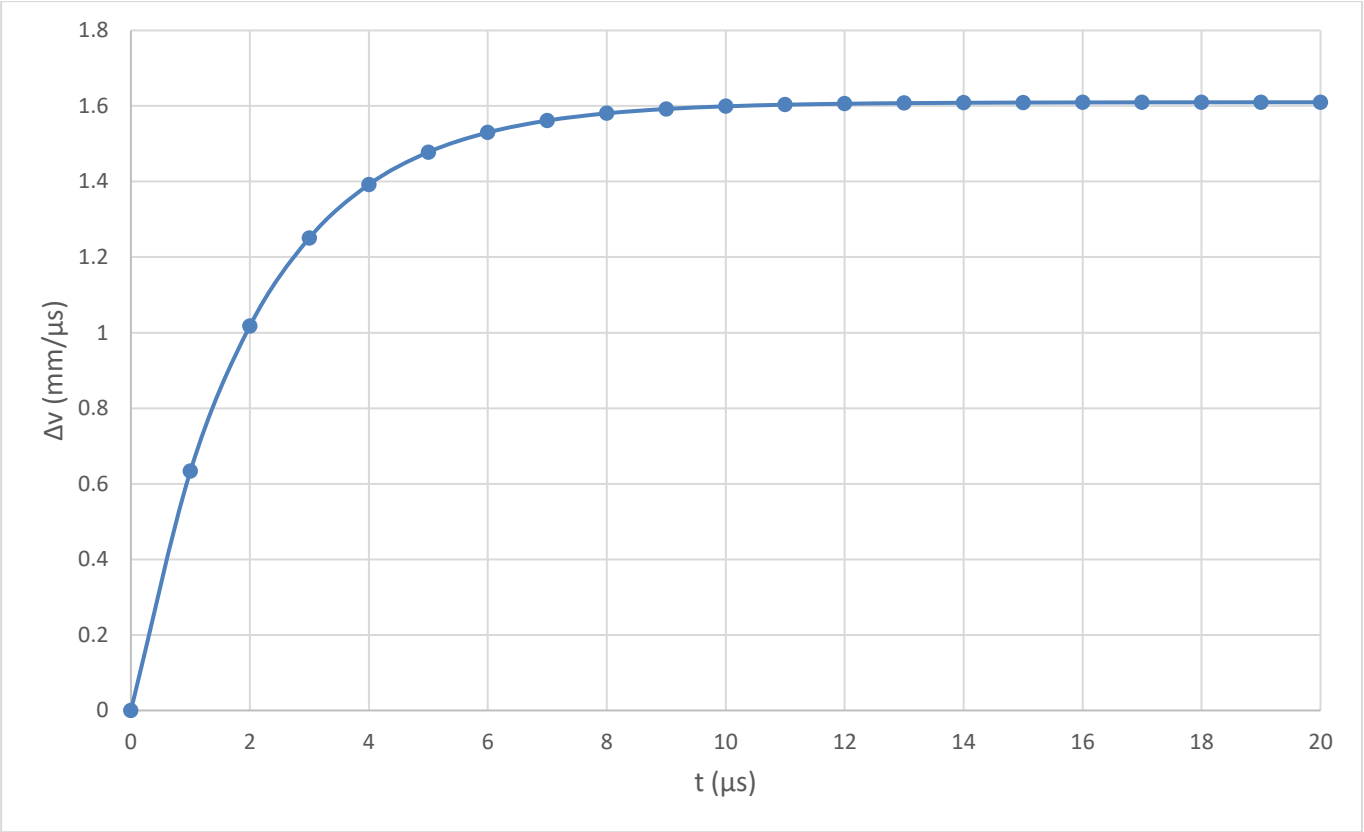

Figure 8-11: The radial expansion velocity of (ONTELIT-1).

ONTELIT -2:

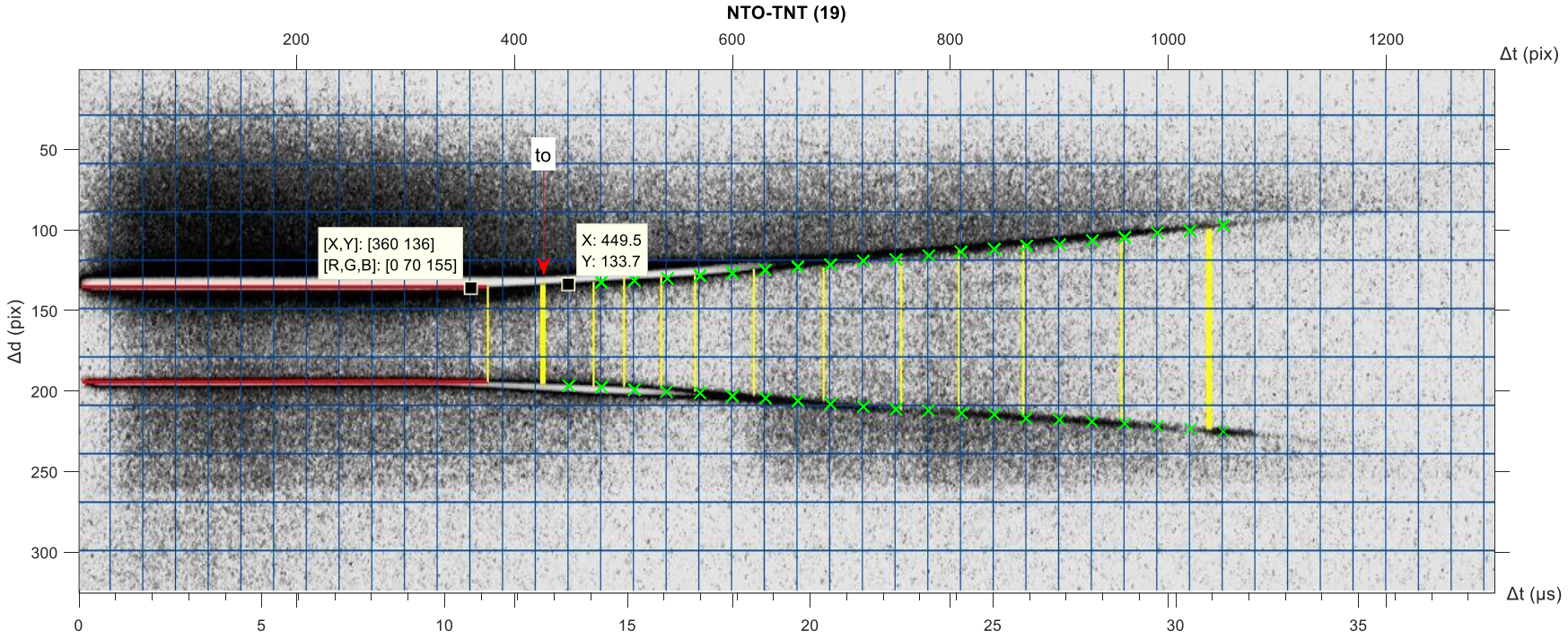
NTO-TNT (19)
200
400
600
800
1000
1200
Δt (pix)
50
100
150
200
250
300
Δd (pix)
to
[X,Y]: [360 136]
[R,G,B]: [0 70 155]
X: 449.5
Y: 133.7
0
5
10
15
20
25
30
35
Δt (μs)

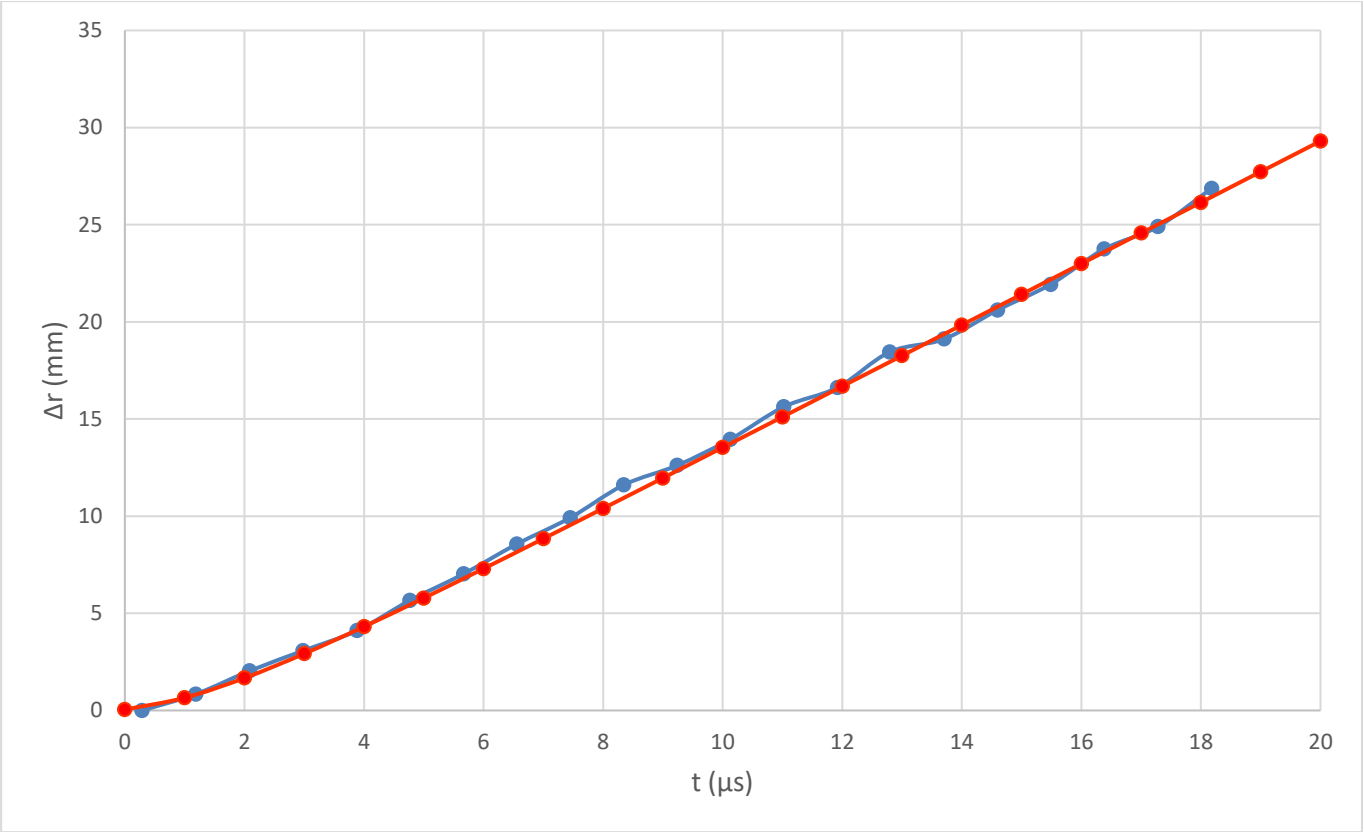

Figure 8-12: The radial position of the cylinder wall with respect to time for (ONTELIT -2).

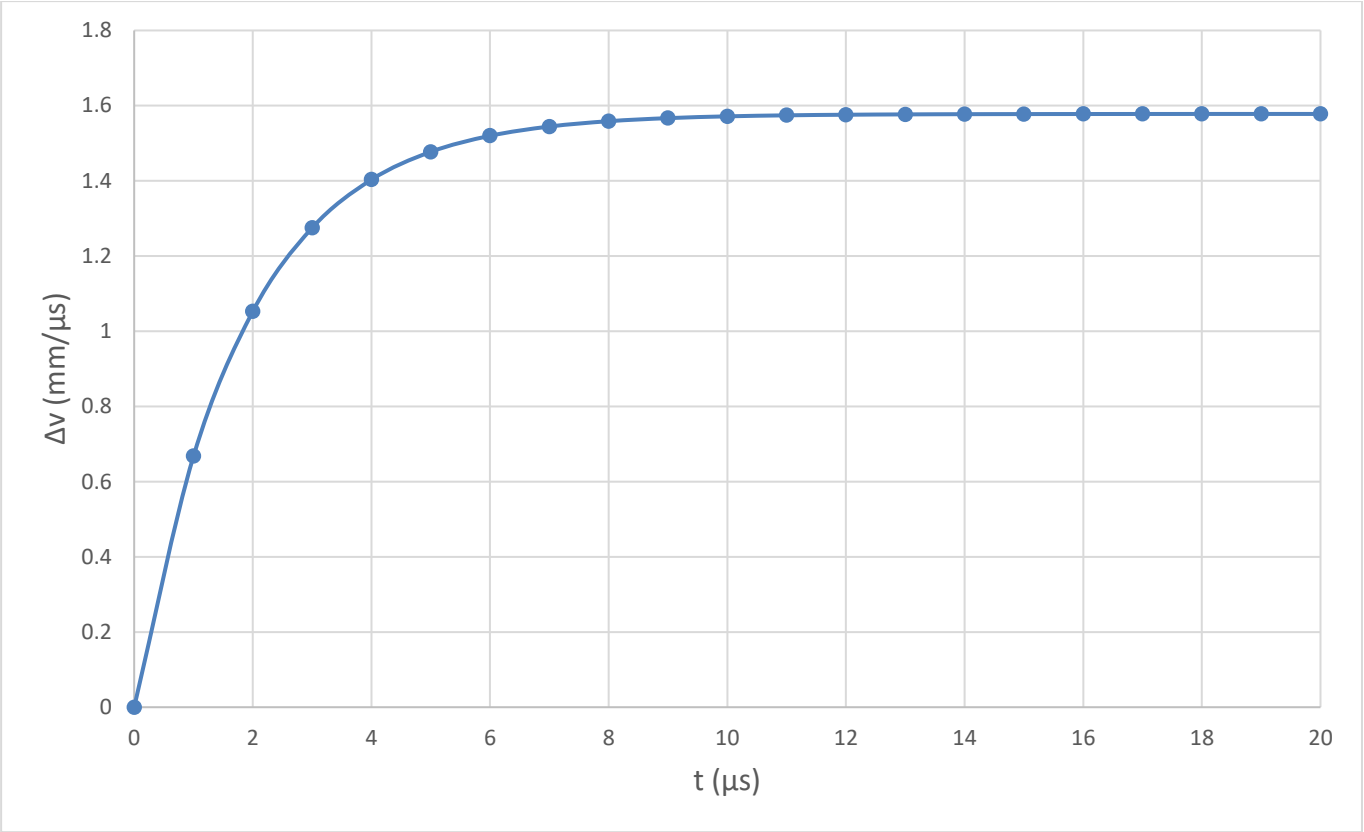

Figure 8-13: The radial expansion velocity of (ONTELIT-2).

MCX-6002-1:

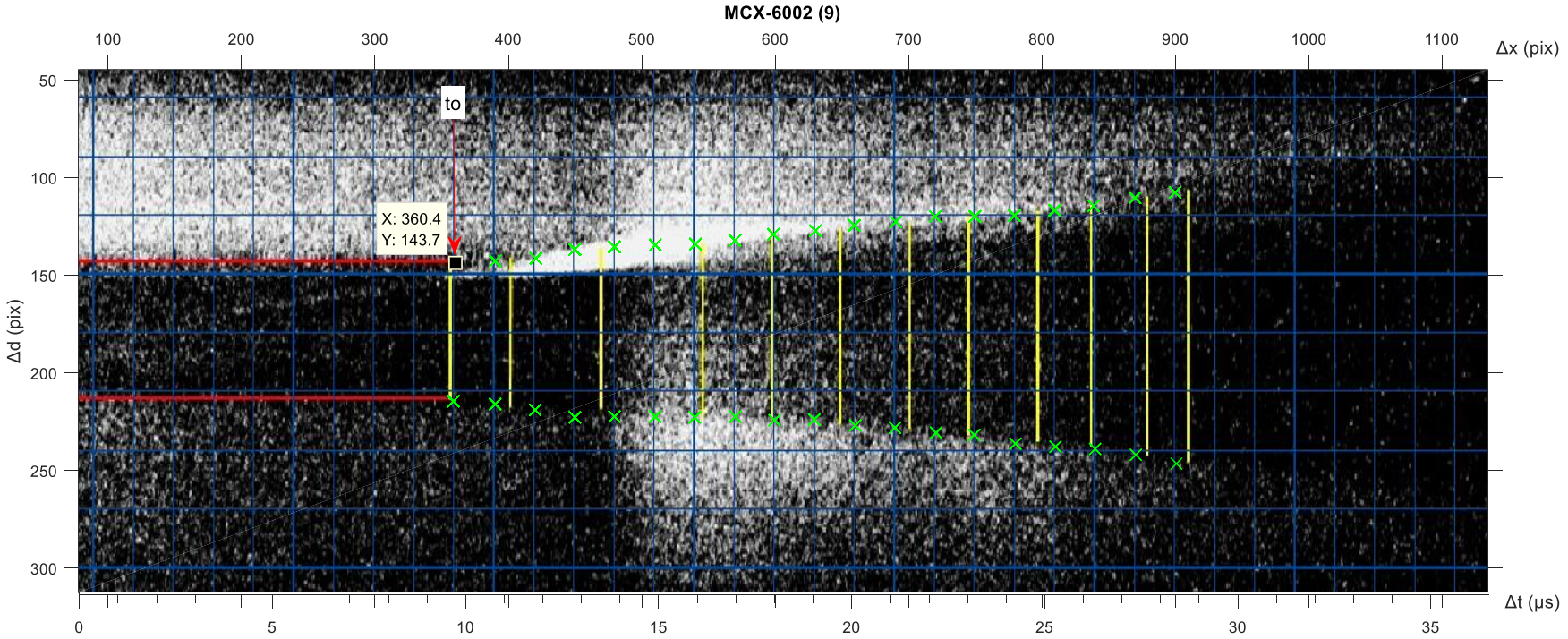
MCX-6002 (9)
Δx (pix)
Δd (pix)
Δt (μs)
to
X: 360.4
Y: 143.7
100
200
300
400
500
600
700
800
900
1000
1100
50
100
150
200
250
300
0
5
10
15
20
25
30
35

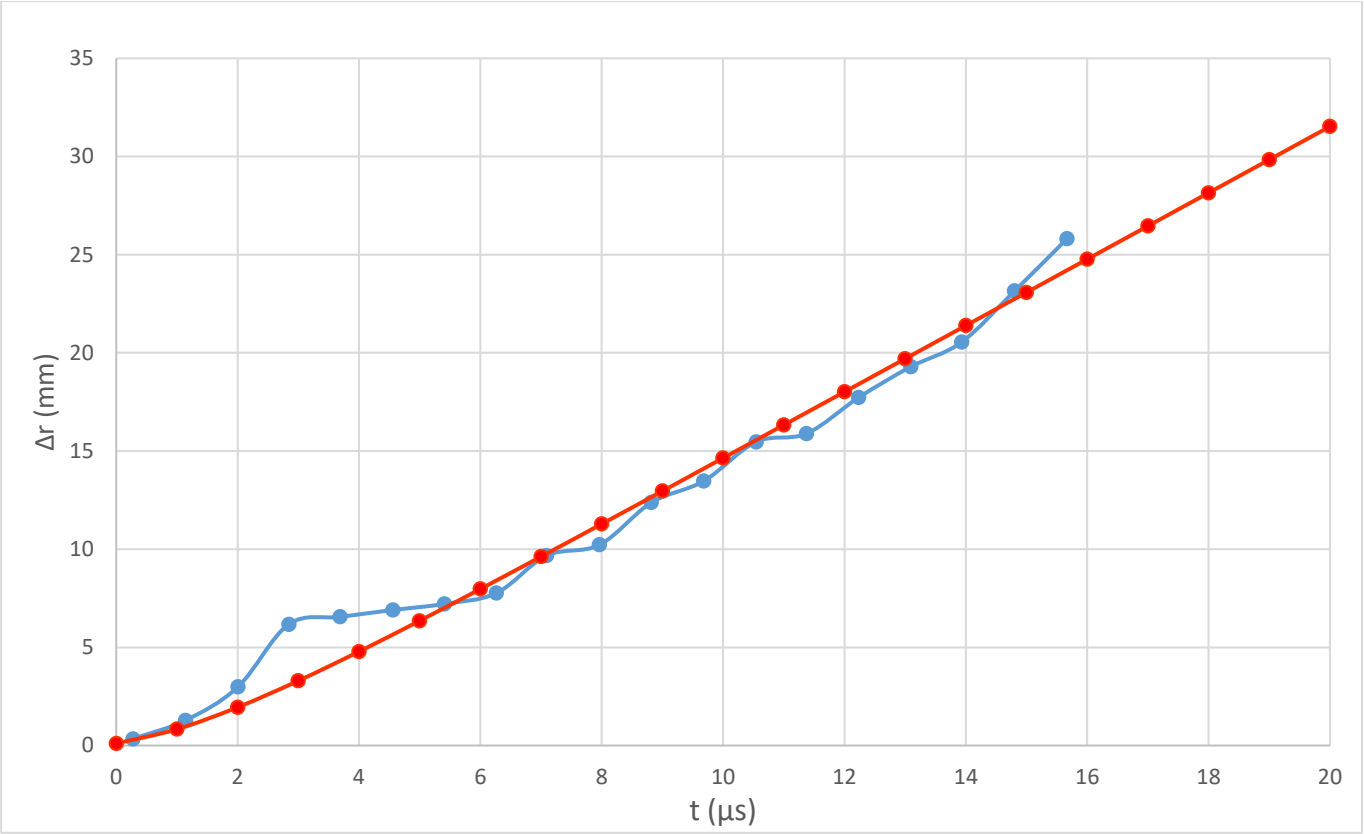

Figure 8-14: The radial position of the cylinder wall with respect to time for (MCX-6002-1).

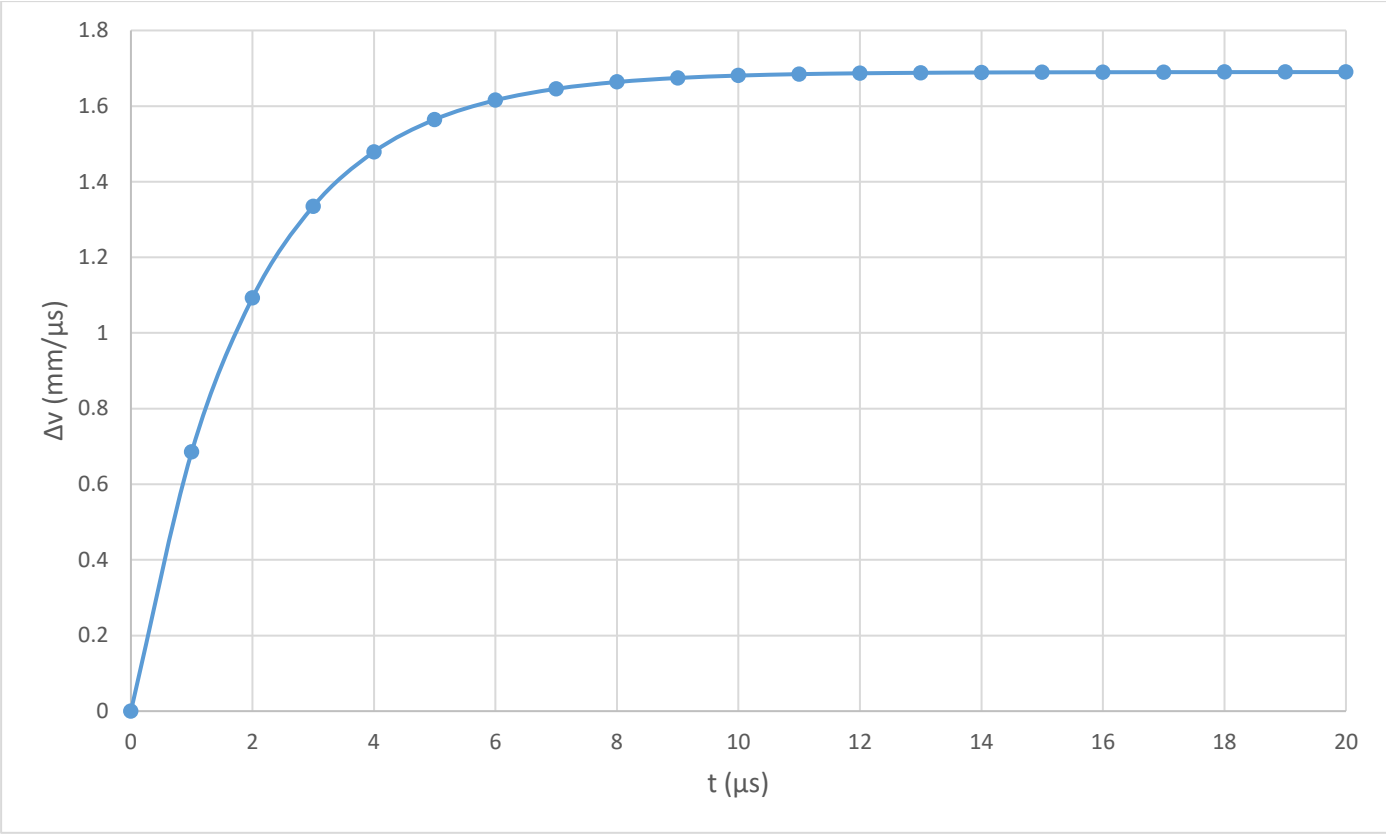

Figure 8-15: The radial expansion velocity of (MCX-6002-1).

RXHT-80-1:

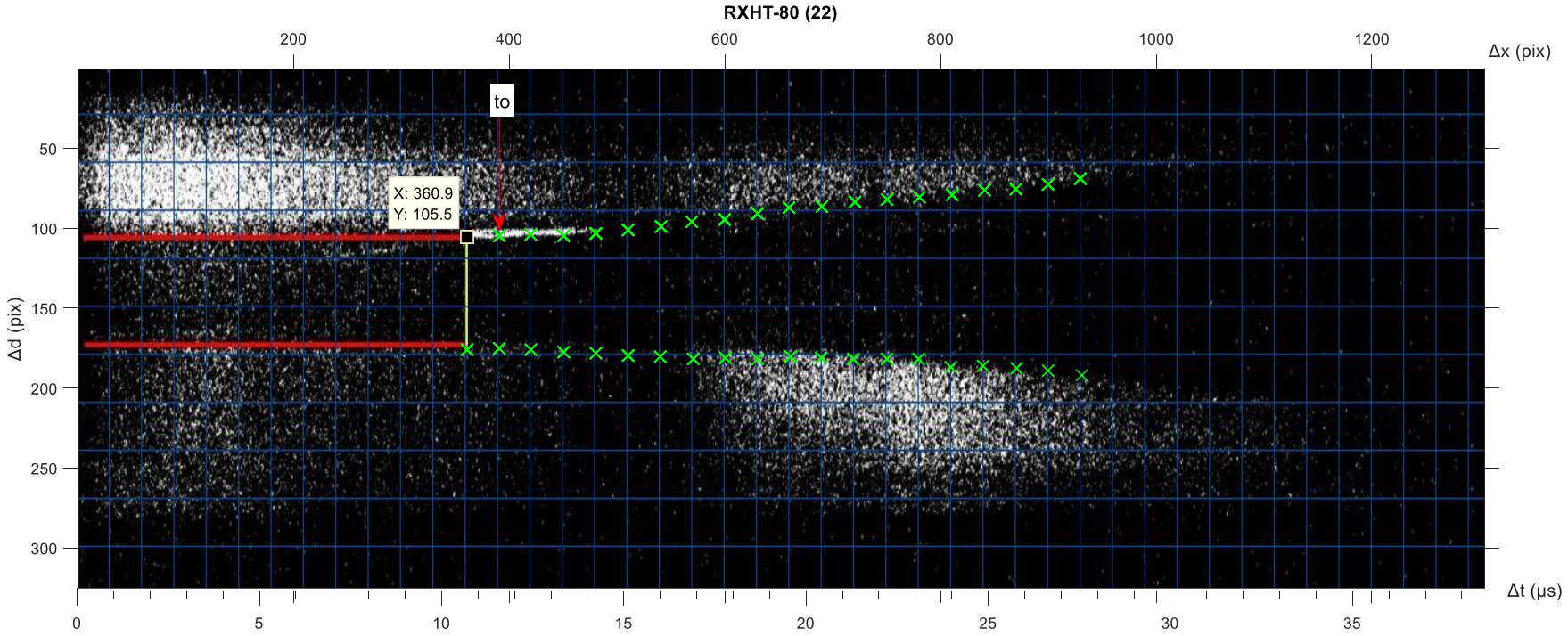
RXHT-80 (22)
Δx (pix)
200
400
600
800
1000
1200
to
X: 360.9
Y: 105.5
Δd (pix)
50
100
150
200
250
300
Δt (μs)
0
5
10
15
20
25
30
35

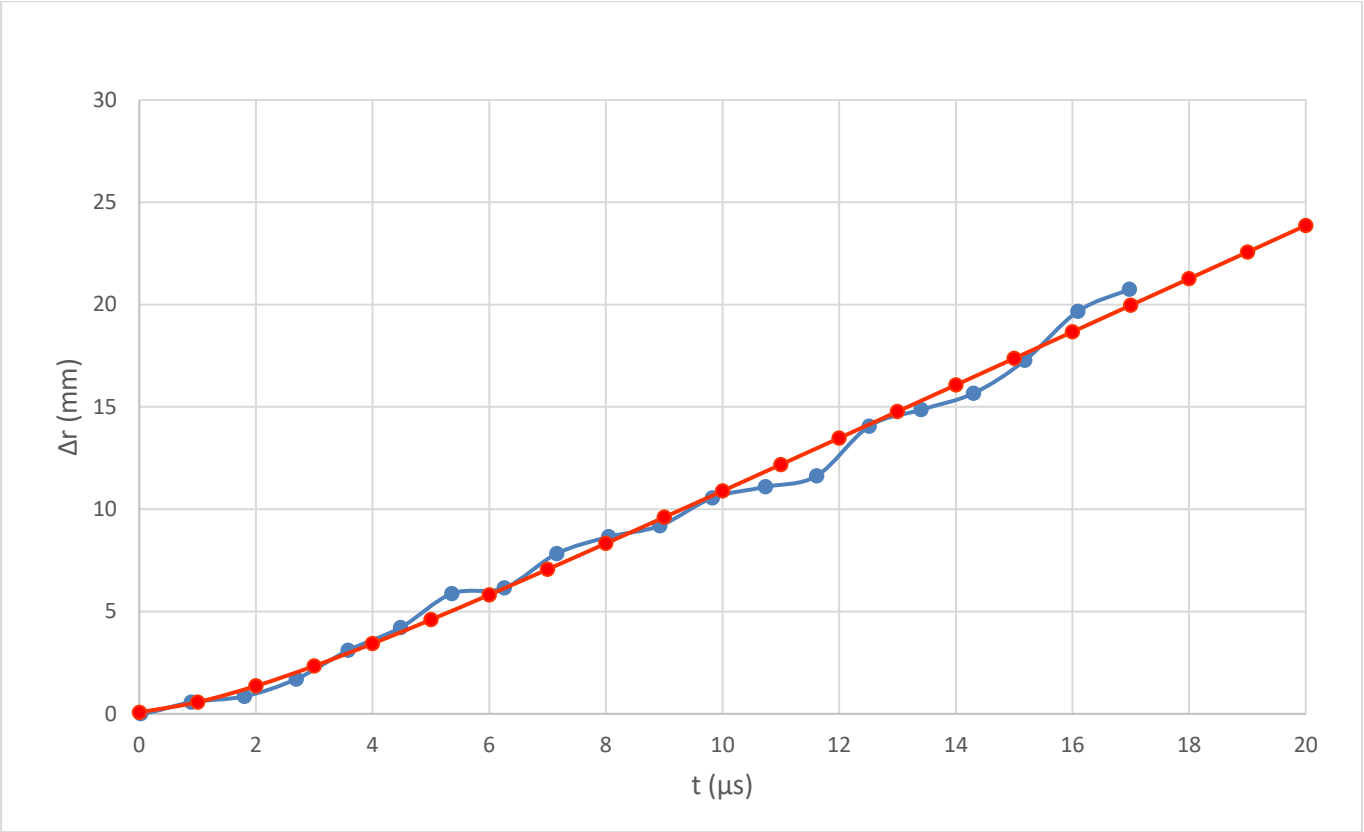

Figure 8-16: The radial position of the cylinder wall with respect to time for (RXHT-80-1).

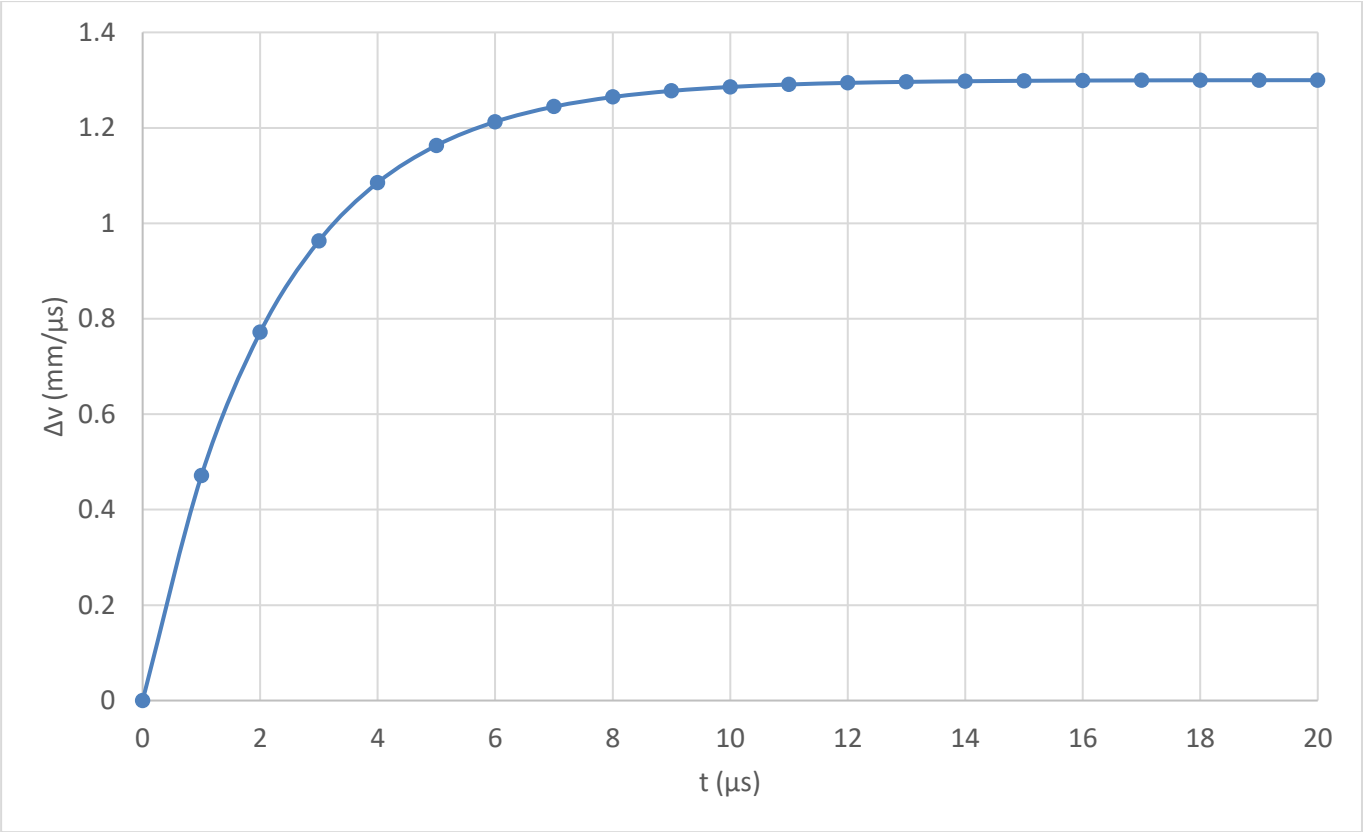

Figure 8-17: The radial expansion velocity of (RXHT-80-1).

Equation of motion parameters:

		TNT	RXHT-80	Comp-B	MCX-6002	ONTELIT
to	1	0.7		0.12		0.12
	2	0.25	0.3	0.2	0.3	0.2
	ave	0.475		0.16		0.16
a	1	1.23		1.78		1.61
	2	1.32	1.3	1.6	1.69	1.578
	ave	1.275		1.69		1.594
b	1	0.3		0.48		0.5
	2	0.5	0.45	0.5	0.52	0.55
	ave	0.4		0.49		0.525